Master's thesis

NTNU
Norwegian University of Science and Technology
Faculty of Natural Sciences
Department of Biotechnology and Food Science

Thea Isabel Bakken

Exploring the potential of using alternative carbon sources for the fermentative production of riboflavin with engineered *Corynebacterium glutamicum*

Master's thesis in Chemical Engineering and Biotechnology
Supervisor: Prof. Trygve Brautaset
Co-supervisor: Dr. Fernando Pérez-García
June 2022

NTNU
Norwegian University of Science and Technology

Thea Isabel Bakken

Exploring the potential of using alternative carbon sources for the fermentative production of riboflavin with engineered *Corynebacterium glutamicum*

Master's thesis in Chemical Engineering and Biotechnology
Supervisor: Prof. Trygve Brautaset
Co-supervisor: Dr. Fernando Pérez-García
June 2022

Norwegian University of Science and Technology
Faculty of Natural Sciences
Department of Biotechnology and Food Science

NTNU
Norwegian University of
Science and Technology

Preface

This master thesis is submitted for the conclusion of my degree in Master of Science through the study program of Chemical Engineering and Biotechnology at NTNU in the spring of 2022. The thesis is a continuation of the specialisation project completed in the fall of 2021, for the department of Biotechnology and Food Science, within the Molecular Genetics team.

I would like to acknowledge my gratitude to Prof. Trygve Brautaset for making it possible for me to be part of the molecular genetics team at NTNU.

To my supervisor, Dr. Fernando Pérez-García, deserving a special thanks for helping with the creation of the idea and being my mentor, teaching and giving me the experience needed to perform the experiments and techniques utilised in this project. Furthermore, always supporting me and answering my questions when needed.

I want to further thank the Cell Factories group members, particularly my lab bench partner Vilde Andrea Tonheim, for creating a friendly and pleasant working atmosphere.

Declaration of Compliance

Trondheim, June 22, 2022

Thea Isabel Bakken

Abstract

The B_2 vitamin, also known as riboflavin, is categorised as an essential nutrient for cells[1]. A deficiency of riboflavin would affect the proper functions of the cells and cause effects such as the increased risk of vascular disease and the production of cancer cells[2][3]. Riboflavin is therefore industrially produced for utilisation as a supplement in feed and food additives.

Corynebacterium glutamicum is a microbial host commonly used for the industrial production of amino acids, in particular l-glutamic acid and l-lysine. Furthermore, it has been engineered for the production of different added value compounds, such as the vitamin riboflavin[4][5]. It is unique because of its capability to utilise multiple carbon sources simultaneously, caused by it lacking the carbon catabolite repression system[6][7] and being successfully modified to use non-native carbon sources[8].

Six strains of *C. glutamicum* were successfully modified through this thesis to analyse how the consumption of different native and non-native carbons sources would affect the growth rate of the strains and the riboflavin production. Glucose, fructose, mannitol and xylose were carbon sources analysed as sole carbon sources and in combinations. The strain, modified with the ability for mannitol consumption, with the highest riboflavin production, yielded a titer of 0.39 $\pm$ 0.12 g/L over 25 hours, utilising a combination of 1 % glucose and 1% mannitol as carbon source.

Furthermore, xylose as sole carbon source showed an improvement in riboflavin's specific productivity. Therefore, the process was scaled-up in bioreactors. The fermentation was divided into a batch and a feed phase, with the total fermentation time at 72 hours. The batch phase consisted of 1 % xylose, while the feed added had a concentration of 5% xylose. The final biomass value, riboflavin titer and product yield values for the fed-batch fermentation were found to be 3.29 g/L, 0.85 g/L and 0.065 g/g.

Through the work done in this master thesis, it has been proven that the use of non-conventional and sustainable substrates for *C. glutamicum* is a powerful tool within industrial biotechnology. Further exploration and exploitation is needed to continue developing sustainable bioprocesses and enforcing the circular bioeconomy.

Sammendrag

B_2 -vitaminet, også kjent som riboflavin, er kategorisert som et essensielt næringsstoff for cellene[1]. Mangel på riboflavin vil påvirke de essensiele funksjonene til cellene og forårsake økt risiko for vaskulær sykdom og produksjon av kreftceller[2][3]. Riboflavin er derfor industrielt produsert for bruk som tilskudd i fôr og mattilsetninger.

Corynebacterium glutamicum er en mikrobiell vert som vanligvis brukes til industriell produksjon av aminosyrer, spesielt l-glutaminsyre og l-lysin. Videre har den blitt modifisert for produksjon av forskjellige verdiskapende forbindelser, slik som vitaminet riboflavin[4][5]. Den er unikt på grunn av dens evne til å bruke flere karbonkilder samtidig, som er forårsaket av dens mangel på det komplekse karbonkatabolitt-undertrykkelses-systemet[6][7] og er videre vellykket modifisert for bruken av non-native karbonkilder[8].

Seks stammer av *C. glutamicum* ble modifisert gjennom denne oppgaven for å analysere hvordan forbruket av forskjellige native og non-native karbonkilder ville påvirke veksthastigheten til stammene og riboflavinproduksjonen. Glukose, fruktose, mannitol og xylose var karbonkildene brukt for analyse, både som eneste karbonkilde og i kombinasjoner. Stammen modifisert med evnen til mannitolforbruk, med den høyeste riboflavinproduksjonen, ga en konsentrasjon på 0,39 ± 0,12 g/L over 25 timer, ved å bruke kombinasjon av 1 % glukose og 1 % mannitol som karbonkilde. Videre viste xylose som eneste karbonkilde en forbedring i riboflavins spesifikke produktivitet. Derfor ble prosessen oppskalert i bioreaktorer. Fermenteringen ble delt inn i en batch og en fôrfase, med total fed-batch-fermenterings tid på 72 timer. Batchfasen bestod av 1 % xylose, mens tilsatt fôr hadde en konsentrasjon på 5 % xylose. Den endelige biomasseverdien, riboflavinkonsentrasjonen og produktutbytteverdien for fed-batch-fermenteringen ble funnet til å være 3.29 g/l, 0.85 g/l og 0.065 g/g.

Gjennom arbeidet i denne masteroppgaven har det blitt bevist at bruk av ikkekonvensjonelle og bærekraftige substrater for *C. glutamicum* er et kraftig verktøy innen industriell bioteknologi. Ytterligere leting og utnyttelse er nødvendig for å fortsette å utvikle bærekraftige bioprosesser og håndheve den sirkulære bioøkonomien.

Table of Contents

List of Abbreviation

Abbreviation	Non abbreviated form
ATP	Adenosine triphosphat
BHI	Brain Heart Infusion
BHIS	Brain Heart Infusion solution with Sorbitol
CGXII	Salt solution
DNA	Deoxyribonucleic acid
EPB1	Electroporation buffer 1
EPB2	Electroporation buffer 2
EtOH	Ethanol
FAD	Flavin adenine dinucleotide
FMN	Flavin mononucleotide
F-PTS	Fructose-specific phosphotranspherase system
G-PTS	Glucose-specific phosphotranspherase system
GTP	Guanosine triphosphate
HEPES	4-(2-hydroxyethyl)-1-piperazineethanesulfonic acid
HPLC	High-performance liquid chromatography
IPTG	Isopropyl Thiogalactopyranoside
KOH	Potassium hydroxide
K_2PO_4	Tripotassium phosphate
MOPS	3-(N-morpholino)propanesulfonic acid
MtlA	importer protein for mannitol
NADH	Nicotinamide adenine dinucleotide
NADPH	nicotinamide adenine dinucleotide phosphate
OD	Optical Density
P	Phosphate
PCA	Protocatechuic acid
PCR	Polymerase chain reaction
PPP	Pentose Phosphate pathway
P_{taq}	taq-promoter
P_{trc}	trc-promoter
Redox reaction	Reduction-oxidation reaction
TCA cycle	Tricarboxylic acid cycle
TES	Trace element solution
TEA	Tris-acetate-EDTA
2TY	2x Yeast Extract Tryptone

1 Introduction

The B_2 vitamin, also known as riboflavin, is categorised as an essential nutrient for cell function[1]. Riboflavin is connected to the electron transport chain as a precursor for the coenzymes flavin mononucleotide (FMN) and flavin adenine dinucleotide (FAD)[2][3]. It implies that a deficiency of riboflavin affects the main metabolism of the cells. Health effects such as the increased risk of vascular disease and the production of cancer cells have also been shown to be dependent on riboflavin[3]. The ability to take B_2 vitamin supplements is therefore essential and made possible through the industrial production of riboflavin.

Riboflavin has been produced chemically and through microbial fermentation for many years[9]. In 2000 the chemical process was replaced with microbial through *Bacillus subtilis*[9]. Today, there is a multitude of industrial producers that have been genetically altered specifically to produce riboflavin.[10]

The gram-positive bacteria *C. glutamicum* as an industrial producer is beneficial because of its high growth rate and ability to achieve high cell density[11][10]. Its optimal growth rate temperature is at 30 °C[12], indicating a lower cost for incubation compared to other organisms, such as *Escherichia coli* which grows best at 37 °C[13]. Furthermore, it can utilise multiple carbon sources simultaneously caused by its lacking carbon catabolite repression system[6][7], as well as being successfully modified to use non-native carbon sources[8]. It has been employed as an industrial-scale producer of amino acids, organic acids, carotenoids and vitamins[4][5]. *C. glutamicum* is a common microbial workhorse, resulting in a broad genetic toolbox available for genetic modifications[11][4].

1.1 Previous Project Work

Previous work connected to the master thesis, the specialisation project "Riboflavin production from genetically modified *Corynebacterium glutamicum*", was coordinated in autumn 2021. The main objective of this project was to establish and optimise the production of riboflavin in *C. glutamicum*, through the genetic modification of overexpressing the biosynthetic operon *riboGCAH* (named *riboCg* in this project) from *C. glutamicum*. This was further connected with an analysis of the effect different concentrations of the primary carbon source glucose had on the growth and riboflavin production performances.

Through the project, it was possible to conclude that the strains that overexpressed the riboflavin biosynthetic operon had a higher riboflavin production than the empty vector strains. Furthermore, it was shown that producing a high amount of riboflavin affected the cell's growth rate and causes a decrease in the final biomass compared to the strains that did not have overexpression of the riboflavin biosynthetic operon. Laying the groundwork for this master thesis.

2 | Theoretic Background

In this chapter, the theoretical background for the thesis is presented. Subchapters 2.1 and 2.2 provides an initial knowledge of the product riboflavin and the microbial host, *C. glutamicum*, utilised in this thesis. These subchapters have furthermore their bases from the specialisation project "Riboflavin production from genetically modified *Corynebacterium glutamicum*". Subchapter 2.3 delves into different possible carbon source pathways for *C. glutamicum*, with the additional connection of possible genetically modifications that could affect the flux of riboflavin production.

2.1 Riboflavin, the B_2 vitamin

For the function of cells, riboflavin, also known as the B_2 vitamin, is categorised as an essential nutrient[1]. Its chemical structure is represented in Figure 2.1[14]. Some attributes of riboflavin are its sensitivity to light and its tendency to photodegrade. Furthermore, the characteristics of riboflavin's chemical structure, specifically the presence of hydroxy groups, make it soluble in water. The solubility is further temperature-dependent and increases with increasing temperature[2]. Additionally, when riboflavin is in its solid form by crystallisation, it obtains a yellow-orange colour, which is utilised to examine samples[3].

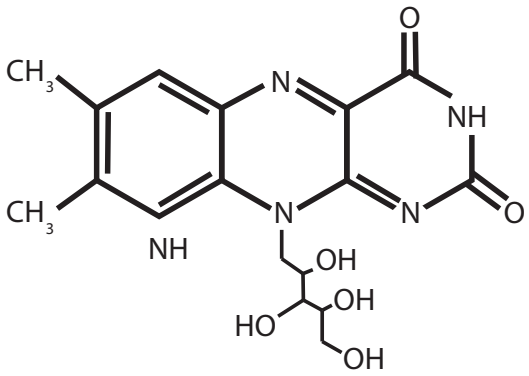

Figure 2.1: Riboflavin's chemical structure is represented here. C, H, N, and O represent the chemicals carbon, hydrogen, nitrogen, and oxygen with their singular- or double-bonded connections.

In connection with its biological role and cell utilisation, riboflavin is a precursor for the coenzymes FMN and FAD. It is inadvertently essential for the cell as the

coenzymes are directly connected to the electron transport chain, involved in the reduction-oxidation(redox) reactions[2] [3]. The most natural source for uptake of riboflavin is as the compounds FMN and FAD. These compounds bind with proteins, therefore protein rich food, such as meat, seafood, dairy and eggs, have a high concentration of the coenzymes[1] [2].

2.1.1 Riboflavin production in cells

The specific pathway for riboflavin production in *C. glutamicum*, as microbial host in this project, is represented in Figure 2.2[15]. The riboflavin biosynthetic prodution has two starting points connected to central metabolic pathways. The oxidative pentose phosphate pathway(PPP) and the purine pathway. Through the compounds Ribulose 5-phosphate(Riboluse-5-P) and guanosine triphosphate(GTP), respectively. Both routes connect when 6,7-Dimethyl- 8-ribityllumazine is synthesised, following then the production of riboflavin. The enzymes associated with riboflavin production are bifunctional riboflavin-specific deaminase/reductase[16], riboflavin synthase[17], GTP cyclohydrolase II/3,4-dihydroxy-2-butanone-4-phosphatesynthase[18] and riboflavin synthase beta chain[19]. The proteins are encoded by a group of gene sequences present in a biosynthetic operon from *C. glutamicum*, called *riboCG*. The specific gene sequences encoding the enzymes are respectively *ribG*, *ribC*, *ribA* and *ribH*. This operon is subsequently essential for riboflavin production, indicating that overexpressing the genes increases the flux through the production pathway.

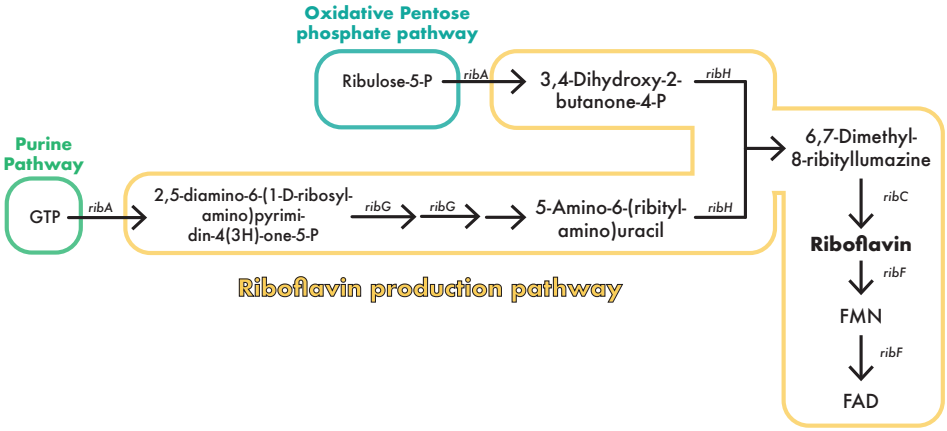

Figure 2.2: The specific production pathway of riboflavin in *C. glutamicum* is shown marked in yellow, with its two starting points connected to the purine pathway(marked in green) and the oxidative PPP(marked in blue). Slanted names refer to specific genes coding for enzymes associated with the reactions. *ribG* encoding for bifunctional riboflavin-specific deaminase/reductase, *ribC* encoding for Riboflavin synthase, *ribA* encoding for GTP cyclohydrolase II/3,4-dihydroxy-2-butanone-4-phosphatesynthase and *ribH* encoding for the riboflavin synthase beta chain. Compounds are represented in regular black writing, where the abbreviations stand for phosphate(P), guanosine triphosphate(GTP), Flavin mononucleotide(FMN) and flavin adenine dinucleotide(FAD)

Riboflavin has two degradation products; FMN and FAD. The degradation flux is dependent on the expression of *ribF*[20]. It codes for the enzymes bifunctional riboflavin kinase and FMN adenylyltransferase that catalyses the reactions producing FMN and FAD, respectively.

2.1.2 Importance of Riboflavin

As an essential nutrient for cells, a deficiency of riboflavin would affect the proper functions of the cells. In connection with the two coenzymes, FMN and FAD, and their association with the electron transport chain, a deficiency of riboflavin would affect the cell's production of energy[2][3]. A reduction in the two coenzymes would further affect the metabolisms of different nutrients, particularly the metabolism of other B-vitamins[3].

Health effects such as the increased risk of vascular disease and the production of cancer cells have also been shown to be dependent on riboflavin. The coenzyme FAD is associated with the metabolism of homocysteine. A decrease in FAD amount decreases the metabolism of homocysteine, inadvertently increasing the risk for vascular disease. The deficiency of riboflavin has further been theorised to affect the activation of carcinogens, which are substances that directly affect the production of cancer cells. In conclusion, a deficiency of riboflavin would cause multiple health effects[2][3], resulting in riboflavin commonly being used as a feed and food additives.

2.1.3 Industrial producers of riboflavin

Riboflavin has been produced chemically and through microbial fermentation for many years. *Ashbya gossypii*, a fungus, *Candida famata*, a yeast, and the Gram-positive bacterium *B. subtilis* are the three main microorganisms employed for commercial riboflavin synthesis over the years and are still widely utilised[9].

MacLaren discovered in 1952 that increasing purine derivatives in the growth medium of *Eremothecium ashbyii* boosted riboflavin synthesis[21]. Pure chemical production of riboflavin was discovered by Kurth et al.(1996)[22], when D-ribose and 3,4-xylidine were combined with ethanol. Although organic solvents were used in this chemical method, the highest significant yield was merely 60%. Furthermore, compared to the *B. subtilis* procedure realised in 1996 by Vanloon[23], the process used 25% more energy. Therefore, the switch to a biotechnical approach, with *B. subtilis*, to replace the chemical process was proposed in 2000. One of the primary reasons being that the organism had a large number of genetic tools that could be employed, making it an extremely efficient workhorse involving genetic engineering[9].

Today, there is a multitude of industrial producers that have been genetically altered specifically to produce riboflavin. Different species have been included in Table 2.1. They are represented with their associated riboflavin titer, the carbon source with the given amount, and the time interval set for riboflavin production[10]. When evaluating the total riboflavin titer for the different microorganisms, the distinction of carbon source amount coupled with the production time used should be considered.

Table 2.1: Distinct industrial producer genetically modified and utilized for the production of riboflavin, with there corresponding riboflavin production titer, carbon source amount and the time interval of production.

Organism	Strain	Carbon source and amount	Time	Titer	Related referance
Bacteria	*C. glutamicum* KCCM11223P	Glucose 1 g	48 h	245 mg/L	Park et al.(2014) [24]
	B. subtilis RH44	Glucose 80 g; Yeast extract 5 g	48 h	16.36 g/L	Wu et al.(2007) [25]
Fungi	*A. gossypii* W 122032	Corn steep liquor 60 g; Gelatin 30 g	9 days	13.7 g/L	Park et al.(2011) [26]
Yeast	*Pichia pastoris* X-33 ScRIB1	Glucose·H_2O 550 g	24-50 h	0.175 g/L	Marx et al.(2008) [27]

2.2 *C. glutamicum* as a microbial host

C. glutamicum was discovered in Japan the year 1965 [11]. Mainly because of its ability to accumulate l-glutamic acid under limiting concentrations of biotin. It is a Gram-positive bacteria with a rod-shaped form, and is represented in Figure 2.3 [28]. Furthermore, *C. glutamicum* is a non-pathogenic bacteria and non spore forming [29].

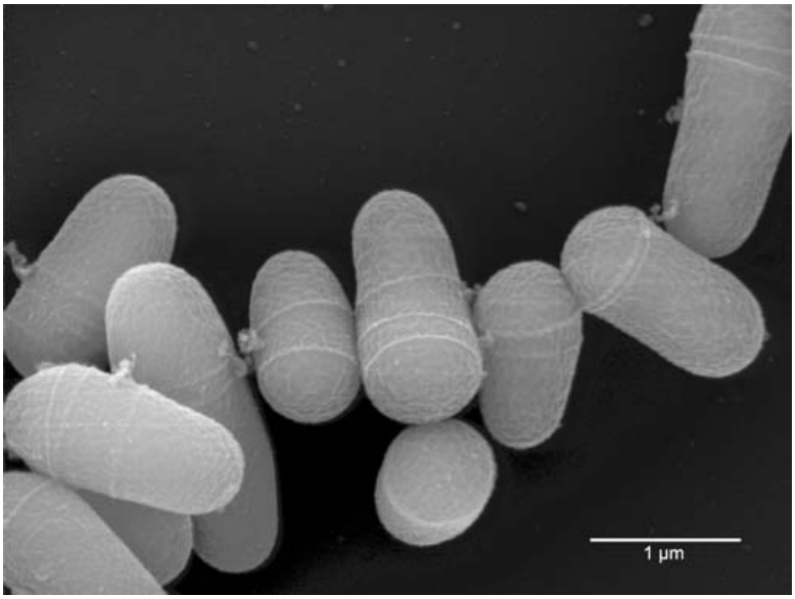

Figure 2.3: Raster electron micrograph depicting *Corynebacterium glutamicum* ATCC 13032 taken from the unpublished results of Krömer, Heinzle and Wittmann 2006 [30] [28].

As a microbial host for industrial purposes and basis research, *C. glutamicum* is beneficial because of its high growth rate, lack of a complex carbon repression regulation, the presence of an extensive genetic toolbox, and ability to achieve high cell density [11] [11] [4] [6]. Among other things, *C. glutamicum* has been the microbial host most often used for the industrial production of amino acids, in particular l-glutamic acid and l-lysine. Additionally, it has been engineered for the production of different added value compounds, such as organic acids, carotenoids and vitamins [4] [5].

2.2.1 Riboflavin biosynthetic pathway in *C. glutamicum*

The riboflavin biosynthetic pathway in *C. glutamicum*, represented in Figure 2.2, is connected with central metabolism pathways. These connections are depicted

in Figure 2.4[31] [15]. Riboflavin synthesis is directly linked to the oxidative phase of the pentose phosphate pathway (PPP) as well as indirectly connected to the non-oxidative PPP through the purin pathway. Both parts of the PPP are connected to the glycolysis, directly and indirectly, inadvertently connecting them to the tricarboxylic acid(TCA) cycle. In other words, the riboflavin biosynthesis is interconnected with the central carbon metabolism, and therefore to the formation of biomass and energy through the electron transport chain.

Genetic modifications to change the carbon flux through the riboflavin production pathway would cause a change in carbon flux through the other main metabolic pathways of the cell, affecting the cell's total energy production and growth rate.

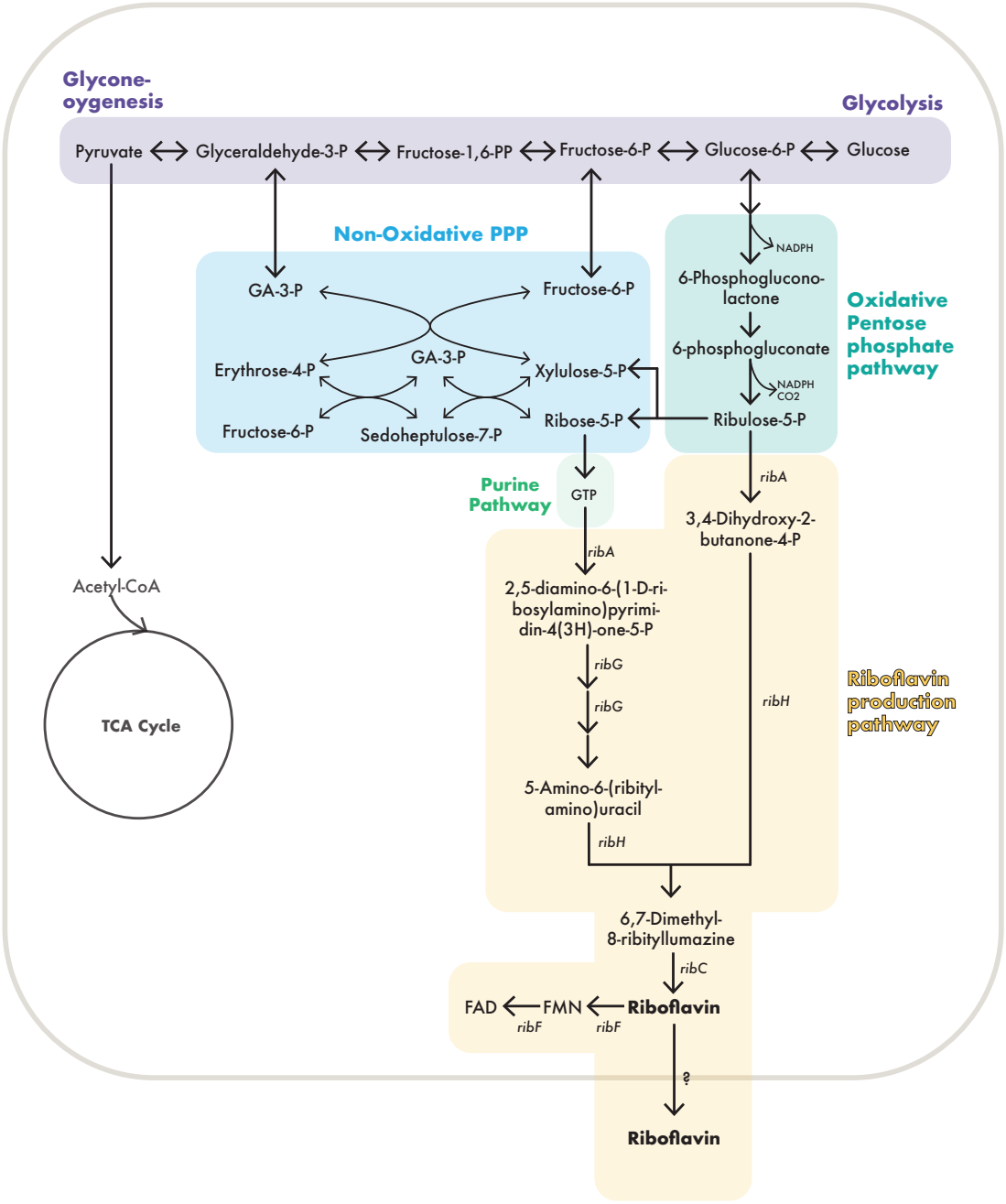

Figure 2.4: The riboflavin synthesis pathway is depicted together with its connections to the primary metabolic pathways of *C. glutamicum*. Ribulose-5-P and GTP function as connecting points. GTP is a product of the purine pathway, which is linked to the non-oxidative PPP. Ribulose-5-P is a product of the oxidative PPP. Distinct colours are used to depict different metabolite routes. The TCA cycle is illustrated in black, while glycolysis is represented in purple. Blue/green and blue depict the oxidative and non-oxidative PPP, respectively. The purin pathway is displayed in green, whereas the riboflavin pathway is yellow. The chemicals in the reactions are written in standard black text, whereas the genes that code for the enzymes used in the various reactions are written in italic.

2.3 *C. glutamicum's* different carbon sources

C. glutamicum has the ability to utilise numerous carbon sources for growth and energy production, where the two most utilised native monosaccharides are glucose and fructose[32]. As shown by Dominguez et al.(1998), *C. glutamicum* has a higher growth rate when utilising glucose as a carbon source compared to fructose[33]. *C. glutamicum* has additionally been successfully modified to use non-native carbon sources[8]. Such carbon sources include mannitol and xylose[34] [35] [36].

Compared to other organisms, *C. glutamicum* has the ability to utilise multiple carbon sources simultaneously[6] [7]. This is caused by it lacking the complex carbon catabolite repression system, that is present in most organisms, such as *E. coli* and *B. subtilis* as shown by for example Görke et al.(2008)[37].

The different carbon source uptake pathways and their connection to the main metabolic pathways in *C. glutamicum* are represented in Figure 2.5[34] [35] [38] [36] [39].

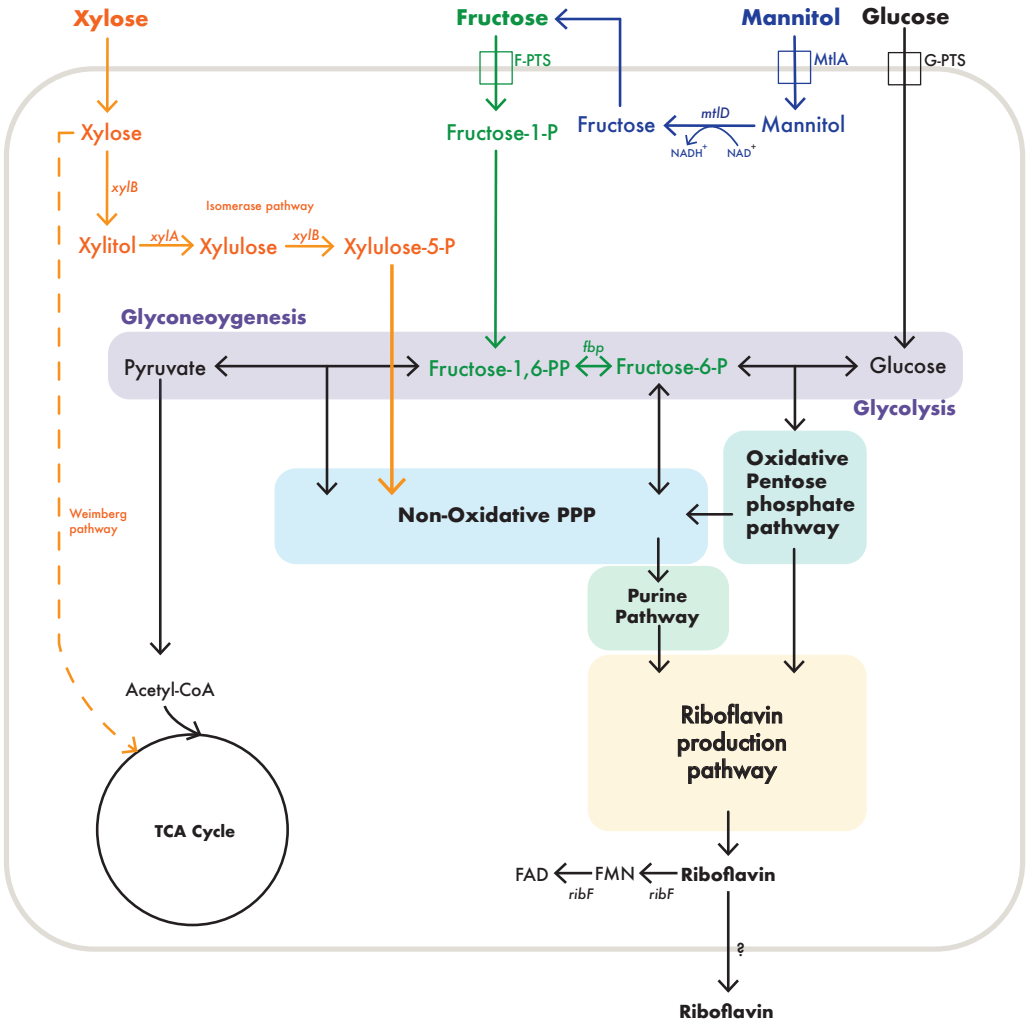

Figure 2.5: The carbon uptake pathway of glucose, mannitol, fructose and xylose are depicted together with their connections to the primary metabolic pathways of *C. glutamicum*. They are illustrated in black, blue, green and orange respectively. The importer proteins for the pathways are represented with boxes. G-PTS, is the glucose specific phosphotranspherase system transporting glucose [32], MtLA is the importer protein for mannitol [35], and F-PTS is the fructose specific phosphotranspherase system transporting fructose into the cell [35]. The chemicals in the reactions are written in standard text, whereas the genes that code for the enzymes used in the various reactions are written in italic. *fbp* codes for the Fructose-1,6-bisphosphatase [40] and effects the flux through glyconeogenesis. *mtlD* codes for the oxidative enzyme mannitol 2-dehydrogenase [34], catalysing the reaction from mannitol to fructose. *xylA* and *xylB* code for xylose isomerase [41] and xylosidase [42] and are the enzymes needed for xylose accumulation.

2.3.1 Fructose

The carbon source pathway for fructose is portrayed in green in Figure 2.5. Fructose enters the cell by utilising the fructose-specific phosphotranspherase system (F-PTS). When transporting fructose, F-PTS phosphorylates the compound into fructose-1-phosphate [35]. The compound enters the glycolysis metabolic pathway and can either be transformed into fructose-6-P or Glyceraldehyde-3-P [38]. Both compounds are further connected to the non-oxidative PPP that correlates with the riboflavin production pathways through the purine pathway.

In connection with the flux through the riboflavin production pathway, a change in the expression of the *fbp* gene from *C. glutamicum* could affect the cell's utilisation of fructose as a carbon source. *fbp* codes for the enzyme Fructose-1,6-bisphosphatase catalysing glyconeogenesis step for transforming fructose-1,6-PP to fructose-6-P [40] [38], and would increase the flux through the PPP and therefore in riboflavin production.

2.3.2 Mannitol

Mannitol is a sugar that can be derived from different alternative carbon sources such as brown seaweed [43]. As a non-native carbon source for *C. glutamicum*, it can only be utilised when it undergoes genetic modifications. MtlA is the importer protein for mannitol [35], importing the sugar in to the cell. The *altR* gene, as shown by Laslo et al.(2012) [34], is the transcription repressor of arabitol utilisation genes, such as the *mtlD* and *mtlA* genes. When arabitol is present in the medium, the protein AltR stops repressing these genes. Mannitol and arabitol are sugars that share similar chemical structure and, hence the arabitol utilization genes act with mannitol as well. *mtlD* codes for mannitol 2-dehydrogenase, which is an enzyme catalysing the oxidisation reaction from mannitol to fructose. When the *altR* gene is deleted, the *mtlD* and *mtlA* genes are transcribed enabling arabitol and mannitol consumption by *C. glutamicum*. The pathway is represented in blue in Figure 2.5. For the produced fructose molecule to be phosphorylated, it is transported out of the cell and then transported back in through the F-PTS [35]. The uptake of mannitol further follows the same pathway as the carbon source path for fructose, as explained earlier.

2.3.3 Xylose

The sugar xylose is a derivative from lignocellulose, and is a non native carbon source for *C. glutamicum*. It can be consumed by the cell if it is genetically modified with the genes *xylA* and *xylB* from *Xanthomonas campestris* and *C.glutamicum* respectively [44]. The pathway is represented in orange in Figure 2.5. The genes encode respectively for the enzymes xylose isomerase [41] and xylosidase [42] [36]. They are catalysts for the reactions in the isomerase pathway that produces xylulose-5-P, which is, in turn, the connection point to the cell's metabolic pathways [39]. This through the non-oxidative PPP. When imported into the cell, xylose can have an additional pathway, the Weimberg pathway, connected to the cell's TCA cycle [39]. Overexpressing *xylAB* enables utilisation of xylose as a carbon source by *C. glutamicum* and, in turn, the production of riboflavin.

3 | Objectives of the Thesis

The main objective of the master thesis is to continue the analysis of the strain *C. glutamicum*(pECXT99a-*riboCg*), produced in the specialisation project, and the effect different carbon sources could have on the flux through the central metabolic pathways of the strain, affecting the growth rate and riboflavin production. Both native and non-native carbon sources were to be utilised, comparing the primary carbon source, glucose, with the effect another carbon source would have alone, but also in combination with glucose.

4 | Material and Methods

The following chapter consists of the earlier work produced, the experimental idea that builds on the earlier work and the materials and methods utilised through the thesis.

4.1 Earlier work

This subchapter will represent a summary of genetic modification and produced strains from earlier work, with the connected growth experiments performed on them.

4.1.1 Strains, vectors and growth experiments performed

During the specialisation project, the vector (pECXT99a) was cloned by utilising Gibson assembly to include the riboflavin biosynthetic operon *ribo Cg*, producing the vector (pECXT99a-*riboCg*). This was then transformed into *C. glutamicum*, creating the strain *C. glutamicum*(pECXT99a-*riboCg*).

Two growth experiments, with the carbon source condition of 0.5 % and 2 % glucose, were performed on the strains *C. glutamicum*(pECXT99a-*riboCg*) and *C. glutamicum*(pECXT99a).

4.2 The main experiment idea for this thesis

The main experimental idea for this thesis was built on the *C. glutamicum*(pECXT99a-*riboCg*) strain, and to further construct strains that would be able to consume non-native carbon sources and have an increased flux through these and the native carbon source pathways. The strains were then analysed through growth experiments to see which combination of carbon source utilisation was most promising for riboflavin production. This information was then used to choose a strain that would be analysed closer by upscaling the fermentation to a bioreactor scale.

4.3 Vectors and strains

Vectors pECXT99a and pVWEx1 were utilised in this project. They are respectively depicted in Figure 4.1a and 4.1b.

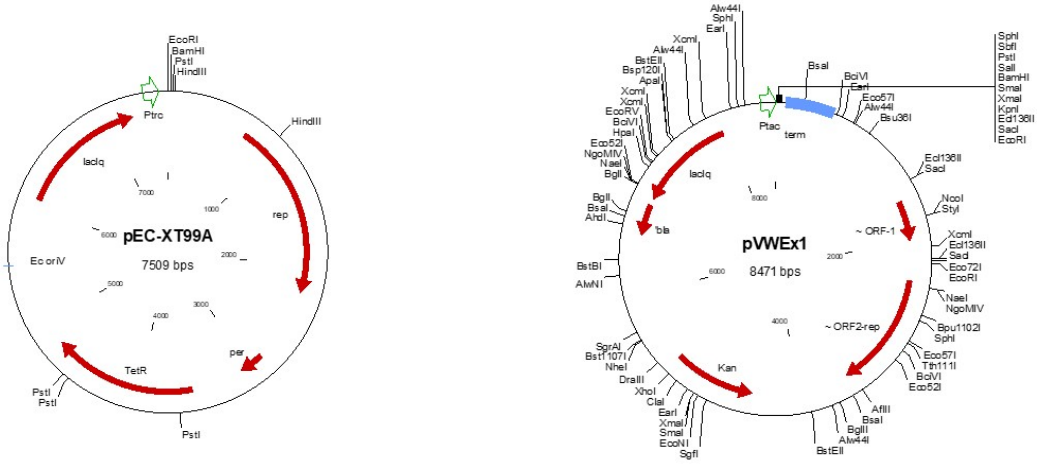

(a) Visualisation of plasmid pECXT99a

(b) Visualisation of plasmid pVWEx1

Figure 4.1: In subfigure (a) and (b) the plasmid pECXT99a and pVWEx1 are respectively depicted. The pECXT99a vector includes a trc-promoter(Ptrc), multiple cloning sites and the gene sequence for Tetracycline resistance. Vector pVWEx1 includes a taq-promoter(Ptaq), multiple cloning sites and the gene sequence coding for Kanamycine resistance.

The vectors used in this work are listed in Table 4.1.

Table 4.1: Vectors utilised in the thesis are represented in this table, including details of their characteristics and source.

Vector	Details	Source
pECXT99a	Tet_R, *C. glutamicum/E. coli* shuttle plasmid(P_{trc}, *lacI*, pGA1, $OriV_{Cg}$)	Kirchner and Tauch 2003 [45]
pECXT99a-*ribo*	Tet_R, pECXT99a vector carrying the biosynthetic operon *riboCg* from *C. glutamicum* [*riboGCAH*]	Bakken 2021 [46]
pVWEx1	Kan_R, *C. glutamicum/E. coli* shuttle plasmid(P_{taq}, *lacI*, pHM1519, $OriV_{Cg}$)	Peters-Wendisch et al.(2001) [47]
pVWEx1-*fbp*	Kan_R, pVWEx1 vector carrying the *fbp* gene from *C. glutamicum*	This work
pSH1	Kan_R, *C. glutamicum/E. coli* shuttle plasmid (P_{tuf}, pHM1519, $OriV_{Cg}$)	Henke et al.(2016) [48]
pSH1-*xylAB*	Kan_R, pSH1 overexpressing *xylA* from *Xanthomonas campestris* and *xylB* from *Corynebacterium glutamicum*	Pérez-García et al.(2021) [44]

Strains utilised in the thesis are represented in Table 4.2. The cloning host utilised was the *E. coli* DH5α. The vectors pVWEx1, pSH1, pSH1-*xyIAB*, where extracted from the existing strains E.coli(pVWEx1), E.coli(pSH1) and E.coli(pSH1-*xyIAB*) respectively. These vectors, including pVWEX1-*fbp* produced in this project, were then transformed into the *C. glutamicum* strain Cg(pECXT99a-*riboCg*). Yielding the strains Cg(pECXT99a-*riboCg*)(pVWEx1), Cg(pECXT99a-*riboCg*)(pVWEx1-*fbp*), Cg(pECXT99a-*riboCg*)(pSH1) and Cg(pECXT99a-*riboCg*)(pSH1-*xylAB*). Furthermore, the vectors pECXT99a and pECXT99a-*riboCg* were extracted and transformed into the *C. glutamicum* strain CgΔ*altR*. Yielding the strains CgΔ*altR*(pECXT99a) and CgΔ*altR*(pECXT99a-*riboCg*) .

Table 4.2: Strains utilised in the thesis are represented in this table, with details of their characteristics and source.

Strain	Details	Source
Escherichia coli DH5α	Δ*lac*U169 (ϕ80*lacZ* ΔM15), *sup*E44, *hsd*R17, *rec*A1, *end*A1, *gyr*A96, *thi*-1, *rel*A1	Hanahan(1983)[49]
Corynebacterium glutamicum	Wild-type strain ATCC 13032, auxotrophic for biotin	Abe(1967)[50]
CgΔ*altR*	*C. glutamicum*Δ*altR*, *C. glutamicum* with a truncated *atlR* gene	Laslo et al.(2012)[51]
Cg(pECXT99a-*riboCg*)(pVWEx1)	*C. glutamicum*(pECXT99a-*riboCg*)(pVWEx1)	This work
Cg(pECXT99a-*riboCg*)(pVWEx1-*fbp*)	*C. glutamicum*(pECXT99a-*riboCg*)(pVWEx1-*fbp*)	This work
Cg(pECXT99a-*riboCg*)(pSH1)	*C. glutamicum*(pECXT99a-*riboCg*)(pSH1)	This work
Cg(pECXT99a-*riboCg*)(pSH1-*xylAB*)	*C. glutamicum*(pECXT99a-*riboCg*)(pSH1-*xylAB*)	This work
CgΔ*altR*(pECXT99a)	*C. glutamicum*ΔaltR(pECXT99a)	This work
CgΔ*altR*(pECXT99a-*riboCg*)	*C. glutamicum*ΔaltR(pECXT99a-*riboCg*)	This work

4.4 Growth conditions

During this project, *E. coli* and *C. glutamicum* were the bacteria utilised. Their optimal growth conditions are respectively at 37[13] and 30[12] degrees celsius. These temperatures were used during the incubation of precultures and during growth fermentations of the different bacterium.

For the cultivation of the precultures, the different bacteria were inoculated with brian heart infusion(BHI) solution or BHI with sorbitol(BHIS) solution, or on agar plates. Liquid solutions were inoculated in shake flasks at 150 rpm. For both cultivation methods, the temperatures were set to the optimal growth temperature of the bacterium. Recipes and procedures for producing BHI, BHIS and selective solid medium are represented in Appendix A.2.1, A.2.2, A.2.4.

Cultivating the main strains of *C. glutamicum* during the growth experiments was done utilising minimal media solution. In Appendix A.4 the specific recipes used during the different experiments are represented. The composition of the minimal media correlates to the different carbon source conditions explained in Section 4.6.

By measuring the Optical Density(OD) values at 600 nm, utilising the spectrophotometer WPA CO 8000 Biowave Cell Density Meter from Biochrom Ltd[52], of the solution during cultivation in the biolector, it was possible to acquire cell growth. The final estimated biomass values given from the biolector were utilised with the final measured OD_{600} values of each sample to calculate a correlation coefficient, which was further used to calculate every OD_{600} value and the correlating growth rates. The calculations form the values given by the biolector experiments are represented in Appendix D, while the results are given in Section 5.2.1. The raw OD_{600} values and calculations for the bioreactor fermentation are represented in Appendix F.1 and F.2, and the results are given in Section 5.4.

Furthermore, the biomass and biomass yield of each strain was calculated utilising the OD_{600} values and a specific correlation factor for the given bacterium. For the particular procedure and calculations, see Appendix D.4 and F.2.4. From personal communication with Dr. Pérez-García, the correlation factor employed for biomass calculations of *C. glutamicum* was set to 0.343.

4.5 Molecular genetic techniques

This Subchapter will include all the molecular genetic techniques utilised for cloning the main strains used in the growth experiments.

4.5.1 Gel electrophoresis

To verify the success of different cloning techniques, gel electrophoresis was performed. More specifically, to verify DNA and plasmid extractions, cut plasmids and DNA, cloning and transformations.

Agarose 0.8% with 20 μL GelRed was the stationary phase of the gel electrophoresis, while Tris-Acetate-EDTA (TAE) buffer was the mobile phase. The conditions were set to 100 V and a run time between 30-37 minutes, depending on the length of the gel. Thermo Scientific™ O'GeneRuler 1 kb DNA Ladder, Ready-to-Use- 250-10,000 bp[53] was the molecular weight size standard used to analyse the appearing bands.

4.5.2 Primers utilised

In Table 4.3 the primers utilised during the thesis are represented. The solutions were resuspended with Mili-Q water to obtain the concentration of 100 μM, before being diluted 1:10.

Table 4.3: The primers used in this thesis, along with their sequence and annealing temperature are represented in this table. The vector overlapping sequence is depicted in black, the ribosomal binding site is represented in red, and the annealing sequence is represented in blue.

Primer name	Sequence	Annealing temperature [C°]
EC Fw	TTTGCGCCGACATCATAACG	53
EC Rv	TACTGCCGCCAGGCAAATTC	
X1Fw	CATCATAACGGTTCTGGC	57
X1Rv	ATCTTCTCTCATCCGCCA	
fbpFw2	GATTACGCCAAGCTTGCATGCCTGCAGGTCGACTCTAGAGGAAAGGAGGCCCTTCAGATGAACCTAAAGAACCCCG	55
fbpRv2	AAACGACGGCCAGTGAATTCGAGCTCGGTACCCGGGGATCTTAGGTCGCGGTGGTGTAGTC	

4.5.3 Plasmid extraction

The procedure for performing plasmid extractions is as follows. *E. coli* strains carrying different plasmids were inoculated overnight at 37 °C, 155 rpm, in 25 mL of BHI solution. 12.5 μL of antibiotics were supplemented to the solution, which antibiotic depended on the plasmids antibiotic resistances. The Plasmid miniprep kit from QIAGEN[54] was then utilised to perform plasmid extraction on the selected strains.

4.5.4 Polymerase chain reaction

Polymerase chain reaction(PCR) is a method used to increase and accumulate different known DNA samples[55] [56]. This method is employed for various purposes; for this thesis, the uses are described further in this Subchapter.

4.5.4.1 High fidelity amplification

For high fidelity amplification of the *fbp* gene from *C. glutamicum*, the protocol for CloneAmp HiFi PCR Premix[57] was utilised. The concentrations and amounts used of the reactants and CloneAmp HiFi PCR premix are given in Table 4.4. The primers utilised where fbpFw2 and fbpRv2, their complete sequence is given in Table 4.3, while the DNA template was from *C. glutamicum*.

With less than 100 ng/μL of the DNA template, the thermal cycle program utilised is represented in Table 4.5. The time interval in step three is dependent on the size of the DNA template used. For the *fbp* DNA fragment, with a length of 1.075 kb, the time interval was set to 5.5 seconds.

Table 4.4: This table shows the correlating concentration and amount of premix, primers, template and Milli-Q water needed for high fidelity PCR. The concentration of the amount extracted is used to compute the amount of template added, which is less than 100 ng/μL.

Reactant	Final Volume	Unit	Final concentration
CloneAmp HiFi PCR Premix	12.5	μL	1x
Primer 1	0.3 - 0.5	μL	0.2-0.3 μM
Primer 2	0.3 - 0.5	μL	0.2-0.3 μM
Template	< 100 / 1	ng / μL	-
Milli-Q water	up to 25	μL	
Total volume	25.0	μL	

Table 4.5: The high fidelity PCR thermal cycle program. The thermal steps are represented with their given temperature, time and the number of cycles the steps should be performed. The last thermal step at 4 °C runs until the samples are retrieved.

Step	Temperature [°C]	Time	Number of cycles
Denaturation	98	10 sec	
Annealing	55	5 or 15 sec	35
Extension	72	5 sec/kb	
Soak	4	∞	1

4.5.4.2 Gibson assembly

Gibson assembly, established by Gibson et al.(2009)[58], is a cloning method that employs the homologous overlapping parts of the DNA molecules for assembly. It is

performed in one single step, making this method more rapid [59], but it also enables the possibility of cloning more than two fragments simultaneously [60], as well as assembling larger fragments than in other techniques.

The procedure for the assembly of the *fbp* fragment from *C. glutamicum* and the vector pVWEx1 was dependent on the concentration, the equimolar mass and the size of each fragment. These values for the vector pVWEx1 and the gene *fbp* are represented in Table 4.6, along with the calculated amounts used for the mixture. The thermal cycle program set for Gibson assembly is at 50 °C for 60 minutes.

Preparatory to using the vector pVWEx1, it was cut using the restriction enzyme BamHi HiFi with a ratio of 1 μL:1 μg respectively of enzyme and vector purified by utilising the PCR product purification protocol from QIAGEN [61].

Table 4.6: This table shows the amount of vector and gene solution used in the Gibson assembly for this project, as well as their concentrations and equimolar mass.

DNA	Size [bp]	Concentration [ng/μL]	Equimolar mass[ng]	Needed volume [μL]
Vector	8471	5.5	90	16.36
Gene	1075	22.8	11.42	0.5

4.5.4.3 Colony PCR

The protocol GoTaq®DNA Polymerase by Promega [62] was used for conducting colony PCR on *E. coli* strains that had been transformed with a possible successful cloned vector. The method for transformation in *E. coli* is given in Section 4.5.6. In Table 4.7 the concentrations and amounts of the reactants used are represented. The upstream and downstream primer utilised for analysing the template DNA are respectively X1Fw and X1Rv, their complete sequences are given in table 4.3. Here, the template DNA is defined as one colony of the transformed *E. coli* strain harbouring a possible successful cloned vector.

The thermal cycle program for colony PCR is represented in Table 4.8. The initial denaturation, final extension and soaking steps are set to run once within a specific timeframe, while the denaturation, annealing and extension steps are set to 35 cycles. The time for the annealing step is furthermore dependent on the DNA template's length. For the *fbp* fragment with a length at about 1.075 kb the extension time was set to 1 minute and 10 seconds. Colony PCR was performed multiple times, increasing the annealing time for every failed attempt, resulting in a final extension time set to 1 minute and 40 seconds.

Table 4.7: This table shows the required concentrations and amounts of PCR nucleotide mix, upstream and downstream primers, DNA polymerase, DNA template, and Milli-Q water for colony PCR. The concentration of the amount extracted is used to compute the amount of template added, which is less than 0.01 μg/μL.

Reactant	Final volume	Unit	Final concentration
5x Green or colorless GoTaq® Reaction Buffer	10	μL	1x
PCR Nucleotide Mix	1	μL	0.2 μM
Upstream primer		μL	0.1-1.0 μM
Downstream primer		μL	0.1-1.0 μM
GoTaq® DNA Polymerase	0.25	μL	1.25u
Template DNA	0.01	μg/μL	-
Milli-Q water	Fill to 50	μL	
Total volume	50	μL	

Table 4.8: The colony PCR thermal cycle method. The thermal steps are represented with their given temperature, time and number of cycles the steps should be performed. The last thermal step at 4 °C is run until the samples are retrieved.

Step	Temperature [°C]	Time[min]	Number of cycles
Initial Denaturation	95	10	1
Denaturation	95	1	
Annealing	42 - 65	1	35
Extension	72	1 min/kb	
Final Extension	72	5	1
Soak	4	∞	1

4.5.5 Production of competent cells

For this project the strains produced into competent cells are Cg(pECXT99a-*riboCg*), E.coli(pECXT99a-*riboCg*) and E.coli(pVWEX1-*fbp*). Competent cells from earlier works have also been utilised.

Depending on the bacteria, either the strain were inoculated and incubated overnight in 5 mL of lysogeny broth(LB) or BHI at the optimal growth temperature. 1 mL of overnight culture was then incorporated with 25 mL of BHIS solution, thereupon put back to incubate at optimal growth temperature for 2 to 4 hours or until the OD_{600} value reached 0.6. At this point, 0.75 μL or 15 μL of ampicillin was added, with concentrations respectively at 100 mg/mL or 5 mg/mL. The solution was again placed for incubation at optimal growth temperature, now for 1 to 1.5 hours. The mixture was centrifuged for 7 minutes at 4 °C at 4000 rpm. The pellet was resuspended with 30 mL of Electroporation buffer 1(EPB1) and put on ice for 5 minutes, three times, before being resuspended with Electroporation buffer 2(EPB2). The solution was then distributed to eppendorfs and frozen at -80 °C.

4.5.6 Transformation in *E. coli*

With the solution from Gibson assembly, transformation in *E. coli* was performed on the *E. coli* DH5α strain. Pre-made competent cells of *E. coli* DH5α were defrosted, before being mixed with 10 μL Gibson assembly solution and incubated on ice for 15 minutes. The solution was exposed to a heat shock at 42 °C for 1.5 minutes, thereupon being put back on ice for 60 seconds. 500 μL of LB was then incorporated into the solution, followed by 45 to 60 minutes of incubation at 37 °and 450 rpm. The pellet formed after centrifuging the mixture was thereafter plated on selective medium and cultivated overnight for further use.

4.5.7 Transformation in *C. glutamicum*

After confirming a successful cloning, the modified vector was extracted from *E. coli* and transformed into *C. glutamicum*. The procedure used was as following. The competent cells, when defrosted, were mixed with 300 to 600 ng of the vector DNA, before being electroporated in one single puls at 2.5 kV, 25 Fv and 200 Ω. The solution was mixed with 1 mL 46 °C preheated BHIS medium, thereupon being placed for incubation at 46 °C for 6 minutes and thereafter at 30 °C, at 450 rpm for 1 hour. The solution was plated on selective medium and incubated at *C. glutamicum's* optimal growth temperature overnight.

4.6 Growth Experiments

Three growth experiments utilising a biolector were performed for this project, with results used to determine what strain and conditions used could be upscaled to a bioreactor fermentation. Each experiment included two strains set under three different carbon source conditions. For the biolector fermentation, the specific conditions for the different strains are represented in Table 4.9.

Table 4.9: The different carbon source conditions utilised in the biolector scale fermentation's are represented here with their correlating strains.

Strains	Carbon source 1	Carbon source 2	Carbon source 3
Cg(pECXT99a-*riboCg*)(pVWEx1) Cg(pECXT99a-*riboCg*)(pVWEx1-*fbp*)	Glucose 1%	Gluose 1% + Fructose 1 %	Fructose 1 %
CgΔ*altR*(pECXT99a) CgΔ*altR*(pECXT99a-*riboCg*)	Glucose 1%	Gluose 1% + Mannitol 1 %	Mannitol 1 %
Cg(pECXT99a-*riboCg*)(pSH1) Cg(pECXT99a-*riboCg*)(pSH1-*xylAB*)	Glucose 1%	Gluose 1% + Xylose 1 %	Xylose 1 %

4.6.1 Precultures

The strains for this project were plated on selective media and placed overnight at optimal growth conditions for *C. glutamicum* incubation. These cultures were further utilised for the incubation of the precultures used in the growth experiments. The preculture media consisted of 25 mL 2x Yeast Extract Tryptone (2TY) complex media and 12.5 μL of the corresponding antibiotics the strains are resistant against, mainly Tetracyclin and Kanamycin. The antibiotic stock solutions production methodes are represented in Appendix A.1.5. The precultures were inoculated with one colony of a strain, with three parallels, and incubated in baffled 250 mL shake flasks overnight at optimal growth conditions for *C. glutamicum*.

4.6.2 Washing and inoculation

A consistent start concentration for all samples in growth experiment is preferable. The OD values for each sample were taken with the spectrophotometer WPA CO 8000 Biowave Cell Density Meter from Biochrom Ltd[52] at 600 nm. By utilising the Equation 4.6.1 and the OD_{600} values, the amount of preculture(V_1) needed to reach an OD_{600} approximately set to 1(C_2), in a final volume of 1 mL(V_2), can be calculated.

$$V_1 \cdot C_1 = V_2 \cdot C_2 \tag{4.6.1}$$

The amounts calculated, represented in Table C.28, C.29 and C.30 in Section C, were transferred to eppendorf's and centrifuged for 1 minute at 13 500 rpm. Dis-

carding the supernatant, the pellet could be resuspended and washed with salt solution(CGXII) before being centrifuged again for 1 minute at 13 500 rpm. The supernatant was discarded, and the pellet was resuspended with minimal media, including the different concentrations of carbon sources. Procedures for CGXII and minimal media solutions are represented in Section A.3.1 and A.4 respectively.

4.6.3 Biolector

The solutions consisting of minimal media with different carbon source conditions and different strains, were then transferred to one well each in the Biolector Plate from m2p Labs[63] in a sterile environment. The plate was closed with a spesific sealing foil from m2p Labs[64] and placed in the Biolector Pro machine[65].

Each experiment was performed with the conditions at the optimal growth temperature of 30 °C for *C. glutamicum* and 1100 rpm. The program used for sampling estimated biomass values was set to take measurements every 20 minutes of each sample over 25 hours. These results were then extracted and utilised for the calculations of the OD_{600} values, the calculations are shown in Appendix D.1 and D.2. The calculated average OD_{600} values for each strain in each condition, with their correlating deviation factors, are represented in Table 5.1, 5.2 and 5.3.

4.6.4 Bioreactor conditions

The Cg(pECXT99a-*riboCg*)(pSH1-*xylAB*) strain was analysed further under the xylose 1 % carbons source condition in a 3.6 L baffled bioreactor. An Applikon glass bioreactor[66] system was used here, and a stirrer with six blades was placed. The stirring speed was automatically controlled and was set to establish a constant 30% oxygen percentage in the medium. The temperature was set to *C. glutamicum's* optimal growth temperature at 30 °celsius and automatically maintained. To maintain a constant pH of 7.0, the system used 10 % phosphoric acid(P_3HO_4) and 5M potassium hydroxide(KOH) for stabilisation, recipes given in Appendix B.3. Air was constantly applied at a rate of 750 ml/min. When needed, antifoam[67] was added to the system.

The initial volume of 500 mL minimal media, recipe given in Appendix B.1, was to be inoculated with a preculture that had incubated overnight in 2TY medium to achieve an initial OD_{600} value of 1. Because of the Cg(pECXT99a-*riboCg*)(pSH1-*xylAB*) strains low growth rate, this was not possible to accomplish. The initial OD_{600} value was 0.12. Sampling was performed over 48 hours. After 48 hours, a constant 0.7 ml/min of feeding solution with 5 % xylose was started. The formula is given in Appendix B.2. Over the next 24 hour period, 7 more samples were taken. The OD_{600} values for each sample taken were found and are represented in Appendix F.1.

4.6.5 High-performance liquid chromatography

High-performance liquid chromatography (HPLC) was utilised to quantify the amount of extracellular riboflavin in every fermentation solution and the amount of xylose in the solution through the bioreactor fermentation. The procedure consists of separation, identification, and quantitative measurements of the chemicals present [68]. The compounds are then distinguished by the different retention times, specifically found by utilising standards of the compounds.

4.6.5.1 Preparation of sample

The preparation of riboflavin samples for HPLC analysis is contingent on Petteys et al.(2011) [69]. Frozen samples were firstly defrosted before 500μL of each sample was transferred to sterile eppendorf's. 1 mL with 15 % Trichloroacetic acid(TCA) was mixed in before gently agitating the mixture for 1 minute. The mixed samples were incubated in the dark for 20 minutes at 25°C, before being centrifuged for 20 minutes at 7830 rpm at 4°C. 150μL of 2 M Tripotassium phosphate(K_3PO_4) was added to HPLC vials, and mixed with 1 mL of the sample centrifugate. After being vortexed, the samples are ready for the HPLC analysis.

Xylose samples were prepared by diluting them 1:10 with Mili-Q water, and placing them in HPLC vials.

4.6.5.2 HPLC set-up

As shown in Petteys et al.(2011) [69], riboflavin is a compound that can be distinguished by fluorometric detection. Therefore the fluorescence detector 2475 FLR Detector from Waters [70] was utilised, with excitation and emission wavelengths at 370 nm and 520 nm, respectively. The column used in the system was Symmetry ®C18 3.5 μm (4.6x75 mm) column [71], with a flow rate set to 0.8 mL/min. A mixture of pH six 5mM ammonium acetate and methanol was used for the mobile phase, proportioned at 1:3.

Xylose was analyzed with a Hi-Plex column [72] and the refractive index detector shodex [73]. As mobile phase, 5 mM sulfuric acid was used in isocratic mode at a flow rate of 0.6 mL/min.

5 | Results

This Chapter consists of the results achieved and calculated through the thesis. Separating between the accomplished construction of new *C.glutamicum* strains, the results from the fermentation experiments done at biolector scale, the HPLC analysis and the bioprocess fermentation performed.

5.1 Construction of new *C. glutamicum* strains to expand to substrate spectrum

The cloning, of the BamHI predigested vector pVWEx1 and the *fbp* gene from *C. glutamicum*, was successful through Gibson assembly. This vector, including the correlating empty vector pVWEx1, the pSH1-*xylAB* vector, and its correlating empty vector pSH1, were then transformed with the competent cell strain Cg(pECXT99a-*riboCg*) produced in the specialisation project "Riboflavin production from genetically modified *Corynebacterium glutamicum*". Resulting in the Cg(pECXT99a-*riboCg*)(pVWEx1-*fbp*), Cg(pECXT99a-*riboCg*)(pVWEx1), Cg(pECXT99a-*riboCg*)(pSH1-*xylAB*) and Cg(pECXT99a-*riboCg*)(pSH1) strains.

Furthermore the the complete cloned vector pECXT99a-*riboCg* and the correlating empty vector pVWEx1 where transformed with the delition strain CgΔ*altR*, yielding in the strains CgΔ*altR*(pECXT99a-*riboCg*) and CgΔ*altR*(pECXT99a).

5.2 Testing the growth performance of newly constructed strains

As explained in Chapter 4.6, three growth experiments where performed. Firstly on the strains Cg(pECXT99a-*riboCg*)(pVWEx1-*fbp*) and Cg(pECXT99a-*riboCg*)(pVWEx1), for the evaluation of two native carbon sources. As well as the strains CgΔ*altR*(pECXT99a-*riboCg*) and CgΔ*altR*(pECXT99a) , and Cg(pECXT99a-*riboCg*)(pSH1-*xylAB*) and Cg(pECXT99a-*riboCg*)(pSH1) being used for the evaluation of seaweed derived sugars and lignocellulosic sugars respectively.

The growth rates [h^{-1}] for the experiments were found by plotting the OD_{600} values calculated and measured against the time interval of the exponential phase of the

experiments and performing a logarithmic transformation of the values. The specific method and growth equations are given in Appendix D.3. The values were utilised to calculate the average and standard deviation for each strain in different conditions, resulting in the Figures represented further in this Chapter. The Biomass and biomass yield was additionally calculated, with specific calculations and methods in Appendix D.4.

5.2.1 Evaluation of alternative carbon sources

A correlation factor was calculated to utilise the estimated biomass measurements taken every 20 min over 25 hours. This was done using the last measured values and the correlating final OD_{600} values. The method and specific values are represented in Appendix D.1. The average OD_{600} values for the parallels were calculated along with the standard deviations. Calculations are given in Appendix D.2. For each biolector experiment, three plots have been produced connected to the different carbon source conditions. They contain the two strains set under the same condition, with their average OD_{600} values and their correlating standard deviations plotted against the fermentation time. They are represented in the following subchapters.

5.2.1.1 Evaluation of the two native carbon sources glucose and fructose

As explained in Chapter 4.6, the growth experiments for strains Cg(pECXT99a-*riboCg*)(pVWEx1) and Cg(pECXT99a-*riboCg*)(pVWEx1-*fbp*) had carbon sources set to 1 % glucose, a mixture of 1% glucose and 1% fructose, and 1 % fructose. The plot for their average OD_{600} values for both strains in each condition is represented in Subfigures 5.1a, 5.1b and 5.1c respectively. The correlating standard deviations values are expressed as error bar lengths protruding from each point. The parallels of this experiment are biological replicates. Because of technical fluctuations during the experiment, parallel 1 for both strains with 1% glucose was excluded during further calculations. For the two other carbon source conditions, parallel 3 of the Cg(pECXT99a-*riboCg*)(pVWEx1-*fbp*) strain was excluded due to inconclusive data most likely derived from technical fluctuations.

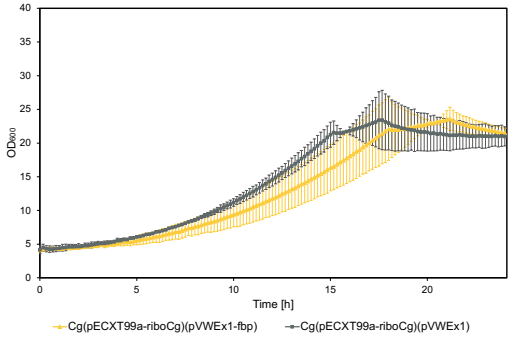

(a) The growth curves for the strains cultivated with a carbon source of 1% glucose.

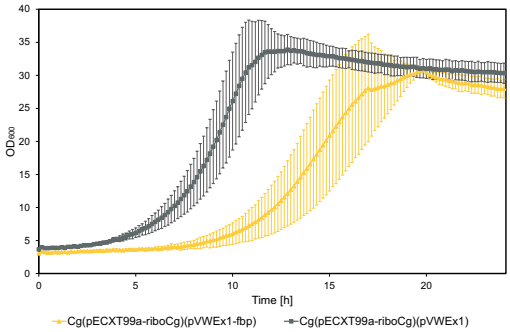

(b) The growth curves for the strains cultivated with a carbon source mixture of 1% glucose and 1% fructose.

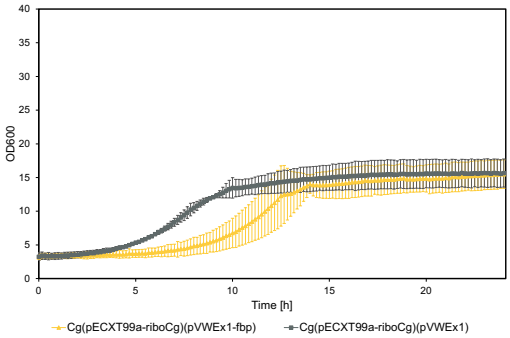

(c) The growth curves for the strains cultivated with a carbon source of 1% fructose.

Figure 5.1: The average growth curves are represented here for the strains Cg(pECXT99a-*riboCg*)(pVWEx1-*fbp*) and Cg(pECXT99a-*riboCg*)(pVWEx1) in the three different carbon source conditions. Cg(pECXT99a-*riboCg*)(pVWEx1) is represented by the grey line with square points, whereas the yellow line with triangle points depicts the Cg(pECXT99a-*riboCg*)(pVWEx1-*fbp*) strains values. The standard deviation values are expressed as the error bars protruding from each point.

The growth rate [h^{-1}] for each growth curve's exponential phases were found. For the Cg(pECXT99a-*riboCg*)(pVWEx1-*fbp*) and Cg(pECXT99a-*riboCg*)(pVWEx1) strains, the growth rates are represented in Table 5.1, along with the correlating biomass and biomass yields. The calculations are given in Appendix D.3.1 and D.4.

Table 5.1: Strains Cg(pECXT99a-*riboCg*)(pVWEx1) and Cg(pECXT99a-*riboCg*)(pVWEx1-*fbp*) and their respective carbon sources represent with the average growth rate, OD_{600} values, biomass and biomass yield values, including the correlating standard deviations.

Carbon source	Amount	Strain	Growth rate [/h]	OD	Biomass [g/L]	Biomass yield [g/g]
Glucose	1%	Cg(pECXT99a-*riboCg*)(pVWEx1-*fbp*)	0.21 ± 0.01	21.50 ± 0.71	7.37 ± 0.24	0.74 ± 0.02
		Cg(pECXT99a-*riboCg*)(pVWEx1)	0.25 ± 0.02	21.00 ± 1.41	7.20 ± 0.49	0.72 ± 0.05
Glucose + Fructose	1% + 1%	Cg(pECXT99a-*riboCg*)(pVWEx1-*fbp*)	0.534 ± 0.047	28.00 ± 1.41	9.60 ± 0.49	0.48 ± 0.02
		Cg(pECXT99a-*riboCg*)(pVWEx1)	0.631 ± 0.037	30.33 ± 1.53	10.40 ± 0.52	0.52 ± 0.03
Fructose	1%	Cg(pECXT99a-*riboCg*)(pVWEx1-*fbp*)	0.490 ± 0.011	15.50 ± 2.12	5.32 ± 0.73	0.53 ± 0.07
		Cg(pECXT99a-*riboCg*)(pVWEx1)	0.488 ± 0.040	15.67 ± 2.08	5.37 ± 0.71	0.54 ± 0.07

The average growth rates, biomass and biomass yield values for the strains Cg(pECXT99a-*riboCg*)(pVWEx1-*fbp*) and Cg(pECXT99a-*riboCg*)(pVWEx1) in different conditions are visualised in Figure 5.2. The correlating standard deviation values are represented as error bars protruding from each point.

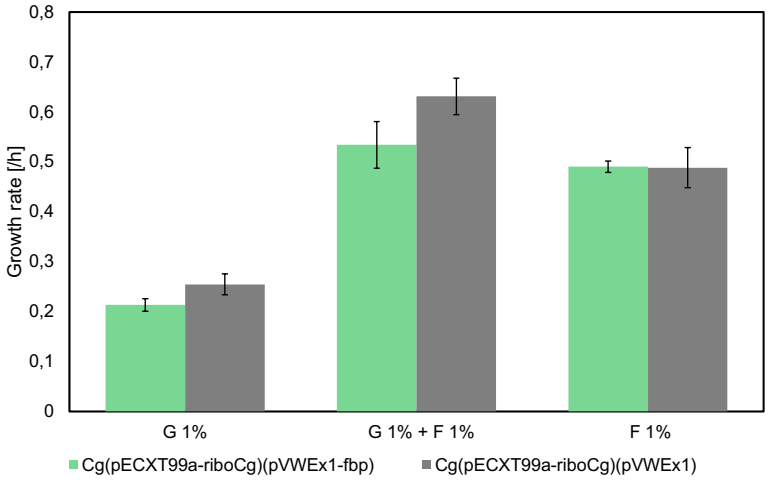

(a) Growth rates

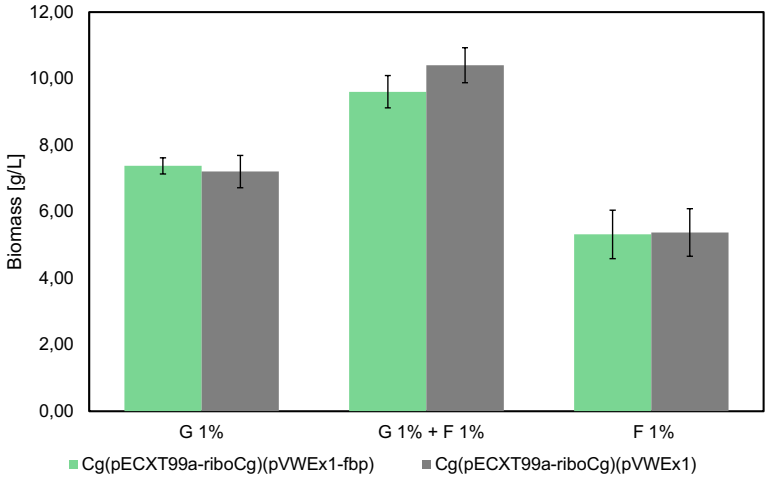

(b) Biomass values

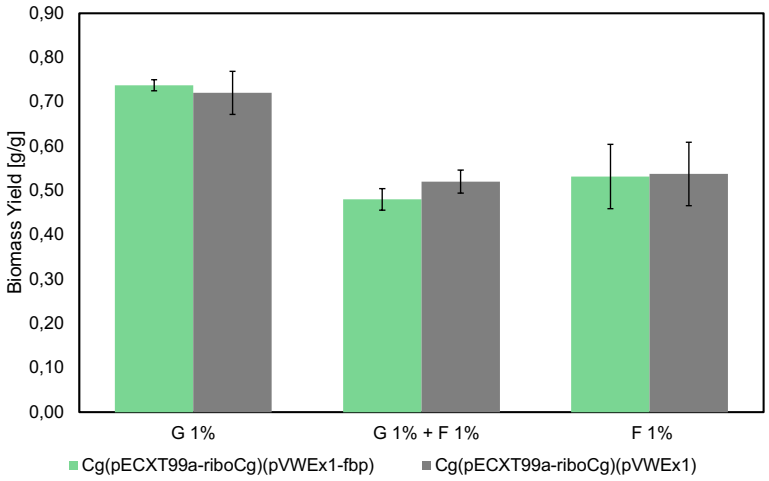

(c) Biomass yield

Figure 5.2: The average growth rates, biomass values and biomass yield values for the strains Cg(pECXT99a-*riboCg*)(pVWEx1-*fbp*) and Cg(pECXT99a-*riboCg*)(pVWEx1) incubated in different carbon source conditions is represented in these subfigures. Their correlating standard deviation values protrude from each point as error bars. The strains are represented in green and grey respectively for the three carbon source conditions. With 1% glucose to the left, a mixture of 1% glucose and 1% fructose in the middle, and 1% fructose on the left of the diagram as the given carbon sources.

5.2.1.2 Evaluation of the seaweed-derived sugar mannitol

For the strains CgΔ*altR*(pECXT99a-*riboCg*) and CgΔ*altR*(pECXT99a), the carbon sources conditions were set to 1 % glucose, a mixture of 1% glucose and 1% mannitol, and 1 % mannitol. The plot for their average OD_{600} values for both strains in each condition is represented in Subfigures 5.3a, 5.3b and 5.3c respectively. The correlating standard deviations values are expressed as error bar lengths protruding from each point. The parallels of this experiment are technical replicates. Due to inconclusive data most likely derived from technical fluctuations during the experiment, parallel 1 for both strains with 1% glucose as carbon source and a mix of 1% glucose and 1% mannitol was excluded during further calculations.

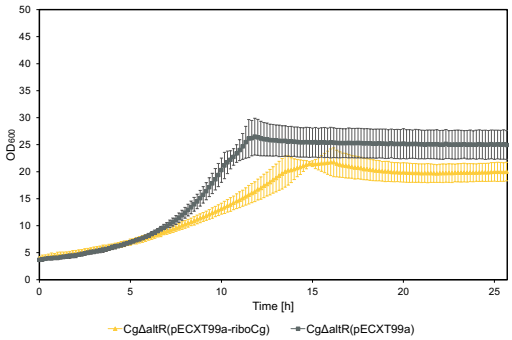

(a) The growth curves for the strains cultivated with a carbon source of 1% glucose.

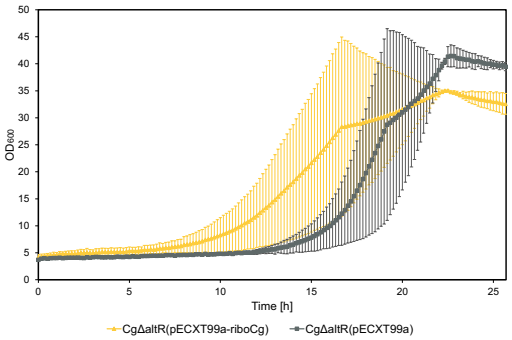

(b) The growth curves for the strains cultivated with a carbon source mixture of 1% glucose and 1% mannitol.

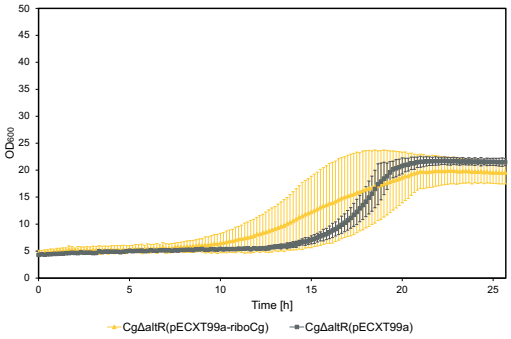

(c) The growth curves for the strains cultivated with a carbon source of 1% mannitol.

Figure 5.3: The average growth curves are represented here for the strains CgΔ*altR*(pECXT99a-*riboCg*) and CgΔ*altR*(pECXT99a) in the three different carbon source conditions. CgΔ*altR*(pECXT99a) is represented by the grey line with square points, whereas the yellow line with triangle points depicts the CgΔ*altR*(pECXT99a-*riboCg*) strains values. The standard deviation values are expressed as the error bars protruding from each point.

From each of the growth curve's exponential phases, the growth rates for the CgΔ*altR* (pECXT99a-*riboCg*) and CgΔ*altR*(pECXT99a) strains were found. The values are represented in Table 5.2, with their connecting biomass and biomass yields values and correlating standard deviations. The calculations are described in Appendix D.3.2 and D.4.

Table 5.2: Strains CgΔ*altR*(pECXT99a) and CgΔ*altR*(pECXT99a-*riboCg*) and their respective carbon sources represent with the average growth rates, OD_{600} values, biomass and biomass yield values, including the correlating standard deviations.

Carbon source	Amount	Strain	Growth rate [/h]	OD_{600}	Biomass [g/L]	Biomass yield [g/g]
Glucose	1%	CgΔ*altR*(pECXT99a-*riboCg*)	0.24 ± 0.03	20.00 ± 1.73	6.86 ± 0.59	0.69 ± 0.06
		CgΔ*altR*(pECXT99a)	0.49 ± 0.02	25.00 ± 2.65	8.58 ± 0.91	0.86 ± 0.09
Glucose + Mannitol	1% + 1%	CgΔ*altR*(pECXT99a-*riboCg*)	0.36 ± 0.09	32.50 ± 2.12	11.15 ± 0.73	0.56 ± 0.04
		CgΔ*altR*(pECXT99a)	0.66 ± 0.11	39.50 ± 0.71	13.55 ± 0.24	0.68 ± 0.01
Mannitol	1%	CgΔ*altR*(pECXT99a-*riboCg*)	0.32 ± 0.04	19.50 ± 2.12	6.69 ± 0.73	0.67 ± 0.07
		CgΔ*altR*(pECXT99a)	0.58 ± 0.02	21.50 ± 0.71	7.37 ± 0.24	0.74 ± 0.02

The average growth rates, biomass and biomass yield values for the strains CgΔ*altR* (pECXT99a-*riboCg*) and CgΔ*altR*(pECXT99a) in different conditions are visualised in Figure 5.4. The correlating standard deviation values are represented as error bars protruding from each point.

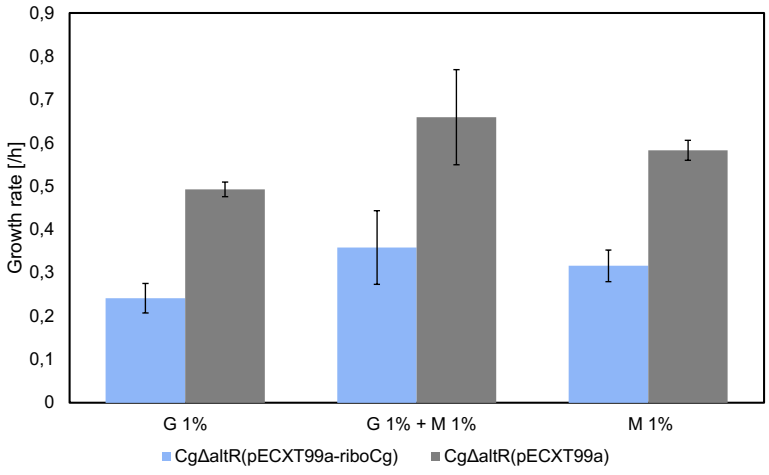

(a) Growth rates

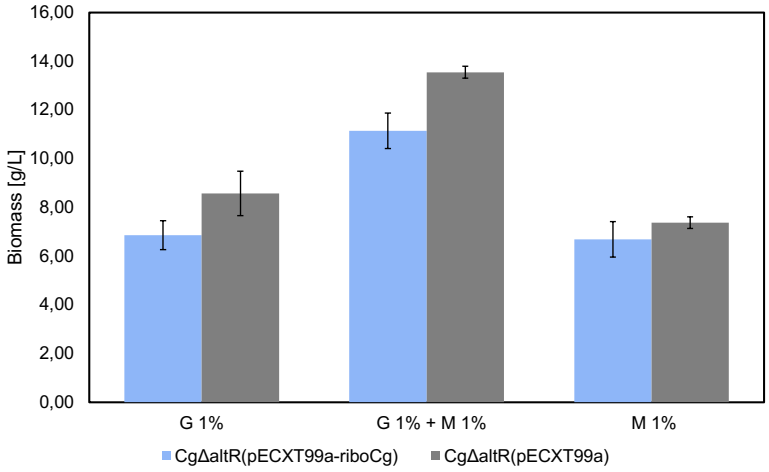

(b) Biomass values

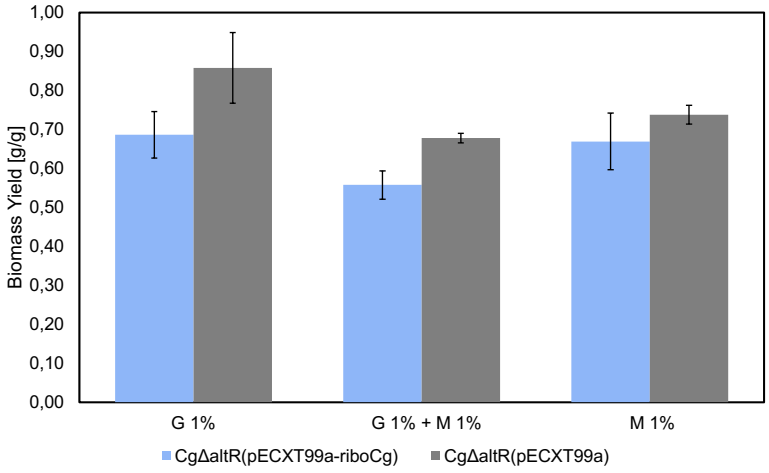

(c) Biomass yield

Figure 5.4: The average growth rates, biomass values and biomass yield values for the strains CgΔ*altR*(pECXT99a-*riboCg*) and CgΔ*altR*(pECXT99a) incubated in different carbon source conditions are represented in these subfigures, with their correlating standard deviation values protruding out from each point as error bars. The strains are represented in blue and grey respectively for the three carbon source conditions. With 1% glucose to the left, a mixture of 1% glucose and 1% mannitol in the middle, and 1% mannitol on the left of the diagram as the given carbon sources.

5.2.1.3 Evaluation of the lignocellulosic sugar xylose

Strains Cg(pECXT99a-*riboCg*)(pSH1-*xylAB*) and Cg(pECXT99a-*riboCg*)(pSH1), were set with carbon sources conditions 1% glucose, a mixture of 1% glucose and 1% xylose, and 1% xylose. The plot for their average OD_{600} values for both strains in each condition is represented in Subfigures 5.5a, 5.5b and 5.5c respectively. The correlating standard deviations values are expressed as error bar lengths protruding from each point. The parallels of this experiment are technical replicates. Due to inconclusive data most likely derived from technical fluctuations during the experiment, parallel 1 for both strains with the carbon source mix of 1% glucose and 1% xylose was excluded during further calculations. For the carbon source condition with only xylose, the parallels 1 and 2 for the Cg(pECXT99a-*riboCg*)(pSH1-*xylAB*) strain have been excluded for further calculations for due to inconclusive data.

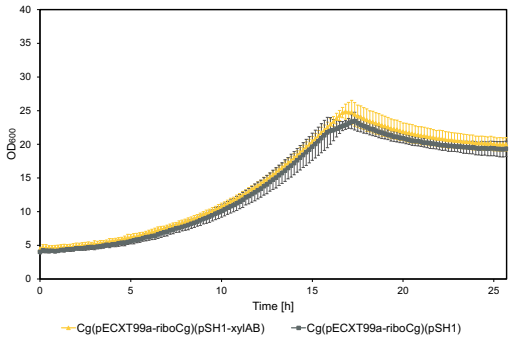

(a) The growth curves for the strains cultivated with a carbon source of 1% glucose.

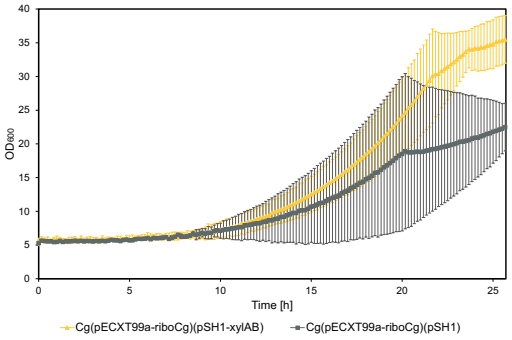

(b) The growth curves for the strains cultivated with a carbon source mixture of 1% glucose and 1% xylose.

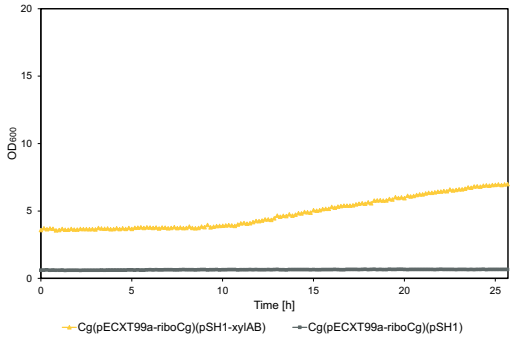

(c) The growth curves for the strains cultivated with a carbon source of 1% xylose.

Figure 5.5: The average growth curves are represented here for the strains Cg(pECXT99a-*riboCg*)(pSH1-*xylAB*) and Cg(pECXT99a-*riboCg*)(pSH1) in the three different carbon source conditions. Cg(pECXT99a-*riboCg*)(pSH1) is represented by the grey line with square points, whereas the yellow line with triangle points gives Cg(pECXT99a-*riboCg*)(pSH1-*xylAB*). The standard deviation values are expressed as the error bars protruding from each point.

From each of the strain's growth curve's exponential phases, the growth rates were found, the values represented in Table 5.3. Furthermore, the biomass and biomass yield values were calculated, also described in Table 5.3, with each correlating standard deviation. The calculations are further represented in Appendix D.3.3 and D.4.

Table 5.3: Strains Cg(pECXT99a-*riboCg*)(pSH1-*xylAB*) and Cg(pECXT99a-*riboCg*)(pSH1) and their respective carbon sources represent with the average growth rates, OD_{600} values, biomass and biomass yield values, including the correlating standard deviations.

Carbon source	Amount	Strain	Growth rate [/h]	OD_{600}	Biomass [g/L]	Biomass yield [g/g]
Glucose	1%	Cg(pECXT99a-*riboCg*)(pSH1-*xylAB*)	0.249 ± 0.003	20.00 ± 1.00	6.86 ± 0.34	0.69 ± 0.03
		Cg(pECXT99a-*riboCg*)(pSH1)	0.263 ± 0.009	19.33 ± 1.15	6.63 ± 0.40	0.66 ± 0.04
Glucose + Xylose	1% + 1%	Cg(pECXT99a-*riboCg*)(pSH1-*xylAB*)	0.258 ± 0.009	35.50 ± 3.54	12.18 ± 1.21	0.61 ± 0.06
		Cg(pECXT99a-*riboCg*)(pSH1)	0.235 ± 0.012	22.50 ± 3.54	7.72 ± 1.21	0.39 ± 0.06
Xylose	1%	Cg(pECXT99a-*riboCg*)(pSH1-*xylAB*)	0.075 ± 0.000	7.00 ± 0.00	2.40 ± 0.00	0.24 ± 0.00
		Cg(pECXT99a-*riboCg*)(pSH1)	0.008 ± 0.0008	0.67 ± 0.06	0.23 ± 0.02	0.02 ± 0.00

The average growth rates, biomass and biomass yield values for the strains Cg(pECXT99a-*riboCg*)(pSH1-*xylAB*) and Cg(pECXT99a-*riboCg*)(pSH1) in different conditions are visualised in Figure 5.6. The correlating standard deviation values are represented as error bars protruding from each point.

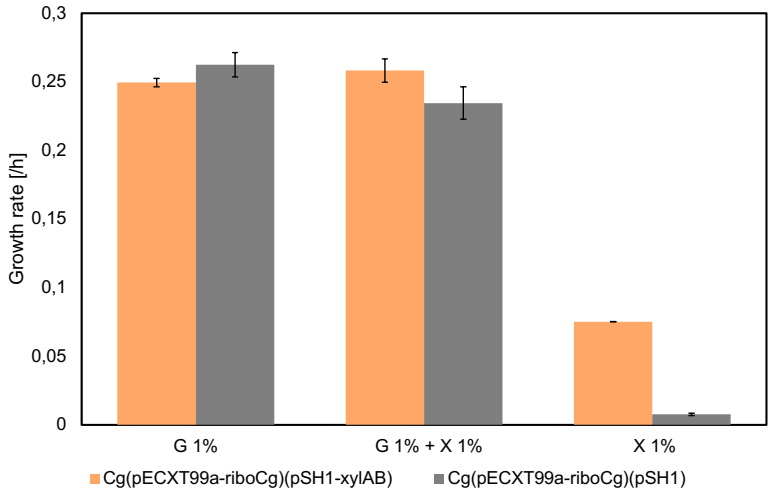

(a) Growth rates

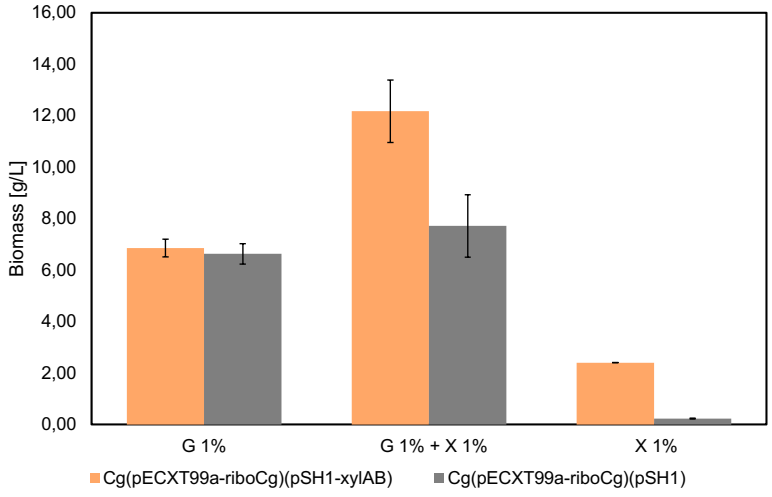

(b) Biomass values

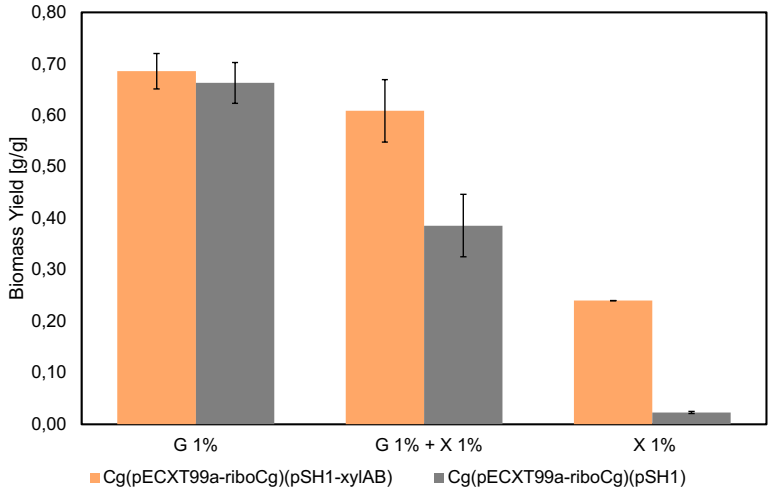

(c) Biomass yield

Figure 5.6: The average growth rates, biomass values and biomass yield values for the strains Cg(pECXT99a-*riboCg*)(pSH1-*xylAB*) and Cg(pECXT99a-*riboCg*)(pSH1) incubated in different carbon source conditions is represented in these subfigures, with their correlating standard deviation values protruding out from each point as error bars. The strains are represented in orange and grey respectively for the three carbon source conditions. With 1% glucose to the left, a mixture of 1% glucose and 1% xylose in the middle, and 1% xylose on the left of the diagram as the given carbon sources.

For the evaluation of the third parallel of the strain Cg(pECXT99a-*riboCg*)(pSH1-*xylAB*) in different conditions, the estimated riboflavin amount produced over time was analysed against the growth curve for the correlating condition. This analysis is represented in Figure 5.7. The figures depict that the growth of the strain is most optimal with both xylose and glucose as a carbon source but has a more extensive lag phase than with just glucose. The growth with only glucose is lower, but both conditions with glucose have a higher value than when the strain only has xylose as sole carbon source. The riboflavin estimated amount for all three conditions results in about the same amount.

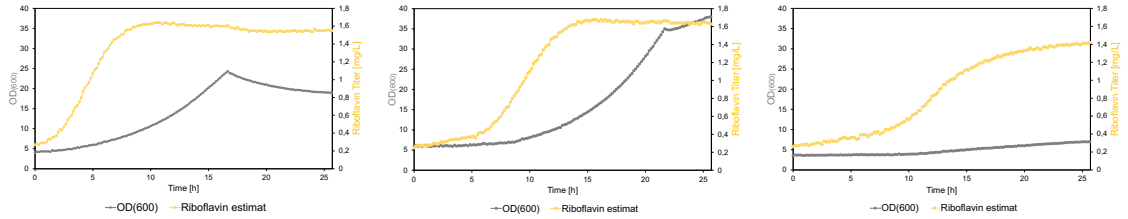

(a) Glucose as carbon source **(b)** Glucose and xylose as carbon sources **(c)** Xylose carbon source

Figure 5.7: A combination plot representing the OD_{600} values and the estimated riboflavin amount over time for the third parallel of strain Cg(pECXT99a-*riboCg*)(pSH1-*xylAB*) is illustrated here. The growth curves are represented in grey lines with round points, while the riboflavin estimated amount is depicted with yellow lines and square points. The left and right y-axis represent the OD_{600} values and the estimated riboflavin production amount for the strain.

5.3 Analysis of carbohydrates and riboflavin

The HPLC was used to analyse the amount of two compounds, the product riboflavin and the carbon source xylose. The retention time of riboflavin and xylose was found to be 4.2 minutes and 10.39 minutes, respectively, and is done by analysing standards for the two components. The standard curves and values are represented in Appendix E.1.

5.3.1 Evaluation of the product riboflavin from alternative carbon sources

One of the final parallel samples in each carbon source condition was analysed for the product riboflavin by HPLC analysis from the strains evaluated with alternative carbon sources. The retention time and height of the peak for each sample are represented in Table5.4.

Table 5.4: The retention time and height found for one of the parallels of the strains Cg(pECXT99a-*riboCg*)(pVWEx1-*fbp*), CgΔ*altR*(pECXT99a-*riboCg*) and Cg(pECXT99a-*riboCg*)(pSH1-*xylAB*), with their correlating carbon source are represented here.

Strain	Carbon source	Sample nr.	Retention time [min]	Height of peak
Cg(pECXT99a-*riboCg*)(pVWEx1-*fbp*)	Glucose 1%	2	4.252	30240709
	Glucose 1% + Fructose 1 %	1	4.274	20648237
	Fructose 1 %	2	4.257	13806302
CgΔ*altR*(pECXT99a-*riboCg*)	Glucose 1%	3	4.283	30072488
	Glucose 1% + Mannitol 1 %	2	4.303	42372466
	Mannitol 1 %	3	4.294	17264714
Cg(pECXT99a-*riboCg*)(pSH1-*xylAB*)	Glucose 1%	3	4.314	33978187
	Glucose 1% + Xylose 1 %	1	4.320	11216126
	Xylose 1 %	3	4.314	11566446

The height values were further used to calculate a correlation factor for each experiment, explained further in Appendix E.2.1. An estimated amount of riboflavin concentration was given through the growth experiments. With the already calculated correlation factors, the height values over time for each sample could then be calculated. The method and calculations are represented in Appendix E.2.1. The final riboflavin titer [g/L], product yield[g/g] and volumetric productivity[g/Lh] (Vol. productivity) for the different strains in different conditions could then be calculated and are represented in Table 5.5, with their correlating standard deviations.

Table 5.5: The average riboflavin titer, product yield and Vol. productivity values, with their correlating standard deviations for each strain in different carbon sources, are represented in this Table. G, F, M and X stands for glucose, fructose, mannitol and xylose.

Carbon source	Amount [g/L]	Strain	Riboflavin Titer [g/L]	Product Yield [g/g]	Vol. Productivity [g/Lh]
G	10	Cg(pECXT99a-*riboCg*)(pVWEx1-*fbp*)	$0.33 \pm 3.72\ 10^{-3}$	$0.033 \pm 3.72\ 10^{-4}$	$1.39\ 10^{-3} \pm 1.55\ 10^{-5}$
		Cg(pECXT99a-*riboCg*)(pVWEx1)	$0.33 \pm 3.28\ 10^{-3}$	$0.033 \pm 3.28\ 10^{-4}$	$1.36\ 10^{-3} \pm 1.37\ 10^{-5}$
G + F	20	Cg(pECXT99a-*riboCg*)(pVWEx1-*fbp*)	$0.22 \pm 2.17\ 10^{-3}$	$0.011 \pm 1.09\ 10^{-4}$	$4.65\ 10^{-4} \pm 4.52\ 10^{-6}$
		Cg(pECXT99a-*riboCg*)(pVWEx1)	$0.22 \pm 3.83\ 10^{-3}$	$0.011 \pm 1.92\ 10^{-4}$	$4.56\ 10^{-4} \pm 7.98\ 10^{-6}$
F	10	Cg(pECXT99a-*riboCg*)(pVWEx1-*fbp*)	$0.15 \pm 2.06\ 10^{-3}$	$0.015 \pm 2.06\ 10^{-4}$	$6.34\ 10^{-4} \pm 8.57\ 10^{-6}$
		Cg(pECXT99a-*riboCg*)(pVWEx1)	$0.15 \pm 2.14\ 10^{-3}$	$0.015 \pm 2.14\ 10^{-4}$	$6.24\ 10^{-4} \pm 8.92\ 10^{-6}$
G	10	CgΔ*altR*(pECXT99a-*riboCg*)	$0.32 \pm 3.12\ 10^{-3}$	$0.032 \pm 3.12\ 10^{-4}$	$1.35\ 10^{-3} \pm 1.30\ 10^{-5}$
		CgΔ*altR*(pECXT99a)	$0.06 \pm 1.18\ 10^{-3}$	$0.006 \pm 1.18\ 10^{-4}$	$2.58\ 10^{-4} \pm 4.91\ 10^{-6}$
G + M	20	CgΔ*altR*(pECXT99a-*riboCg*)	$0.39 \pm 1.23\ 10^{-1}$	$0.020 \pm 6.16\ 10^{-3}$	$8.20\ 10^{-4} \pm 2.57\ 10^{-4}$
		CgΔ*altR*(pECXT99a)	$0.09 \pm 1.51\ 10^{-3}$	$0.004 \pm 7.56\ 10^{-5}$	$1.84\ 10^{-4} \pm 3.15\ 10^{-6}$
M	10	CgΔ*altR*(pECXT99a-*riboCg*)	$0.18 \pm 5.51\ 10^{-3}$	$0.018 \pm 5.51\ 10^{-4}$	$7.64\ 10^{-4} \pm 2.30\ 10^{-5}$
		CgΔ*altR*(pECXT99a)	$0.04 \pm 6.73\ 10^{-4}$	$0.004 \pm 6.73\ 10^{-5}$	$1.49\ 10^{-4} \pm 2.80\ 10^{-6}$
G	10	Cg(pECXT99a-*riboCg*)(pSH1-*xylAB*)	$0.37 \pm 4.96\ 10^{-3}$	$0.037 \pm 4.96\ 10^{-4}$	$1.45\ 10^{-3} \pm 1.93\ 10^{-5}$
		Cg(pECXT99a-*riboCg*)(pSH1)	$0.37 \pm 1.38\ 10^{-3}$	$0.037 \pm 1.38\ 10^{-4}$	$1.43\ 10^{-3} \pm 5.36\ 10^{-6}$
G + X	20	Cg(pECXT99a-*riboCg*)(pSH1-*xylAB*)	$0.12 \pm 2.50\ 10^{-3}$	$5.95\ 10^{-3} \pm 1.25\ 10^{-4}$	$2.32\ 10^{-4} \pm 4.87\ 10^{-6}$
		Cg(pECXT99a-*riboCg*)(pSH1)	$0.10 \pm 2.46\ 10^{-2}$	$4.99\ 10^{-3} \pm 1.23\ 10^{-3}$	$1.94\ 10^{-4} \pm 4.80\ 10^{-5}$
X	10	Cg(pECXT99a-*riboCg*)(pSH1-*xylAB*)	$0.08 \pm 4.36\ 10^{-2}$	$7.59\ 10^{-3} \pm 4.36\ 10^{-3}$	$2.96\ 10^{-4} \pm 1.70\ 10^{4}$
		Cg(pECXT99a-*riboCg*)(pSH1)	$0.02 \pm 5.11\ 10^{-4}$	$2.42\ 10^{-3} \pm 5.11\ 10^{-5}$	$9.43\ 10^{-5} \pm 1.99\ 10^{-6}$

A visualisation of the the final average riboflavin titer and the correlating standard deviation values for the different conditions in the three experiments are represented in the Figures below. Figure 5.8, represents the titers for the Cg(pECXT99a-*riboCg*)(pVWEx1-*fbp*) and Cg(pECXT99a-*riboCg*)(pVWEx1) strains in different conditions, whereas Figure 5.9 and 5.10, illustrates the titers for strains CgΔ*altR*(pECXT99a-*riboCg*) and CgΔ*altR*(pECXT99a) , and strains Cg(pECXT99a-*riboCg*)(pSH1-*xylAB*) and Cg(pECXT99a-*riboCg*)(pSH1) respectively in their different conditions.

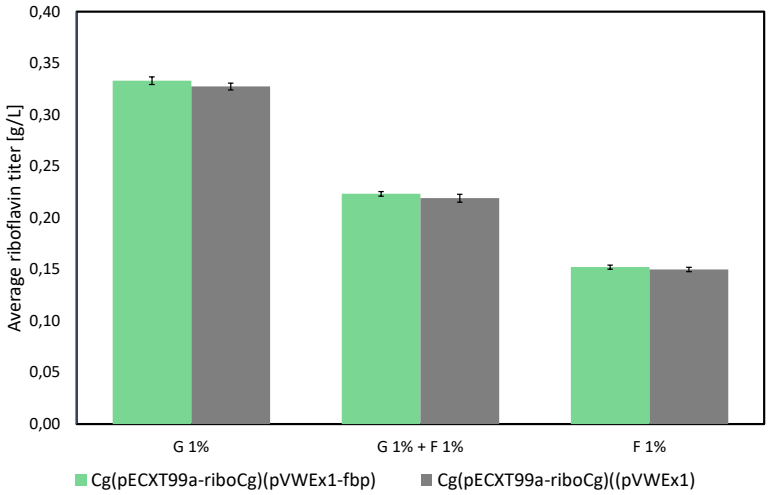

Figure 5.8: The final average riboflavin titer for the strains Cg(pECXT99a-*riboCg*)(pVWEx1-*fbp*) and Cg(pECXT99a-*riboCg*)(pVWEx1) incubated in different carbon source conditions is represented here respectively in green and grey. The titer for the 1% glucose carbon source condition, is represented to the left. With the mixture of 1% glucose and 1% fructose as a carbon source, the titers are given in the middle. At the right, the titer for the strains with 1% fructose as carbon source is represented.

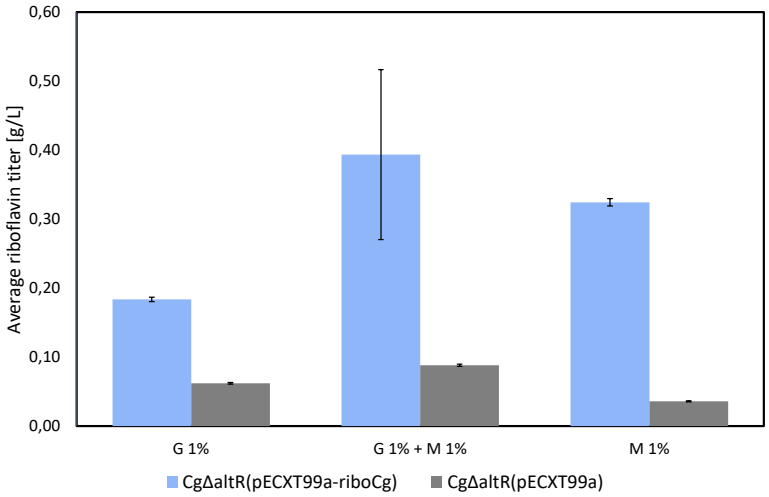

Figure 5.9: The final average riboflavin titer for the strains CgΔ*altR*(pECXT99a-*riboCg*) and CgΔ*altR*(pECXT99a) incubated in different carbon source conditions is represented here with the colors blue and grey respectively. The titer for the carbon source 1% glucose condition, is represented to the left. For the mixture of 1% glucose and 1% mannitol as a carbon source, the titers are given in the middle. At the right, the titer for the strains for the 1% mannitol carbon source condition is represented.

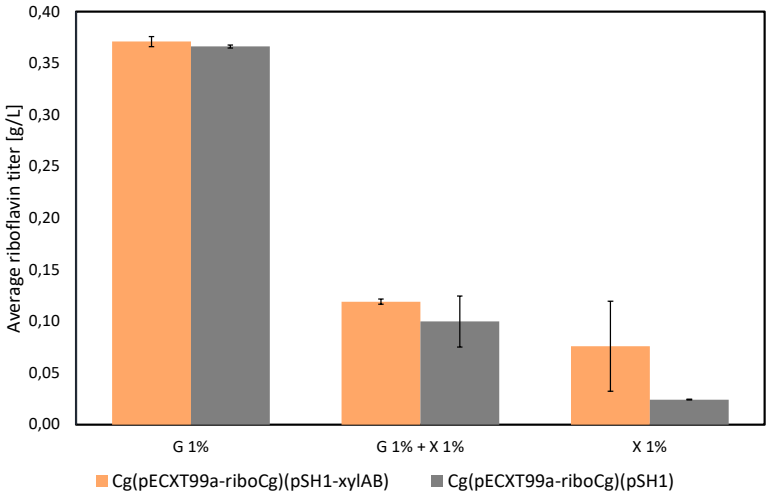

Figure 5.10: The final average riboflavin titer for the strains Cg(pECXT99a-*riboCg*)(pSH1-*xylAB*) and Cg(pECXT99a-*riboCg*)(pSH1) incubated in different carbon source conditions is represented here respectively in orange and grey. The titer for the carbon source 1% glucose condition, to the left, with the mixture of 1% glucose and 1% xylose as a carbon source, the titers are given in the middle, and at the right, titer for the strains with 1% xylose carbon source condition is represented.

5.4 Establishment of a bioprocess in a lab-scale bioreactor using xylose as sole carbon source

The strain Cg(pECXT99a-*riboCg*)(pSH1-*xylAB*) from the growth experiments was analysed in a lab-scale bioreactor, utilising 1 % xylose as the carbon source for the batch phase, adding a feed line, at 48.5 hours, of 5% xylose with a feed rate of 0.7 mL/min for the feeding phase. The OD_{600} values of the fermentation were taken over 72 hours. These values are given in Table F.40, in Appendix F.1, and are plotted against their respective time values in Figure 5.11, showing the growth curve. The fed-batch fermentation is divided into two fragments; in the growth curve the yellow line represents the batch phase from 0 to hour 48.5, and the orange line depicts the growth for the feeding phase from hour 48.5 to hour 72.

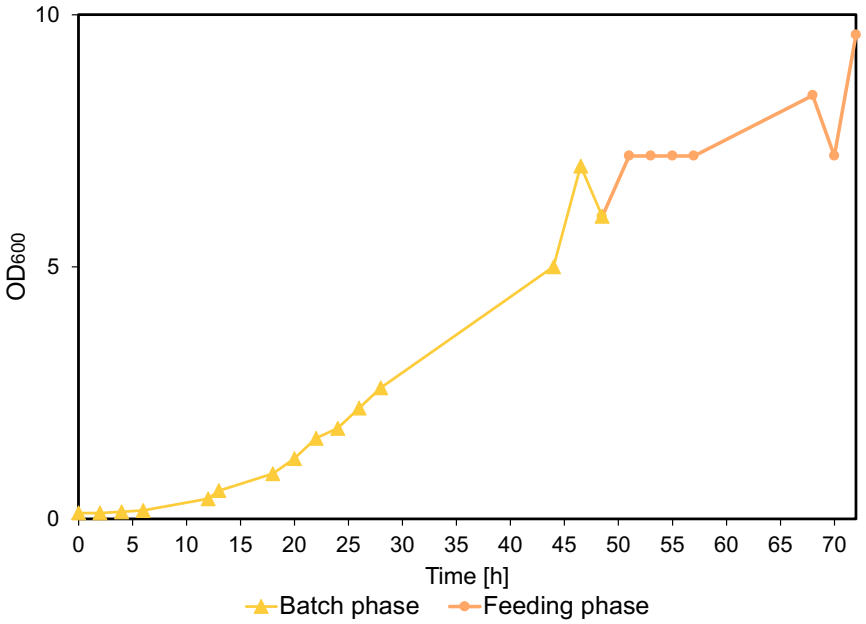

Figure 5.11: Growth curve from the fed-batch fermentation at bioreactor scale, sectioned with the batch phase represented with triangle points with a yellow line, and the feeding phase depicted as circle points with an orange line for the strain Cg(pECXT99a-*riboCg*)(pSH1-*xylAB*).

From the growth curve, the growth rates of the two sections were calculated, specified further in Appendix F.2.1, with the values represented in Table 5.6.

Table 5.6: The growth rate values for the exponential phase of the batch phase and feeding phase are represented in this Table.

Section	Growth rate [/h]
Batch phase	0.06
Feeding phase	0.01

HPLC analysis was performed on each sample taken from the bioreactor for both riboflavin and xylose. The height values given were utilised to calculate the titer of both compounds and are represented in Table 5.7 and 5.8 respectively, including the samples correlating retention times and height values.

Table 5.7: Retention time and height found for the samples of the strain Cg(pECXT99a-*riboCg*)(pSH1-*xylAB*) taken from the bioreactor fermentation with 1% xylose as the main carbon source in the batch phase, until 48.5 hours, adding from that point a feed of 100 mL 5 % xylose at a flow rate of 0.7 mL/min. The table includes furthermore the correlating riboflavin titer, calculated from the other correlating values.

Sample time [h]	Retention time [min]	Height of peak	Riboflavin Titer [mg/L]
0	4,283	3006	0.03
2	4,317	4802	0.05
4	4,332	18852	0.20
6	4,335	68100	0.74
12	4,34	654732	7.12
13	4,334	790673	8.60
18	4,337	1815904	19.74
20	4,333	3186284	34.64
22	4,328	3060694	33.27
24	4,32	3378460	36.73
26	4,323	5297210	57.58
28	4,318	5973051	64.93
44	4,333	17222450	187.22
46.5	4,329	15505409	168.55
48.5	4,338	22368816	243.16
51	4,339	18578936	363.54
53	4,341	18173724	355.61
55	4,345	16693211	326.64
57	4,351	22024422	430.96
68	4,349	43394958	849.12
70	4,354	41463321	811.32
72	4.354	34265886	670.49

Table 5.8: Retention time and height found for the samples of the strain Cg(pECXT99a-*riboCg*)(pSH1-*xylAB*) taken from the bioreactor fermentation with 1% xylose as the main carbon source the batch phase, until 48.5 hours, adding a feed of 100 mL 5 % xylose at a flow rate of 0.7 mL/min. The table includes furthermore the correlating xylose titer, calculated from the other correlating values.

Sample time [h]	Retention time [min]	Height of peak	Xylose Titer [g/L]
0	10.376	48.6	11.41
2	10.373	47.4	11.12
4	19.238	46.9	11.01
6	10.370	44.9	10.54
12	10.378	39.0	9.15
13	10.370	36.7	8.61
18	10.362	34.6	8.12
20	10.365	35.0	8.21
22	10.379	34.5	8.10
24	10.381	32.4	7.60
26	10.366	31.5	7.39
28	10.369	38.9	9.13
44	10.366	27.8	6.52
46.5	19.238	25.9	6.08
48.5	10.36	24.6	5.77
51	10.372	44.5	12.53
53	10.37	48.9	13.77
55	10.373	48.7	13.72
57	10.168	55.2	15.55
68	10.373	44.6	12.56
70	10.368	33.7	9.49
72	10.377	28.7	8.08

The consumed carbon source titers for the final point in the batch phase, at 48.5 hours, at 68 hours into the feed phase and at the last point of fermentation, at 72 hours, were calculated from the xylose titers. Caclulations and values represented in Appendix F.2.3. This enabled the calculation of the biomass and biomass yield for the fermentation. Specific calculations are represented in Appendix F.2.4, where the values are given in Table 5.9.

Table 5.9: The biomass and biomass yield values for the final point in the batch phase, at 48.5 hours, at 68 hours into the feed phase and at the last point of fermentation, at 72 hours, are represented in this table with their correlating carbon consumption titers.

Sample time [h]	Carbon consumed [g/L]	Biomass[g/L]	Biomass yield[g/g]
48.5	7.46	2.40	0.43
68.0	8.62	2.88	0.33
72.0	13.10	3.29	0.25

From the riboflavin titer and carbon consumption values, the product yield and volumetric productivity values for the final point in the batch phase, at 48.5 hours, at 68 hours into the feed phase and at the last point of fermentation, at 72 hours,

were found, results represented in Table 5.10. For specific calculations, see Appendix F.2.5.

Table 5.10: The average riboflavin titer, product yield and Vol. productivity with the correlating standard deviations for the strain Cg(pECXT99a-*riboCg*)(pSH1-*xylAB*) at the final point in the batch phase, at 48.5 hours, at 68 hours into the feed phase and at the last point of fermentation, at 72 hours, are represented in this table.

Sample time [h]	Riboflavin Titer [mg/L]	Product Yield [mg/g]	Vol. Productivity [mg/Lh]
48.5	243.16	43.17	5.01
68.0	849.12	64.84	12.49
72.0	670.49	51.20	9.31

The xylose consumption titer, calculations represented in Appendix F.2.3, over time against riboflavin production titer, represented in Table 5.7, and the biomass values for the Cg(pECXT99a-*riboCg*)(pSH1-*xylAB*) strain, calculations represented in Appendix F.40, are illustrated in Figure 5.12.

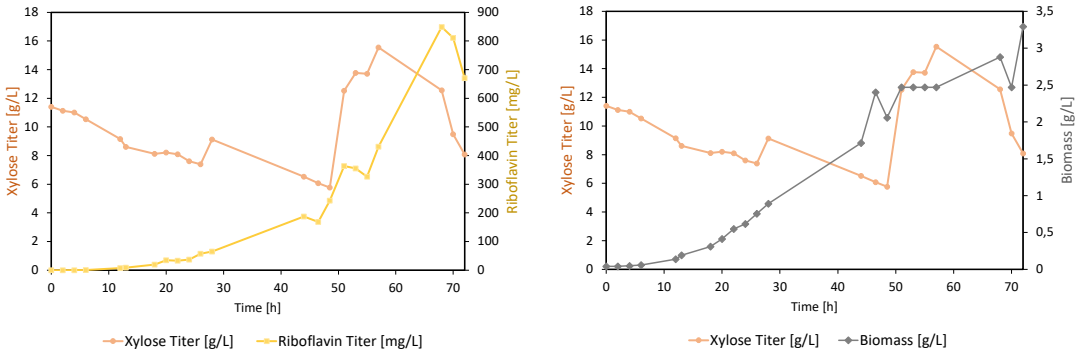

(a) Xylose consumption titer [g/L] and the Riboflavin titer [mg/L] are represented by circular points with an orange line and square points with a yellow line respectively. The values are both plotted against the fermentation time [h].

(b) Xylose consumption titer [g/L] and the biomass values [g/L] are represented by circular points with an orange line and diamond-shaped points with a grey line respectively. The values are both plotted against the fermentation time [h].

Figure 5.12: The different average values calculated for the analysis of the strain Cg(pECXT99a-*riboCg*)(pSH1-*xylAB*) are plotted in the same graf to easier evaluate the correlation between them.

6 | Discussion

6.1 Genetically modified riboflavin producers

Genetically modifying organisms solely for riboflavin production has been done for many years in Bacteria, Fungi and Yeast [9] [10] [21] [23]. Some existing industrial producers analysed at bioprocess fermentation stages are listed in Table 2.1. Wu et al.(2007) [25] produced, through the modified bacteria *B. subtilis*, a titer of 16.36 g/L riboflavin in 5 litres fed-batch fermentor over 48 hours. The genetically modified fungi *A. gossypii* W 122032 from Park et al.(2011) [26] produced a riboflavin titer of 13.7 g/L over 9 days. The experiment was performed in a 3 litre fermentor in batch mode and a working volume of 1.5 L [26]. In 2008 H. Marx and others [27] grew the genetically modified yeast *Pichia pastoris* X-33 ScRIB1 via fed-batch fermentation and a starting volume of 1.75 L over 24-50 hours, which yielded a riboflavin titer of 0.175 g/L. In summary, these industrial producers have a production range of riboflavin between 0.175 g/L and 13.7 g/L. The common genetic modifications performed generally in microorganisms for the optimalisation of riboflavin production, are either to effect the carbon flux through the purine or PPP pathway, all whom are connected to the riboflavin production pathway [10].

Other alternative riboflavin producers, such as *E. coli* and *C. glutamicum*, have in later years been utilised more and more, genetically explicitly modified to overproduce riboflavin. With *E. coli* for example, through genomic deletion of the *pgi* gene, coding for the Glucose-6-phosphate isomerase enzyme [74], causing a redirection of the carbon flux to the oxidative PPP, as well as inhibiting the degradation of riboflavin, by modulating the expression of the gene *ribF*, the *E. coli* strain RF05S-M40 produced by Lin et al.(2014) [75]. It yielded a 1036.1 mg/L riboflavin titer from fermentation done in 25 mL baffled shake flasks with optimised medium.

In 2014 S. H. Park and others [24] produced a *C. glutamicum* strain KCCM11223P that was initially analysed for the expression of the amino acid L-arginine. This was done by enhancing the activity of the correlating enzymes needed, that are expressed by the riboflavin operon. They further found that over 48 hours, the strain had produced 73 times higher riboflavin titer in contrast to the control strain, yielding a titer production of 245 mg/L using a 25 mL baffle shack flask. Taniguchi and Wendisch found in 2015 [76] that the titer of riboflavin would increase when *C. glutamicum* had been modified to overexpress the sigma factor *sigH*. This sigma factor then effectes the initiation of transcription for many genes, among them are the *ribH*, *ribA* and *ribC* genes. As explained in Chapter 2.1.1 by Figure 2.2, these

genes code for essential enzymes utilised for the riboflavin production, and when overexpressed causes an increase in carbon flux through the production pathway. Building on these results, overexpressing the complete riboflavin operon genes in a *C. glutamicum* strain through growth experiments with a 25 mL shake flask and 2% glucose as carbon source was performed. It further concluded that the strains overexpressing the genes would produce more riboflavin than the control strain, showing riboflavin titers of respectively 0.75 ± 0.13 g/L and 0.003 ± 0.000 g/L.

Through the fermentations performed in this thesis, continuing on these finding, the strains Cg(pECXT99a-*riboCg*)(pVWEx1-*fbp*), CgΔ*altR*(pECXT99a-*riboCg*) and Cg (pECXT99a-*riboCg*)(pSH1-*xylAB*) have yielded riboflavin titers at 0.33 ± 0.00 g/L, 0.39 ± 0.12 g/L and 0.37 ± 0.00 g/L over 25 hours. For these three specific riboflavin titer results, the carbon sources conditions were respectively 1 % glucose, a mixture of 1 % glucose and 1 % mannitol, and 1 % glucose. The results for the three strains in different carbon source conditions are represented in Table 5.5. Compared to other riboflavin producers, tested in baffle flasks or upscaled to bioreactor scale fermentations, the strains of the thesis have already produced industrially competitive riboflavin values.

The strain CgΔ*altR*(pECXT99a-*riboCg*) provided the highest riboflavin production value throughout this thesis. Including having the ability to overexpress the complete biosynthetic riboflavin operon *riboCG* in *C. glutamicum*, as the other strains, it has been modified to consume the non native carbon source mannitol. This causes an increase in carbon flux through the glyconeoygenesis, affecting both the oxidative and non-oxidative PPP connected to the riboflavin production pathway, as explained in Chapter 2.3.2. Pérez-García et al.(2022) [43] constructed a *C. glutamicum* strain that could consume mannitol through overexpressing the genes *mtlDBs* and *mtlAFBs*, which codes for mannitol specific phosphotranspherase system and the mannitol-1-phosphate-5-dehydrogenase enzyme from *B. subtilis* [43]. Under the same carbon source conditions, the strain achieved 0.21 g/L higher riboflavin titer, resulting in a final titer of 0.60 ± 0.03 g/L. Indicating that there could be a significant difference in mannitol uptake between the two modifications. Were the overexpression of genes that produce the enzymes vital for mannitol utilisation in *C. glutamicum* is more efficient than the deletion of the *altR* inhibitor gene, that causes the transcription of the *mtlD* gene and therefor the enzyme catalysing the reaction from mannitol to fructose.

When growing the strain that overexpresses the xylose utilisation genes, the highest riboflavin titer was achieved with glucose as sole carbon source. There was growth for both experiments performed with xylose as sole carbon source and a combination of glucose and xylose as carbon source, as represented in Table 5.3, but as depicted in Figure 5.6c, the biomass yield values are lower than in the glucose experiment. Furthermore, the riboflavin titer values for the three experiments indicate that when using xylose the production of riboflavin is lower, as shown in Table 5.5. Suggesting that the overexpression of the *xylAB* genes result in an overall metabolic imbalance.

However, when comparing the growth and riboflavin production values from xylose as sole carbon source, shown in Figure 5.7, the growth rate and final biomass are lower compared to the other carbon source conditions with glucose and a mixture of

glucose and xylose. Still, the riboflavin production was estimated to reach similar values. These results imply that there is a higher flux through the riboflavin production pathway, with xylose as a carbon source has its main flux directly to the PPP and not through the central metabolism pathways of glycolysis and TCA. Hence, the xylose consuming strain was selected to upscale the fermentation at bioreactor scale.

When comparing results given by Pérez-García et al.(2021)[7], which produced a riboflavin titer of 11.7 mg/L from a *C. glutamicum* strain modified to consume lignocellulosic carbon sources, including xylose, over 84 hours in batch fermentation. Shows that all the experiments with the Cg(pECXT99a-*riboCg*)(pSH1-*xylAB*) strain yielded higher riboflavin production values. The values found for the Cg(pECXT99a-*riboCg*)(pSH1-*xylAB*) strain with the different carbon source conditions respectively being 0.3585 g/L , 0.1083 g/L and 0.0683 g/L. Comparing the riboflavin production values for the two strains, indicates that there is a difference in the efficiency of the two accumulation pathways, with the modifications of the strains produced in this thesis seeming to be the better strain for lignocellulosic sugar consumption.

6.2 Alternative carbon sources

As observed by Wendisch et al. in 1997[6], *C. glutamicum* can consume multiple carbon sources simultaneously. This has been found to be caused by *C. glutamicum* lacking the complex carbon catabolite repression system[6].

As shown by further observations, Pérez-García et al.(2021)[7] found that using multiple carbon sources could boost riboflavin production. This was the basis for analysing a combination of two carbon sources for each strain in this thesis. The results are illustrated in Figure 5.8, 5.9 and 5.10. The seaweed-based fed-batch fermentation, performed by F. Pérez-García et al.(2022)[43], indicates that *C. glutamicum*, when consuming both glucose and mannitol simultaneously, increased the riboflavin production, with a result of 1,291.2 mg/L. From this project, only the CgΔ*altR*(pECXT99a-*riboCg*) strain had its highest riboflavin titer value when utilising more than one carbon source, specifically the combination of glucose and mannitol. Indicating that the modifications done here do not negatively affect the cell's metabolism and increase riboflavin production. The difference between the two strains consuming mannitol is 0.9 g/L. However, the strain produced by F. Pérez-García et al.(2022) has already been upscaled to a fed-batch fermentation, while the fermentation values for CgΔ*altR*(pECXT99a-*riboCg*) have only been performed in biolector scale fermentation.

Next, it was assumed that fructose as a native carbon source of *C. glutamicum* would also increase the growth and production of riboflavin in the strain Cg(pECXT99a-*riboCg*)(pVWEx1-*fbp*), as mannitol consumption is connected to the fructose consumption pathway. Illustrated in Figure 2.5. This suggests that the overexpression of the *fbp* gene, increasing glyconeoygenesis and causing a metabolic imbalance in the cell, inhibiting the growth of the cell and the production of riboflavin. Furthermore, the carbon loss in the form of carbon dioxide is higher through the PPP than

through the glycolysis, which may affect the production and of the biomass yields.

The result for the strain Cg(pECXT99a-*riboCg*)(pSH1-*xylAB*) modified to consume xylose, were similar. As depicted in Figure 2.5, the carbon flux of xylose is directly connected to the non-oxidative PPP. Theoretically, adding this as a carbon source would not negatively affect the cell's growth when glucose was available. As shown by the biomass yield values for the three conditions, which are respectively 0.69 ± 0.03 g/g, 0.61 ± 0.06 g/g and 0.24 ± 0.00 g/g, indicating that the strain utilised more of the carbon source for growth with glucose as its sole carbon source. This further indicates that the uptake of xylose affects the metabolic balance negatively. Furthermore, as shown in Table 5.5, the riboflavin titer from the combined xylose and glucose conditions is one third of the amount with glucose as a sole carbon source. Suggesting that there is no increase in carbon flux through the riboflavin production pathway either, that could be caused by a loss of carbon source through the PPP as carbon dioxide.

Utilising alternative carbon sources is essential for developing sustainable bioprocesses and bioeconomy, as well as and making production more eco-friendly. Causing renewable resources to be more sought after and researched.

In 2017 Pérez-García et al.[77] modified *C. glutamicum* for the consumption of glycerol, glucosamine, xylose, arabinose, and soluble starch as carbon sources, for the production of ectoine. Something advantageous about the amino acid glucosamine is that it is both a prime source of carbon and nitrogen. Alongside the amino sugar N-acetylglucosamine, it is a derivative from chitin, a polymer found in abundance, yielding an excellent alternative source[78].

Xylose and arabinose are both lignocelluloses, with an accumulation pathway connected directly to the PPP. Making it a favourable carbon source for riboflavin production and other pathways linked to the PPP, as it does not directly effect the main metabolic pathways for energy production.[78] [79] [80] [81]

Rice Straw Hydrolysate(RSH) is further an alternative feedstock for riboflavin production, as it is made up of xylose (13.6 g/L) and glucose (23.7 g/L). In 2011, Gopinath et al.[81] demonstrates that *C. glutamicum* when modified could utilise rice straw for carbon source consumption. Sasikumar et al. (2021)[82] further showed that RSH could be consumed by *C. glutamicum* when producing the non-proteinogenic amino acid 5-aminovalerate and the diamine putrescine. The use of RSH could be favourable for riboflavin production with *C. glutamicum* as the combination of the two carbon sources, connected to two different primary metabolite pathways, could cause the production of varying compounds to increased without possibly decreasing the organism's growth rate.

Another alternative carbon source is brown seaweed, as it is a combination of glucose and mannitol. It is furthermore also a source of nitrogen, which could be beneficial. It was found by Pérez-García et al.(2022)[43] that *C. glutamicum* could consume brown seaweed extract for the production of riboflavin specifically. In correlation to the CgΔ*altR*(pECXT99a-*riboCg*) strain produced in this thesis, it could be a prime alternative source as the strain created the highest riboflavin amount when utilising these carbon sources. Furthermore, the use of seaweed further substantiates the turn

towards sustainable bioprocesses. Norway has one of the largest reservoirs of seaweed worldwide[83], and in general seaweed has high growth rate and good biomass yield[84][85], further substantiating the development of a sustainable bioeconomy.

6.3 Different processes

The strain Cg(pECXT99a-*riboCg*)(pSH1-*xylAB*) was selected for upscaling fermentation to bioreactor scale using xylose as sole carbon source. The total carbon source consumed after 72 hours was 13.10 g/L, resulting in a final riboflavin titer of 670.49 mg/L, represented in Table 5.10. Concluding that the upscaling of the process with this strain was successful. Interestingly, at 68 hours the riboflavin titer was calculated to be 849.12 mg/L, meaning 178.63 mg/L higher than the final titer. From visual confirmation of the bioreactor, this loss of riboflavin in the solution is caused by the product being precipitated as solid particles between these two sampling points. This fermentation done with a lab scale bioreactor resulted with a riboflavin titer 643.5 mg/L higher than the results found by Pérez-García et al.(2021)[7].

Represented in Figure 5.12 is the correlation between the xylose consumption against the riboflavin production and the biomass concentration of the strain Cg(pECXT99a-*riboCg*)(pSH1-*xylAB*) from the fed-batch fermentation over 72 hours. These plots show when there is consumption of xylose there is a proportional increase in both riboflavin production and biomass production. Further concluding that there is metabolic balance in the strain when utilising xylose, however, the consumption rate is indicated to be slow. The results, when compared to other publications, shows both that the growth rate and the riboflavin production is lower for the strain produced in this thesis, when performed in a similar fed-batch fermentation. Such as represented by Pérez-García et al.(2022)[43], that performed a seaweed-based fed-batch fermentation, with mannitol and glucose. It concluded with the riboflavin final titer and biomass concentration values at 1 291.2 mg/L and 4.8 g L, after 75 h. The final riboflavin titer and biomass value for the Cg(pECXT99a-*riboCg*)(pSH1-*xylAB*) strain after 72 hours are 670.49 mg/L and 3.29 g/L, respectively, indicating a difference of over a 100% in the production of riboflavin and 45 % higher biomass production in the strain produced by Pérez-García et al.(2022)[43].

The fed-batch fermentation examined by Rohles et al.(2016)[86], producing 5- aminovalerate from *C. glutamicum*, had a similar setup to the thesis fed-batch fermentation, having a batch phase and a feed phase. When examining the two product yields for the different phases of both fermentations, both values increase when the feed is added. The values for the Rohles and the thesis fermentation being 0.11 g/g and 0.13 g/g, and 43.17 mg/g and 64.84 mg/g for the batch and feed phases, respectively. The yield values are higher for the Rohles fermentation, indicating that the accumulation and utilisation of the carbon source for the strain in the thesis are lower than other similar fed-batch fermentation. This one can also see when comparing the product yield values with the production results of ectoine produced by the *C. glutamicum* strain from Pérez-García et al.(2017)[77], respectively being 0.065 g/g and 0.456 g/g for the batch and feed phase. Compared to the other fed-batch

fermentation, this one has a 7 times yield increase after the feeding, while the others have at most a 50 % increase. Indicating that this fermentation has a clear shift from biomass fermentation to production when the feed is added compared to the fermentation done for the thesis. The Cg(pECXT99a-*riboCg*)(pSH1-*xylAB*) strain, in other words, did not necessarily reach the stationary phase of growth before the feed was added, as further indicated by the illustration in Figure 5.12b. The carbon source was not solely utilised for the production of riboflavin but also for biomass fermentation, resulting in a lower yield than other similar fermentation.

6.4 Recommendations for Future Work

For future work, many elements can be explored. In connection to the carbon sources, optimisation of the amounts utilised for the different strains could be looked into, as previous work showed that different amounts of carbon sources yielded various biomass and production amounts[46]. Furthermore, analysing different combinations of carbon sources for the different strains, utilising *C. glutamicum's* ability to consume several carbon sources simultaneously[6] could be beneficial[7][43]. One effect could be using two carbon sources, where each carbon source affects separate metabolic pathways, causing the production of the product to increase without decreasing the organism's growth rate.

With this in mind, utilising alternative carbon sources is an exciting aspect. Both when it comes to its effects on the production and growth rates of the strains and for establishing sustainable bioprocesses, thereby supporting the bioeconomy. Here, the analysis of RSH as an alternative carbon source for the Cg(pECXT99a-*riboCg*)(pSH1-*xylAB*) strain could be interesting, as it contains xylose and glucose, further widening the analysis of the strains utilisation of xylose[81]. Brown seaweed is another alternative carbon source and would affect the sustainability of a bioprocess, also being an economical compound to utilise for production in Norway. It could be used as carbon and nitrogen source for the CgΔ*altR*(pECXT99a-*riboCg*) strain, as it is put together by glucose and mannitol[43].

Further work connected to the bioreactor approach would be to establish a continuous fermentation for the Cg(pECXT99a-*riboCg*)(pSH1-*xylAB*) strain. As shown by Hirao, T. et al.(1989)[87], establishing a continuous fermentation increased the production utilising *C. glutamicum* as the microbial host, compared to the results given by fed-batch fermentation. Advantages of continuous fermentation compared to fed-batch fermentation are, among other things, the continuous flow of feed through the system. Resulting in no decrease in carbon source amount or other nutrients. Enabling the possibility of high growth rates for the microorganism and the continuous production of different compounds without reaching a stationary phase.

Further modifications of the *C. glutamicum* strain is the possibility of improving the carbon flux through the PPP. This would increase the riboflavin production, as the production pathway is connected in two points of the PPP, as depicted in 2.4. Another aspect would be to improve the riboflavin exportation rate, as the analysis done in this thesis only considers the riboflavin amount in the solution, not including

the amount present in the cell's cytosol. At this point, there is no clear information on how *C. glutamicum* exports riboflavin and if the presence of riboflavin in the fermentation solution could affect the growth and production performances. In this regard, toxicity tests should be performed to further evaluate *C. glutamicum* as a riboflavin overproducer.

By further expanding the riboflavin pathway, the roseoflavin production could be established in *C. glutamicum*. Riboflavin is the direct precursor of the antimicrobial roseoflavin. Its production could be accomplished by overexpressing the *rosAB* genes from the bacterium *Streptomyces davaonensis* that codes for the enzymes catalysing the production reaction[88].

7 | Conclusion

Production of riboflavin was successfully established, tested and evaluated from different carbon sources using the metabolic engineered *C. glutamicum* as host. The specific strains being Cg(pECXT99a-*riboCg*)(pVWEx1-*fbp*), CgΔ*altR*(pECXT99a-*riboCg*) and Cg(pECXT99a-*riboCg*)(pSH1-*xylAB*). By using xylose as sole carbon source, the riboflavin specific productivity could be greatly improved, and therefore, the process was scaled-up in bioreactors. Compared to other similar fed-batch fermentation's, the results for the strain consuming xylose is not yet at the degree to sufficiently compete with existing publications. As proven in this thesis, the use of non-conventional and sustainable substrates is a powerful tool within industrial biotechnology, which needs further exploration and exploitation to enforce the circular bioeconomy.

Bibliography

[1] J. Pinto et al. Riboflavin. *Advances in Nutrition*, 7(5):973–975, 2016. DOI: https://DOI.org/10.3945/an.116.012716.

[2] Ph.D. Gerald F. Combs, Jr. *The Vitamins - Fundamental aspects in Nutrition and Health*. Elsevier Inc, 3 edition, 2008. doi: DOI:.

[3] H. J. Powers. Riboflavin (vitamin b-2) and health. *The American Journal of Clinical Nutrition*, 77(6):1352–1360, 2003. DOI: https://DOI.org/10.1093/ajcn/77.6.1352.

[4] O. Kirchner and A. Tauch. Tools for genetic engineering in the amino acid-producing bacterium *Corynebacterium glutamicum*. *Journal of biotechnology*, 104:287–299, 2003. DOI: 10.1016/S0168-1656(03)00148-2.

[5] N. A. Henke et al. *Carotenoid Production by Corynebacterium: The Workhorse of Industrial Amino Acid Production as Host for Production of a Broad Spectrum of C40 and C50 Carotenoids*. Intech, 2017. DOI: 10.5772/67631.

[6] V.F. Wendisch et al. Regulation of acetate metabolism in *Corynebacterium glutamicum*: transcriptional control of the isocitrate lyase and malate synthase genes. *Archives of Microbiology*, 168:262–269, 1997. DOI: 10.1007/s002030050497.

[7] F. Pérez-García et al. Dynamic co-cultivation process of *Corynebacterium glutamicum* strains for the fermentative productionof riboflavin. *Fermentation*, 7, 2021. DOI: 10.3390/fermentation7010011.

[8] V. F. Wendisch et al. Updates on industrial production of amino acids using *Corynebacterium glutamicum*. *World J Microbiol Biotechnol*, 32(105), 2016. DOI: 10.1007/s11274-016-2060-1.

[9] K.-P. Stahmann et al. Three biotechnical processes using ashbya gossypii, candida famata, or *Bacillus subtilis* compete with chemical riboflavin production. *Applied Microbiology and Biotechnology*, 53:509–516, 2000. DOI: 10.1007/s002530051649.

[10] L. A. Averianova et al. Production of vitamin b2(riboflavin) by microorganisms: An overview. 2020. DOI: 10.3389/fbioe.2020.570828.

[11] H. Yukawa et al. *Corynebacterium glutamicum Biology and Biotechnology*. Springer, 1 edition, 2013. doi: DOI:10.1007/978-3-642-29857-8.

[12] M. Leszczewicz and P. Walczak. Selection of thermotolerant *Corynebacterium glutamicum* strains for organic acid biosynthesis. *Food Technol Biotechnol*, 57: 249–259, 2019. DOI: 10.17113/ftb.57.02.19.5980.

[13] M. P. Doyle and J. L. Schoeni. Survival and growth characteristics of *Escherichia coli* associated with hemorrhagic colitis. *Applied and environmental microbiology*, 48:855–856, 1984. DOI: 10.1128/aem.48.4.855-856.1984.

[14] LS. Silva et al. Chromatographic determination of riboflavin in the presence of tetracycline in skimmed and full cream milk using fluorescence detection. *JOURNAL OF THE BRAZILIAN CHEMICAL SOCIETY*, 16:1175, 11 2005. DOI: 10.1590/S0103-50532005000700013.

[15] Riboflavin metabolism - *Corynebacterium glutamicum* atcc 13032 (bielefeld). Available at: `https://www.genome.jp/kegg-bin/show_pathway?cgb00740` (Accessed: 20.11.21), 2021.

[16] Riboflavin biosynthesis protein ribd. Available at: `https://www.uniprot.org/uniprot/A4QEG9` (Accessed: 20.12.21)., 2021.

[17] Riboflavin synthase. Available at: `uniprot.org/uniprot/P0AFU8` (Accessed: 06.12.21)., 2021.

[18] Riboflavin biosynthesis protein. Available at: `https://www.uniprot.org/uniprot/A4QEG9` (Accessed: 06.12.21)., 2021.

[19] 6,7-dimethyl-8-ribityllumazine synthase. Available at: `https://www.uniprot.org/uniprot/P11998` (Accessed: 06.12.21)., 2021.

[20] Bifunctional riboflavin kinase/fmn adenylyltransferase. Available at: `https://www.uniprot.org/uniprot/P0AG40` (Accessed: 20.12.21)., 2021.

[21] A. Bacher et al. Biosynthesis of vitamin b2 (riboflavin). *Annual Review of Nutrition*, 7:153–167, 2000. DOI: 10.1146/annurev.nutr.20.1.153.

[22] R. Kurth et al. Ullmann's encyclopedia of industrial chemistry. *VCH, Weinheim*, page pages: 521–530, 1996.

[23] A. P. van Loon et al. Physiology and metabolic fluxes of wild-type and riboflavin-producing *Bacillus subtilis*. *Applied and Environmental Microbiology*, 62(10):3687–3696, 1996. doi: DOI:10.1128/aem.62.10.3687-3696.1996.

[24] S. H. Park et al. Microorganism for simultaneously producing l-amino acid and riboflavin, and method for producing l-amino acid and riboflavin using same. 2014. Patent No.: US 2014/0356518 A1.

[25] QL. Wu et al. Optimization of riboflavin production by recombinant *Bacillus subtilis* rh44 using statistical designs. *Applied Microbiology and Biotechnology*, 76, 2007. DOI: 10.1007/s00253-007-1049-y.

[26] E.Y. Park et al. The improvement of riboflavin production in *Ashbya gossypii* via disparity mutagenesis and dna microarray analysis. *Applied Microbiology and Biotechnology*, 91, 2011. DOI: 10.1007/s00253-011-3325-0.

[27] H. Marx et al. Overexpression of the riboflavin biosynthetic pathway in *Pichia pastoris*. *Microbial Cell Factories*, 7, 2008. DOI: 10.1186/1475-2859-7-23.

[28] C. Wittmann and J. Becker. The l-lysine story:from metabolic pathways to industrial production. *Microbiology Monographs*, 5:43, 24 February 2007. DOI: 10.1007/7171_2006_08.

[29] J. Yang and S. Yang. Comparative analysis of *Corynebacterium glutamicum* genomes: a new perspective for the industrial production of amino acids. *BMC Genomics*, 18:Article nr: 940, 2017. DOI: 10.1186/s12864-016-3255-4.

[30] C. Krömer, J. Wittmann and E. Heinzle. Metabolic pathway analysis for rational design of l-methionine production by *Escherichia coli* and *Corynebacterium glutamicum*. *Metabolic Engineering*, 8, July 2006. DOI: 10.1016/j.ymben.2006.02.001.

[31] J. Kovářová and M. P. Barrett. The pentose phosphate pathway in parasitic trypanosomatids. *Applied and Environmental Microbiology*, 32, 2016. DOI: 10.1016/j.pt.2016.04.010.

[32] A. Zahoor et al. Metabolic engineering of *Corynebacterium glutamicum* aimed at alternative carbon sources and new products. *Computational and structural biotechnology journal*, 3, 2012. DOI: 10.5936/csbj.201210004.

[33] H. Dominguez et al. Carbon-flux distribution in the central metabolic pathways of *Corynebacterium glutamicum* during growth on fructose. *European Journal of Biochemistry*, 254:pages: 96 – 102, 1998. DOI: 10.1046/j.1432-1327.1998.2540096.x.

[34] T. Laslo et al. Arabitol metabolism of *Corynebacterium glutamicum* and its regulation by atlr. *Journal of Bacteriology*, 194:941–955, 2012. DOI: 10.1128/jb.06064-11.

[35] X. Peng et al. Characterization of the mannitol catabolic operon of *Corynebacterium glutamicum*. *Applied Microbiology and Biotechnology*, 91:1375–1387, 2011. DOI: 10.1007/s00253-011-3352-x.

[36] H. Kawaguchi et al. Engineering of a xylose metabolic pathway in *Corynebacterium glutamicum*. *Applied and Environmental Microbiology*, 72(5):3418–3428, 2006. DOI: 10.1128/AEM.72.5.3418-3428.2006.

[37] B. Görke and J. Stülke. Carbon catabolite repression in bacteria: many ways to make the most out of nutrients. *Nature Reviews Microbiology*, 6:613–624, 2008. DOI: 10.1038/nrmicro1932.

[38] I. Krahn et al. Evolving a new efficient mode of fructose utilization for improved bioproduction in c*Corynebacterium glutamicum*. *Frontiers in Bioengineering and Biotechnology*, 9, 2021. DOI: 10.3389/fbioe.2021.669093.

[39] A. Radek et al. Engineering of *Corynebacterium glutamicum* for minimized carbon loss during utilization of d-xylose containing substrates. *Journal of Biotechnology*, 192:156–160, 2014. DOI: 10.1016/j.jbiotec.2014.09.026.

[40] Fructose-1,6-bisphosphatase. Available at: https://www.uniprot.org/uniprot/P0A993 (Accessed: 20.12.21)., 2022.

[41] Xylose isomerase. Available at: https://www.uniprot.org/uniprot/Q4UTU6 (Accessed: 20.12.21)., 2021.

[42] Xylosidase. Available at: https://www.uniprot.org/uniprot/Q8P9U0 (Accessed: 20.12.21)., 2021.

[43] F. Pérez-García et al. From brown seaweed to a sustainable microbial feedstock for the production of riboflavin. *Fronteirs in Bioengineering and Biotechnology*, 10, 2022. DOI: 10.3389/fbioe.2022.863690.

[44] F. Pérez-García et al. Dynamic co-cultivation process of *Corynebacterium glutamicum* strains for the fermentative productionof riboflavin. *Fermentation*, 7 (5), 2021. DOI: 10.3390/fermentation7010011.

[45] O. Kirchner and A. Tauch. Tools for genetic engineering in the amino acid-producing bacterium *Corynebacterium glutamicum*. *Journal of Biotechnology*, 104:287–299, 2003. DOI: 10.1016/S0168-1656(03)00148-2.

[46] T. Bakken. Riboflavin production from genetically modified *Corynebacterium glutamicum*. *Specialization project, NTNU*, 2021.

[47] P. G. Peters-Wendisch et al. Pyruvate carboxylase is a major bottleneck for glutamate and lysine production by *Corynebacterium glutamicum*. *Journal of Molecular Microbiology and Biotechnology*, 3:295–300, 2001.

[48] N.A. Henke et al. Production of the marine carotenoid astaxanthin by metabolically engineered *Corynebacterium glutamicum*. *Marin drugs*, 14, 2016. DOI: 10.3390/md14070124.

[49] D. Hanahan. Studies on transformation of *Escherichia coli* with plasmids. *Journal of Molecular Biology*, 166, 1983. DOI: 10.1016/S0022-2836(83)80284-8.

[50] s. Abe et al. Taxonomical studies on glutamic acid-producing bacteria. *The Journal of General and Applied Microbiology*, 13, 1967. DOI: 10.2323/jgam.13.279.

[51] T. Laslo et al. Arabitol metabolism of *Corynebacterium glutamicum* and its regulation by *AltR*. *Journal of bacteriology*, 194, 2012. DOI: 10.1128/JB.06064-11.

[52] Biochrom wpa range of colorimeters and spectrophotometers. Available at: http://www.biochrom.co.uk/product/20/biochrom-wpa-co8000-cell-density-meter.html (Accessed: 17.04.22).

[53] *Thermo Scientific™ O'GeneRuler 1 kb DNA Ladder, Ready-to-Use- 250-10,000 bp.* https://www.fishersci.no/shop/products/fermentas-o-generuler-ready-to-use-1kb-dna-ladder/11551615 (Accessed: 04.09.21)., 2021.

[54] *QIAprep® Spin Miniprep Kit.* https://www.qiagen.com/cn/resources/download.aspx?id=56b0162c-23b0-473c-9229-12e8b5c8d590&lang=en (Accessed: 07.04.22)., 2015.

[55] P. Dixon. *Basic Science in Obstetrics and Gynaecology.* Churchill Livingstone, 4 edition, 2013. doi: DOI:10.1007/978-3-642-29857-8.

[56] R. M. Steinberg. Pcr. *Encyclopedia.com.* Available at: https://www.encyclopedia.com/science/news-wires-white-papers-and-books/pcr (Accessed: December 9, 2021)., 2018.

[57] Inc. A Takara Bio Company Clontech Laboratories. Cloneamp™ hifi pcr premix protocol-at-a-glance. Available at: https://www.takarabio.com/documents/User%20Manual/CloneAmp%20HiFi%20PCR%20Premix%20Protocol/CloneAmp%20HiFi%20PCR%20Premix%20Protocol-At-A-Glance_092612.pdf (Accessed: 15.02.22)., 2012.

[58] D. G. Gibson et al. Enzymatic assembly of dna molecules up to several hundred kilobases. *Nature Methods*, 6, 2009. DOI: 10.1038/nmeth.1318.

[59] S. Thomas et al. Dna library construction using gibson assembly. *Nat Methods*, 12, 2015. DOI: 10.1038/nmeth.f.384.

[60] Gibson assembly cloning guide. *Synthetic Genomics, Inc. Company*, 2:6, 2017.

[61] QIAquick Spin Handbook. Qiaquick pcr purification kit protocol. Available at: http://2012.igem.org/wiki/images/a/a3/QIAquick_PCR-purification.pdf (Accessed: 23.02.22)., 2008.

[62] Promega. Gotaq® dna polymerase. Available at: https://no.promega.com/resources/protocols/product-information-sheets/g/gotaq-dna-polymerase-m300-protocol/ (Accessed: 28.02.22)., 2018.

[63] m2p Labs. Biolector pro - microfluidic bioprocess control. Available at: https://pdf.medicalexpo.com/pdf/m2p-labs-microbioreactors/biolector-pro/112726-227059.html (Accessed: 30.04.22)., 2020.

[64] m2p Labs. Biolector pro - microfluidic bioprocess control. Available at: https://pdf.medicalexpo.com/pdf/m2p-labs-microbioreactors/biolector-pro/112726-227059.html (Accessed: 30.04.22)., 2020.

[65] m2p Labs. Biolector pro - microfluidic bioprocess control. Available at: https://pdf.medicalexpo.com/pdf/m2p-labs-microbioreactors/biolector-pro/112726-227059.html (Accessed: 30.04.22)., 2020.

[66] ASISTEC. Applikon autoclavable bioreators. Available at: https://asistec.ie/product/applikon-autoclavable-bioreators/ (Accessed: 15.05.22).

[67] Sigma-Aldrich. Antifoam 204. Available at: https://www.sigmaaldrich.com/NO/en/product/sigma/a6426 (Accessed: 10.05.22).

[68] P. C. Sadek. *The HPLC Solvent Guide.* 2 edition, 2002. ISBN ISBN: 978-0-471-41138-3.

[69] B. J. Petteys and E. L. Frank. Rapid determination of vitamin b2 (riboflavin) in plasma by hplc. *Clinica Chimica Acta*, 412:38–43, 2011. DOI: 10.1016/j.cca.2010.08.037.

[70] *2475 Fluorescence (FLR) Detector.* https://www.waters.com/waters/en_US/2475-Fluorescence-%28FLR%29-Detector/nav.htm?cid=514434&locale=en_US#:~:text=The%20Waters%202475%20Fluorescence%20(FLR,derivatized%20with%20a%20fluorescent%20tag. (Accessed: 10.04.22)., 2021.

[71] *Symmetry C18 Column, 100Å, 3.5 µm, 4.6 mm X 75 mm, 1/pk.* https://www.waters.com/nextgen/us/en/shop/columns/wat066224-symmetry-c18-column-100a-35--m-46-mm-x-75-mm-1-pk.html (Accessed: 17.04.22)., 2022.

[72] Agilent. Hi-plex. Available at: https://www.agilent.com/en/product/small-molecule-columns/ion-exclusion-ligand-exchange-columns/hi-plex#:~:text=Agilent%20Hi%2DPlex%20HPLC%20columns,require%20ion%20regeneration%20or%20suppressors. (Accessed: 25.05.22).

[73] Shodex. Refractive index detector : Shodex ri-501,502,504. Available at: https://www.shodex.com/en/da3/b3/01/1d.html#! (Accessed: 25.05.22).

[74] Glucose-6-phosphate isomerase. Available at: https://www.uniprot.org/uniprot/Q1R3R3 (Accessed: 12.05.22)., 2022.

[75] Z. Lin et al. Metabolic engineering of *Escherichia coli* for the production of riboflavin. *Microbial Cell Factories*, 13, 2014. DOI: 10.1186/s12934-014-0104-5.

[76] H. Taniguchi and V. F. Wendisch. Exploring the role of sigma factor gene expression on production by *Corynebacterium glutamicum*: sigma factor h and fmn as example. *Fronteirs in Microbiology*, 6, 2015. DOI: 10.3389/fmicb.2015.00740.

[77] F. Pérez-García et al. Improved fermentative production of the compatible solute ectoine by *Corynebacterium glutamicum* from glucose and alternative carbon sources. *Journal of Biotechnology*, 258, 2017. DOI: 10.1016/j.jbiotec.2017.04.039.

[78] A. Uhde et al. Glucosamine as carbon source for amino acid-producing *Corynebacterium glutamicum*. *Applied Microbiology and Biotechnology*, 97, 2013. DOI: 10.1007/s00253-012-4313-8.

[79] H. Kawaguchi et al. Engineering of a xylose metabolic pathway in *Corynebacterium glutamicum*. *Applied and Environmental Microbiology*, 72, 2006. DOI: 10.1128/AEM.72.5.3418-3428.2006.

[80] M. Sasaki et al. Simultaneous utilization of d-cellobiose, d-glucose, and d-xylose by recombinant *Corynebacterium glutamicum* under oxygen-deprived conditions. *Applied Microbiology and Biotechnology*, 81, 2008. DOI: 10.1007/s00253-008-1703-z.

[81] V. Gopinath et al. Amino acid production from rice straw and wheat bran hydrolysates by recombinant pentose-utilizing *Corynebacterium glutamicum*. *Applied Microbiology and Biotechnology*, 92, 2011. DOI: 10.1007/s00253-011-3478-x.

[82] K. Sasikumar et al. Production of biopolyamide precursors 5-amino valeric acid and putrescine from rice straw hydrolysate by engineered *Corynebacterium glutamicum*. *Frontiers in Bioengeneering an Biotechnology*, 2021. DOI: 10.3389/fbioe.2021.635509.

[83] P. Stévant et al. Seaweed aquaculture in norway: recent industrial developments and future perspectives. *Aquaculture International*, 25(12), 2017. DOI: 10.1007/s10499-017-0120-7.

[84] S. Sharma. Production of microbial protein from brown seaweed and spruce wood and its use as a novel feed ingredient in aquaculture. *Faculty of Chemistry, Biotechnology and Food Science, Norwegian University of Life Sciences*, 2018. ISSN: 1894-6402, ISBN: 978-82-575-1518-8.

[85] S. Sharma and S. J. Horn. Enzymatic saccharification of brown seaweed for production of fermentable sugars. *Bioresource Technology*, 213, 2016. DOI: 10.1016/j.biortech.2016.02.090.

[86] C. M. Rohles et al. Systems metabolic engineering of *Corynebacterium glutamicum* for the production of the carbon-5 platform chemicals 5-aminovalerate and glutarate. *Microbial Cell Factories*, 15, 2016. DOI: 10.1186/s12934-016-0553-0.

[87] T Hirao et al. L-lysine production in continuous culture of an l-lysine hyperproducing mutant of *Corynebacterium glutamicum*. *Applied Microbiology and Biotechnology*, 32, 1989. DOI: 10.1007/BF00184972.

[88] F. Jankowitsch et al. Genome sequence of the bacterium *Streptomyces davawensis* jcm 4913 and heterologous production of the unique antibiotic roseoflavin. *Journal of Bacteriology*, 194, 2012. DOI: 10.1128/JB.01592-12.

Appendix

The appendix includes the procedure for the medium and solutions, as well as values and calculations performed and utilised for the master thesis.

A Medium and Solutions

This section will contain the recipe information for each medium and solution utilised during experiments. When necessary, the solutions were sterilised by autoclavation or filtration.

A.1 Stock solutions

The stock solutions utilised are given in this section.

A.1.1 Biotin

The biotin stock solution recipe is given in Table A.1.

Table A.1: This table includes the components utilised for the production of the biotin stock solution, with the compounds corresponding concentrations and amounts.

Compound	Concentration	Unit	Quantity in final solution	Unit
Biotin	0.2	g/L	0.02	g
NaOH 1M			100	mL
Final volume			100	mL

A.1.2 IPTG stock

The construction of the IPTG stock solution at 1M is represented in Table A.2.

Table A.2: This table includes the components utilised for the production of the IPTG stock solution, with the compounds corresponding concentrations and amounts.

Compound	Concentration	Unit	Quantity in final solution	Unit
IPTG	2.38	g/L	0.238	g
Milli-Q water			100	mL
Final volume			100	mL

A.1.3 PCA solution

Protocatechuic acid (PCA) stock solution was made by following the description in Table A.3.

Table A.3: This table includes the compounds utilised for the production of the PCA stock solution, with the compounds corresponding concentrations and amounts.

Compound	Concentration in final volume	Unit	Quantity in final solution	Unit
PCA	30	g/L	0.3	g
NaOH 1 M			10	mL
Final volume			10	mL

A.1.4 Trace element solution

The trace element solution(TES) is made by mixing half the Milli-Q water amount and the dry elements, represented in Table A.4. The pH is adjusted to 1 with HCl, before adding the rest of the Milli-Q water, so that the final volume is 100 mL.

Table A.4: This table includes the components utilised for the production of the trace element solution, with the compounds corresponding concentrations and amounts.

Compound	Concentration	Unit	Quantity in final solution	Unit
FeSO4 x7 H2O	16.4	g/L	1.64	g
MnSO4 x H2O	10	g/L	1	g
ZnSO4 x7 H2O	1	g/L	0.1	g
CuSO4 x5 H2O	0.31	g/L	0.031	g
NiCl2 x6 H2O	0.02	g/L	0.002	g
Milli-Q water			100	mL
Final volume			100	mL

A.1.5 Antibiotics

This section will describe the methods for preparing the different antibiotic solutions. The solutions are filtrated and aliquoted to smaller volumes, before being frozen at - 20°C.

Tetracycline stock
The tetracycline stock with a final concentration at 10 g/L is made by following the protocol represented in Table A.5, utilising ethanol(EtOH) 70 %.

Table A.5: This table includes the components utilised for the production of the antibiotic stock solution of tetracycline, with the compounds corresponding concentrations and amounts.

Compound	Final concentration	Unit	Quantity in final solution	Unit
Tetracycline	10	g/L	0.5	g
EtOH			50	mL
Final volume			50	mL

Kanamycin stock
Following the amounts represented in Table A.6, the kanamycin stock solution at 50 g/L is made.

Table A.6: This table includes the components utilised for the production of the antibiotic stock solution of kanamycin, with the compounds corresponding concentrations and amounts.

Compound	Final concentration	Unit	Quantity in final solution	Unit
Kanamycin	50	g/L	2.5	g
Milli-Q water			50	mL
Final volume			50	mL

A.1.6 Glycerin 89%

The glycerin solution at 89 % is produced by mixing the compounds represented in Table A.7.

Table A.7: This table includes the components utilised for the production of the glycerin stock solution, with the compounds corresponding concentrations and amounts, resulting in a final concentration at 89%.

Compound	Concentration	Unit	Quantity in final solution	Unit
Glycerin	99.5	%	89.45	mL
Milli-Q water			10.55	mL

A.2 Complex media

All the complex media used in the thesis is represented in this section.

A.2.1 BHI

BHI solution is made by utilising Brain heart infusion(BHI) mixture. The specific amounts used for the final solution at 400 mL is given in Table A.8.

Table A.8: This table includes the components utilised for the production of the BHI solution, with the compounds corresponding concentrations and amounts.

Compound	Concentration	Unit	Quantity in final solution	Unit
BHI	37	g/L	37	g
Milli-Q water			1000	mL
Final volume			1000	mL

A.2.2 BHIS

BHIS solution is the combination of the BHI solution represented in Appendix A.2.1, and a sorbitol solution, given in Table A.9.The ratio between the to solutions are represented in Table A.10.

Table A.9: This table includes the components utilised for the production of the sorbitol solution, with the compounds corresponding concentrations and amounts.

Compound	Concentration	Unit	Quantity in final solution	Unit
Sorbitol	455	g/L	45.5	g
Milli-Q water			100	mL
Final volume			100	mL

Table A.10: This table includes the components utilised for the production of the BHIS solution, with the compounds corresponding amounts.

Compound	Quantity in final solution	Unit
BHI solution	100	mL
Sorbitol solution	1000	mL
Final volume	400	mL

A.2.3 2TY

The 2TY complex media is produced combining the components represented in Table A.11.

Table A.11: This table includes the components utilised for the production of the 2TY complex media solution, with the compounds corresponding concentrations and amounts.

Compound	Concentration	Unit	Quantity in final solution	Unit
Yeast extract	10	g/L	20	g
Triptone	16	g/L	32	g
NaCl	5	g/L	10	g
Milli-Q water			2000	mL
Final volume			2000	mL

A.2.4 Solid selective medium

To produce the solid selective medium of agarplates, utilised in the thesis, BHI solution was mixed with agar. The amounts represented in Table A.12. After the solution was autoclaved, 250 μL of one or plural antibiotics were added to the solution in sterile conditions.

Table A.12: This table includes the components utilised for the production of the solution used for producing selective agarplates, with the compounds corresponding concentrations and amounts.

Compound	Quantity in final solution	Unit
BHI	500	mL
Agar	18.5	g
Final volume	500	mL

A.3 Stock solutions for minimal media

The stock solutions needed for the different minimal medias produced for the thesis is represented in this section.

A.3.1 Salt solution - CGXII

The salt solution, CGXII, is produced by following the description in Table A.13, as well as adjusting the pH value to 7 by adding potassium hydroxide(KOH).

Table A.13: This table includes the components utilised for the production of the salt solution, with the compounds corresponding concentrations and amounts.

Compound	Concentration	Unit	Quantity in final solution	Unit
(NH4)2SO4	10	g/L	5	g
KH2PO4	1	g/L	0.5	g
K2HPO4	1	g/L	0.5	g
UREA	5	g/L	2.5	g
MOPS	42	g/L	21	g
Ca-stock 1000X	1	mL/L	0.5	mL
Mg-stock 1000X	1	mL/L	0.5	mL
MiLLi-Q water	-	-	400	mL
Final volume			100	mL

A.3.2 Carbon source stock solutions

The carbon source solutions of glucose, fructose, mannitol and xylose are respectively represented in Table A.14, A.15, A.16 and A.17.

Table A.14: This table includes the components utilised for the production of the glucose solution, with the compounds corresponding concentrations and amounts.

Compound	Concentration	Unit	Quantity in final solution	Unit
Glucose	400	g/L	200	g
Milli-Q water			500	mL
Final volume			500	mL

Table A.15: This table includes the components utilised for the production of the fructose solution, with the compounds corresponding concentrations and amounts.

Compound	Concentration	Unit	Quantity in final solution	Unit
Fructose	400	g/L	200	g
Milli-Q water			500	mL
Final volume			500	mL

Table A.16: This table includes the components utilised for the production of the mannitol solution, with the compounds corresponding concentrations and amounts.

Compound	Concentration	Unit	Quantity in final solution	Unit
Mannitol	200	g/L	40	g
Milli-Q water			200	mL
Final volume			200	mL

Table A.17: This table includes the components utilised for the production of the xylose solution, with the compounds corresponding concentrations and amounts.

Compound	Concentration	Unit	Quantity in final solution	Unit
Xylose	100	g/L	20	g
Milli-Q water			200	mL
Final volume			200	mL

A.4 Minimal media

This section includes the minimal media produced for the experiments performed in the biolector for the strains Cg(pECXT99a-*riboCg*)(pVWEx1-*fbp*) and Cg(pECXT99a-*riboCg*)(pVWEx1), CgΔ*altR*(pECXT99a-*riboCg*) and CgΔ*altR*(pECXT99a), and Cg(pECXT99a-*riboCg*)(pSH1-*xylAB*) and Cg(pECXT99a-*riboCg*)(pSH1).

A.4.1 For the Cg(pECXT99a-*riboCg*)(pVWEx1-*fbp*) and Cg(pECXT99a-*riboCg*)(pVWEx1) strains

The minimal media produced for the experiments with the strains Cg(pECXT99a-*riboCg*)(pVWEx1-*fbp*) and Cg(pECXT99a-*riboCg*)(pVWEx1) are a combination of the compounds represented in Table A.18 and the specific amounts of carbon and correlating amount of sterile water given in Table A.19 for the different carbon sources. Giving the final carbon source concentrations at 1 % glucose, a mixture of 1 % glucose and 1 % fructose, and 1 % fructose for the different minimal medias.

Table A.18: This table includes the components utilised for the production of the minimal media used for the Cg(pECXT99a-*riboCg*)(pVWEx1-*fbp*) and Cg(pECXT99a-*riboCg*)(pVWEx1) strains, with the compounds corresponding concentrations and amounts.

Compound	Concentration	Unit	Quantity in final solution	Unit
CGXII	-	-	20	mL
Biotin	0.2	g/L	25	μL
PCA	20	g/L	25	μL
TES	-	-	25	μL
Tetracylin	10	g/L	12.5	μL
Kanamycin	50	g/L	12.5	μL
IPTG	0.5	M	62.5	μL

Table A.19: This table includes the different carbon source and sterile water amounts for the different conditions for the Cg(pECXT99a-*riboCg*)(pVWEx1-*fbp*) and Cg(pECXT99a-*riboCg*)(pVWEx1) strains, to be mixed with the components represented in Table A.18 making the different minimal medias for the strains.

Compound	Concentration	Unit	Quantity in final solution	Unit
Glucose solution	1	%	625	μL
Sterile water	-	-	4.212	mL
Glucose solution	1	%	625	μL
Fructose solution	1	%	700	μL
Sterile water	-	-	3.512	mL
Fructose solution	1	%	700	μL
Sterile water	-	-	4.137	mL

A.4.2 For the CgΔ*altR*(pECXT99a-*riboCg*) and CgΔ*altR*(pECXT99a) strains

The minimal media produced for the experiments with the strains CgΔ*altR*(pECXT99a-*riboCg*) and CgΔ*altR*(pECXT99a) are a combination of the compounds represented in Table A.20 and the specific amounts of carbon and correlating amount of sterile water given in Table A.21 for the different carbon sources. Giving the final carbon source concentrations at 1 % glucose, a mixture of 1 % glucose and 1 % mannitol, and 1 % mannitol for the different minimal medias.

Table A.20: This table includes the components utilised for the production of the minimal media used for the CgΔ*altR*(pECXT99a-*riboCg*) and CgΔ*altR*(pECXT99a) strains, with the compounds corresponding concentrations and amounts.

Compound	Concentration	Unit	Quantity in final solution	Unit
CGXII	-	-	20	mL
Biotin	0.2	g/L	25	μL
PCA	30	g/L	25	μL
TES	-	-	25	μL
Tetracylin	10	g/L	12.5	μL
IPTG	0.5	M	62.5	μL

Table A.21: This table includes the different carbon source and sterile water amounts for the different conditions for the CgΔ*altR*(pECXT99a-*riboCg*) and CgΔ*altR*(pECXT99a) strains, to be mixed with the components represented in Table A.20 making the different minimal medias for the strains.

Compound	Concentration	Unit	Quantity in final solution	Unit
Glucose solution	1	%	625	μL
Sterile water	-	-	4.225	mL
Glucose solution	1	%	625	μL
Mannitol solution	1	%	1250	μL
Sterile water	-	-	3.137	mL
Mannitol solution	1	%	1250	μL
Sterile water	-	-	3.762	mL

A.4.3 For the Cg(pECXT99a-*riboCg*)(pSH1-*xylAB*) and Cg(pECXT99a-*riboCg*)(pSH1) strains

The minimal media produced for the experiments with the strains Cg(pECXT99a-*riboCg*)(pSH1-*xylAB*) and Cg(pECXT99a-*riboCg*)(pSH1) are a combination of the compounds represented in Table A.22 and the specific amounts of carbon and correlating amount of sterile water given in Table A.23 for the different carbon sources. Giving the final carbon source concentrations at 1 % glucose, a mixture of 1 % glucose and 1 % xylose, and 1 % xylose for the different minimal medias.

Table A.22: This table includes the components utilised for the production of the minimal media used for the Cg(pECXT99a-*riboCg*)(pSH1-*xylAB*) and Cg(pECXT99a-*riboCg*)(pSH1) strains, with the compounds corresponding concentrations and amounts.

Compound	Concentration	Unit	Quantity in final solution	Unit
CGXII	-	-	20	mL
Biotin	0.2	g/L	25	μL
PCA	30	g/L	25	μL
TES	-	-	25	μL
Tetracylin	10	g/L	12.5	μL
Kanamycin	50	g/L	12.5	μL
IPTG	0.5	M	62.5	μL

Table A.23: This table includes the different carbon source and sterile water amounts for the different conditions for the Cg(pECXT99a-*riboCg*)(pSH1-*xylAB*) and Cg(pECXT99a-*riboCg*)(pSH1) strains, to be mixed with the components represented in Table A.20 making the different minimal medias for the strains.

Compound	Concentration	Unit	Quantity in final solution	Unit
Glucose solution	1	%	625	μL
Sterile water	-	-	4.212	mL
Glucose solution	1	%	625	μL
Xylose solution	1	%	2500	μL
Sterile water	-	-	1.712	mL
Xylose solution	1	%	2500	μL
Sterile water	-	-	2.337	mL

B Bioreactor solutions

This section includes the solutions utilised during the bioreactor fermentation.

B.1 Minimal media

The minimal media produced with the final concentration of 1 % xylose as carbon source is represented in Table B.24.

Table B.24: This table includes the components utilised for the production of the minimal media used for the fed-batch fermentation of the Cg(pECXT99a-*riboCg*)(pSH1-*xylAB*) strains, with a concentration of 1 % xylose. The compounds are represented with their corresponding concentrations and amounts.

Compound	Concentration	Unit	Quantity in final solution	Unit
CGXII	-	-	400	mL
Xylose solution	10	%	50	mL
Biotin	0.2	g/L	500	μL
PCA	30	g/L	500	μL
TES	-	-	500	μL
Tetracylin	10	g/L	250	μL
Kanamycin	50	g/L	250	μL
IPTG	0.5	M	500	μL

B.2 Feed solution

In Table B.25 the composition of the xylose 5 % feed solution, utilised during the bioreactor fermentation, is represented.

Table B.25: This table includes the components utilised for the production of feed solution used during fermentation, with the final 5 % xylose concentration. The compounds use are represented with their corresponding concentrations and amounts.

Compound	Concentration	Unit	Quantity in final solution	Unit
Xylose solution	10	%	50	mL
Milli-Q water			50	mL
Final volume			100	mL

B.3 Acid and base solution

For the adjustment of the pH in the bioreactor fermentation the phosphoric acid (P_3HO_4) and potassium hydroxide(KOH), solutions used are represented in table B.26 and B.27.

Table B.26: This table includes the components utilised for the production of the acid solution used during fermentation, made of phosphoric acid (P_3HO_4), with the compounds corresponding concentrations and amounts.

Compound	Concentration	Unit	Quantity in final solution	Unit
P_3HO_4	85	%	23.53	mL
Milli-Q water			200	mL

Table B.27: This table includes the components utilised for the production of the base solution used during fermentation, made of potassium hydroxide (KOH), with the compounds corresponding concentrations and amounts.

Compound	Concentration	Unit	Quantity in final solution	Unit
KOH			56.11	g
Milli-Q water			200	mL

C Calculations from precultur OD_{600} values

To optimise an equal starting point for each sample in different conditions performed in the same biolector, the OD_{600} values of the precultures were measured to calculate the amount needed for a starting point of 1 OD_{600}. The equation utilised is;

$$V_1 \cdot C_1 = V_2 \cdot C_2 \tag{C.1}$$

C_1 is the OD_{600} value of the preculture, C_2 is the intended OD_{600} value starting point for the experiment and is set to 1 OD_{600}, while V_2 is the starting volume of the experiment at 1 mL. V_1 is the volume to be calculated, and correlates to the amount of preculture used for inoculation of experiment. In Table C.28, C.29 and C.30 the OD_{600} values and the correlating inoculation amount for the strains Cg(pECXT99a - *riboCg*)(pVWEx1 - *fbp*), CgΔ*altR*(pECXT99a-*riboCg*) and Cg(pECXT99a - *riboCg*)(pSH1 - *xylAB*) are shown respectively.

Table C.28: OD_{600} values taken of precultures from strains Cg(pECXT99a - *riboCg*)(pVWEx1-*fbp*) and Cg(pECXT99a - *riboCg*)(pVWEx1), and the correlating amount calculated for further inoculation.

Strain	Sample	OD_{600}	Amount used for inoculation [μL]
Cg(pECXT99a - *riboCg*)(pVWEx1 - *fbp*)	1	17	59
	2	18	56
	3	6	167
Cg(pECXT99a - *riboCg*)(pVWEx1)	1	6	167
	2	8	125
	3	13	77

Table C.29: OD_{600} values take of precultures from strains CgΔ*altR*(pECXT99a - *riboCg*) and CgΔ*altR*(pECXT99a) , and the correlating amount calculated for further inoculation.

Strain	Sample	OD_{600}	Amount used for inoculation [μL]
CgΔ*altR*(pECXT99a - *riboCg*)	1	5	200
	2	3	333
	3	3	333
CgΔ*altR*(pECXT99a)	1	0.5	1667
	2	5	200
	3	5	200

Table C.30: OD_{600} values taken of precultures from strains Cg(pECXT99a - *riboCg*)(pSH1-*xylAB*) and Cg(pECXT99a - *riboCg*)(pSH1), and the correlating amount calculated for further inoculation.

Strain	Sample	OD_{600}	Amount used for inoculation [μL]
Cg(pECXT99a - *riboCg*)(pSH1-*xylAB*)	1	9	111
	2	9	111
	3	8	125
Cg(pECXT99a - *riboCg*)(pSH1)	1	10	100
	2	8	125
	3	10	100

D Biolector experiment calculations

This sections represents all the calculations performed for the biolector experiments done on the strains Cg(pECXT99a-*riboCg*) (pVWEx1-*fbp*) and Cg(pECXT99a-*riboCg*)(pVWEx1), CgΔ*altR*(pECXT99a-*riboCg*) and CgΔ*altR*(pECXT99a), and Cg(pECXT99a-*riboCg*)(pSH1-*xylAB*) and Cg(pECXT99a-*riboCg*)(pSH1).

D.1 Calculation of correlation coefficient from final OD_{600} values measured from Biolector

To utilise the measurements taken from the biolector, a correlation coefficient was calculated from the last measured value and the correlating OD_{600} value. This was done for each sample of both strains in their corresponding conditions. The correlation factor is calculated by utilising Equation D.1. r_i is the correlation coefficient for sample i calculated by dividing the initial OD_{600} value for sample i, x_i, with the measured value for sample i given by the biolector, y_i.

$$r_i = \frac{x_i}{y_i} \tag{D.1}$$

OD_{600} values, the measured value from the biolector and the corresponding correlation coefficient for each sample of the strains Cg(pECXT99a - *riboCg*)(pVWEx1-*fbp*), CgΔ*altR*(pECXT99a - *riboCg*) and Cg(pECXT99a - *riboCg*)(pSH1-*xylAB*) in the different conditions set are represented in Table D.31, D.32 and D.33 respectively.

Table D.31: OD_{600} values and the measured value from the biolector taken at the final point of the experiment for each sample of the strains Cg(pECXT99a - *riboCg*)(pVWEx1-*fbp*) and Cg(pECXT99a - *riboCg*)(pVWEx1) are represented in this table with their corresponding correlation coefficient. The samples are divided into sections of the different carbon source conditions; 1% glucose, 1% glucose with 1% fructose, and 1% fructose.

Carbon source	Strain	Sample	OD_{600}	Value from Biolector	Correlation coefficient
Glucose 1%					
	Cg(pECXT99a - *riboCg*)(pVWEx1-*fbp*)	1	35	140.67	0.25
	Cg(pECXT99a - *riboCg*)(pVWEx1-*fbp*)	2	22	132.21	0.17
	Cg(pECXT99a - *riboCg*)(pVWEx1-*fbp*)	3	21	134.19	0.16
	Cg(pECXT99a - *riboCg*)(pVWEx1)	1	25	123.71	0.20
	Cg(pECXT99a - *riboCg*)(pVWEx1)	2	20	128.8	0.16
	Cg(pECXT99a - *riboCg*)(pVWEx1)	3	22	115.46	0.19
Glucose 1%, Fructose 1%					
	Cg(pECXT99a - *riboCg*)(pVWEx1-*fbp*)	1	27	216.68	0.13
	Cg(pECXT99a - *riboCg*)(pVWEx1-*fbp*)	2	29	213.29	0.14
	Cg(pECXT99a - *riboCg*)(pVWEx1-*fbp*)	3	31	238.55	0.13
	Cg(pECXT99a - *riboCg*)(pVWEx1)	1	30	232.72	0.13
	Cg(pECXT99a - *riboCg*)(pVWEx1)	2	32	215.56	0.15
	Cg(pECXT99a - *riboCg*)(pVWEx1)	3	29	201.36	0.14
Fructose 1%					
	Cg(pECXT99a - *riboCg*)(pVWEx1-*fbp*)	1	14	118.01	0.12
	Cg(pECXT99a - *riboCg*)(pVWEx1-*fbp*)	2	17	115.89	0.15
	Cg(pECXT99a - *riboCg*)(pVWEx1-*fbp*)	3	16	132.93	0.12
	Cg(pECXT99a - *riboCg*)(pVWEx1)	1	14	139.57	0.10
	Cg(pECXT99a - *riboCg*)(pVWEx1)	2	15	130.76	0.12
	Cg(pECXT99a - *riboCg*)(pVWEx1)	3	18	119.59	0.15

Table D.32: OD_{600} values and the measured value from the biolector taken at the final point of the experiment for each sample of the strains CgΔ*altR*(pECXT99a - *riboCg*) and CgΔ*altR*(pECXT99a) are represented in this table with their corresponding correlation coefficient. The samples are divided into sections of the different carbon source conditions; 1% glucose, 1% glucose with 1% mannitol, and 1% mannitol.

Carbon source	Strain	Sample	OD_{600}	Value from Biolector	Correlation coefficient
Glucose 1%					
	CgΔ*altR*(pECXT99a - *riboCg*)	1	21	122.21	0.17
	CgΔ*altR*(pECXT99a - *riboCg*)	2	18	124.12	0.15
	CgΔ*altR*(pECXT99a - *riboCg*)	3	21	139.6	0.15
	CgΔ*altR*(pECXT99a)	1	22	186.11	0.12
	CgΔ*altR*(pECXT99a)	2	27	178.41	0.15
	CgΔ*altR*(pECXT99a)	3	26	178.07	0.15
Glucose 1%, Mannitol 1%					
	CgΔ*altR*(pECXT99a - *riboCg*)	1	4	56.08	0.07
	CgΔ*altR*(pECXT99a - *riboCg*)	2	31	197.59	0.16
	CgΔ*altR*(pECXT99a - *riboCg*)	3	34	205.25	0.17
	CgΔ*altR*(pECXT99a)	1	43	328.52	0.13
	CgΔ*altR*(pECXT99a)	2	40	282.56	0.14
	CgΔ*altR*(pECXT99a)	3	39	291.94	0.13
Mannitol 1%					
	CgΔ*altR*(pECXT99a - *riboCg*)	1	14	100.87	0.14
	CgΔ*altR*(pECXT99a - *riboCg*)	2	18	111.53	0.16
	CgΔ*altR*(pECXT99a - *riboCg*)	3	21	118.39	0.18
	CgΔ*altR*(pECXT99a)	1	21	167.19	0.13
	CgΔ*altR*(pECXT99a)	2	22	143.73	0.15
	CgΔ*altR*(pECXT99a)	3	21	145.88	0.14

Table D.33: OD_{600} values and the measured value from the biolector taken at the final point of the experiment for each sample of the strains Cg(pECXT99a - *riboCg*)(pSH1-*xylAB*) and Cg(pECXT99a - *riboCg*)(pSH1) are represented in this table with their corresponding correlation coefficient. The samples are divided into sections of the different carbon source conditions; 1% glucose, 1% glucose with 1% xylose, and 1% xylose.

Carbon source	Strain	Sample	OD_{600}	Value from Biolector	Correlation coefficient
Glucose 1%					
	Cg(pECXT99a - *riboCg*)(pSH1-*xylAB*)	1	21	124.02	0.169
	Cg(pECXT99a - *riboCg*)(pSH1-*xylAB*)	2	20	116.96	0.171
	Cg(pECXT99a - *riboCg*)(pSH1-*xylAB*)	3	19	115.51	0.165
	Cg(pECXT99a - *riboCg*)(pSH1)	1	18	116.86	0.154
	Cg(pECXT99a - *riboCg*)(pSH1)	2	20	121.05	0.165
	Cg(pECXT99a - *riboCg*)(pSH1)	3	20	115.47	0.173
Glucose 1%, Xylose 1%					
	Cg(pECXT99a - *riboCg*)(pSH1-*xylAB*)	1	14	67.01	0.209
	Cg(pECXT99a - *riboCg*)(pSH1-*xylAB*)	2	33	166.44	0.198
	Cg(pECXT99a - *riboCg*)(pSH1-*xylAB*)	3	38	177.22	0.214
	Cg(pECXT99a - *riboCg*)(pSH1)	1	4	34.5	0.116
	Cg(pECXT99a - *riboCg*)(pSH1)	2	25	122.82	0.204
	Cg(pECXT99a - *riboCg*)(pSH1)	3	20	95.29	0.210
Xylose 1%					
	Cg(pECXT99a - *riboCg*)(pSH1-*xylAB*)	1	1.7	35.78	0.048
	Cg(pECXT99a - *riboCg*)(pSH1-*xylAB*)	2	1.3	32.99	0.039
	Cg(pECXT99a - *riboCg*)(pSH1-*xylAB*)	3	7	52.1	0.134
	Cg(pECXT99a - *riboCg*)(pSH1)	1	0.7	31.2	0.022
	Cg(pECXT99a - *riboCg*)(pSH1)	2	0.7	30.21	0.023
	Cg(pECXT99a - *riboCg*)(pSH1)	3	0.6	27.53	0.022

D.2 Calculated OD_{600} values

With the correlation coefficients given in Appendix D.1, all the OD_{600} values over time for the samples in the biolector were calculated by using Equation D.2.

$$x_i = \frac{r_i}{y_i} \tag{D.2}$$

x_i is the OD_{600} value for a given sample, r_i is the correlation coefficient correlating to the sample, and y_i is the measured value for sample i provided by the biolector.

The average and standard deviation were then calculated for each strain in the different conditions. This was done by utilising Equation D.3 and D.4. n represents the number of parallel samples taken at a specific point, and x represents the specific value one wants to analyse. In this case, x stands for the particular OD_{600} value for the sample i. μ represents the further the mean of the parallels analysed.

$$A = \frac{1}{n} \sum_{i=1}^{n} x_i \tag{D.3}$$

$$\sigma = \sqrt{\frac{\sum (x_i - \mu)^2}{n}} \tag{D.4}$$

In Table 5.1, 5.2 and 5.3, the final average OD_{600} values for each strain in their different carbon source condition, and their correlating standard deviation values are represented.

D.3 Calculations of growth rate

To calculate the growth rate of each sample, the OD_{600} values calculated are plotted against the corresponding time from the 25-hour fermentation timeline. The Y-axis is then converted to logarithmic values, resulting in $Log(OD_{600})$ plotted against time. The equation for this conversion is shown below.

$$y = \log(OD_{600(i)}) \tag{D.5}$$

The logarithmic value of the OD_{600} measurement is represented by y, and i stands for the specific sample taken at a particular time. The plots made for the different experiments with different strains and conditions are represented further in this chapter. For each condition and strain, there are three parallels. The growth curve for each parallel is plotted in one figure for comparison. The exponential growth phase for each parallel has then been plotted separately, and the specific growth rate was found from the trendline. These trend lines are respectively given in Table D.34, D.35 and D.36 for the fermentations performed at biolector scale.

D.3.1 Trendlines for the Cg(pECXT99a-*riboCg*)(pVWEx1-*fbp*) and Cg(pECXT99a-*riboCg*)(pVWEx1) strains

For the three conditions sett for strains Cg(pECXT99a-*riboCg*)(pVWEx1-*fbp*) and Cg(pECXT99a-*riboCg*)(pVWEx1), the trend lines are given in Table D.34. The trend lines are found from the plots given in Figure D.1, D.2, D.3, D.4, D.5 and D.6. From the trendlines, the specific growth rate is found. These values are given in Chapter 5.2.1, Table 5.1.

Table D.34: Equations for the trend lines of strain Cg(pECXT99a-*riboCg*)(pVWEx1-*fbp*) and Cg(pECXT99a-*riboCg*)(pVWEx1) at different carbon source conditions, found from Figures D.1, D.2, D.3, D.4, D.5 and D.6, are represented with their corresponding sample number. G and F stands for glucose and fructose.

Carbon source	Amount [%]	Sample nr	**Cg(pECXT99a-*riboCg*)(pVWEx1-*fbp*)**	**Cg(pECXT99a-*riboCg*)(pVWEx1)**
G	1	1	$y = 4.2716\ e^{0.0966x}$	$y = 3.2309\ e^{0.1046x}$
	1	2	$y = 2.9426\ e^{0.1023x}$	$y = 3.0109\ e^{0.1348x}$
	1	3	$y = 3.5286\ e^{0.111x}$	$y = 3.2815\ e^{0.1198x}$
G and F	1 + 1	1	$y = 0.3478\ e^{0.2504x}$	$y = 1.2145\ e^{0.3313x}$
	1 + 1	2	$y = 0.41\ e^{0.2835x}$	$y = 1.1351\ e^{0.3199x}$
	1 + 1	3	$y = 0.9024\ e^{0.3322x}$	$y = 0.9309\ e^{0.2953x}$
F	1	1	$y = 0.4453\ e^{0.2411x}$	$y = 1.4128\ e^{0.2643x}$
	1	2	$y = 0.6842\ e^{0.2491x}$	$y = 1.4856\ e^{0.244x}$
	1	3	$y = 1.0241\ e^{0.2845x}$	$y = 1.6239\ e^{0.224x}$

Glucose as carbon source

With glucose 1% as the carbon source for strains Cg(pECXT99a-*riboCg*)(pVWEx1-*fbp*) and Cg(pECXT99a-*riboCg*)(pVWEx1), the logarithmic OD_{600} with the corresponding trendlines are plotted in Figure D.1, D.2 respectively.

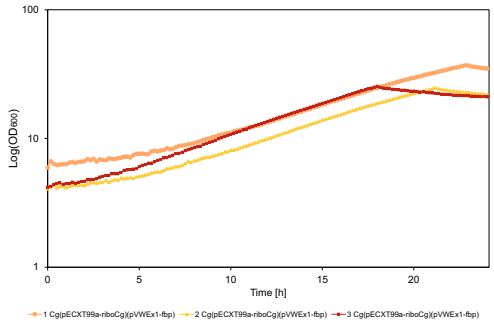

(a) All three parallels with their complete Log(OD_600) values are represented over 25 hours.

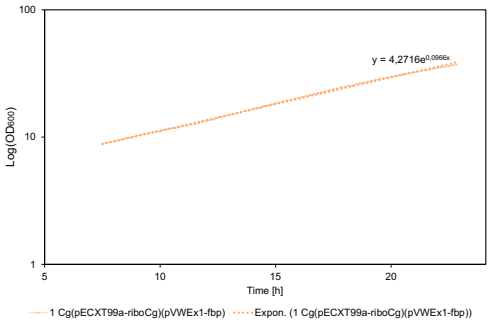

(b) The exponential growth phase of parallel number 3, with its trendline. Equation represented in Table D.34.

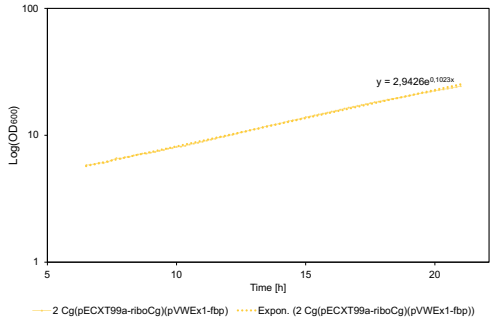

(c) The exponential growth phase of parallel number 2, with its trendline. Equation represented in Table D.34.

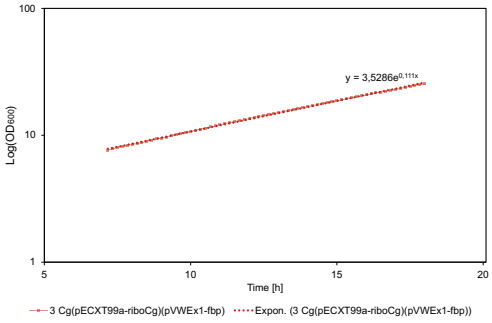

(d) The exponential growth phase of parallel number 3, with its trendline. Equation represented in Table D.34.

Figure D.1: These plots represent the growth curves of three parallels of the strain Cg(pECXT99a-*riboCg*)(pVWEx1-*fbp*) and Cg(pECXT99a-*riboCg*)(pVWEx1), and their corresponding trend lines, in the exponential phase incubated with glucose 1%. The OD_{600} values are plotted against their corresponding time, between the time interval of 0 and 25 hours.

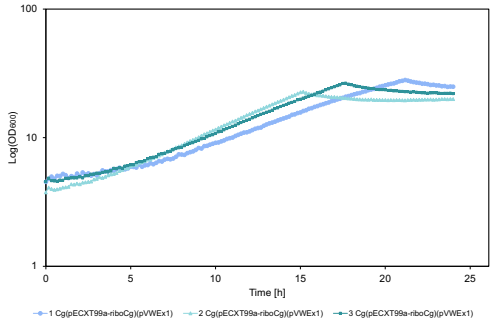

(a) All three parallels with their complete Log(OD_600) values are represented over 25 hours.

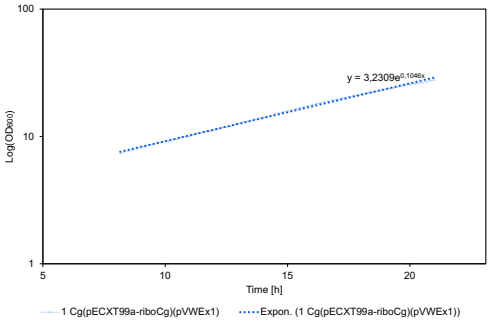

(b) The exponential growth phase of parallel number 1, with its trendline. Equation represented in Table D.34.

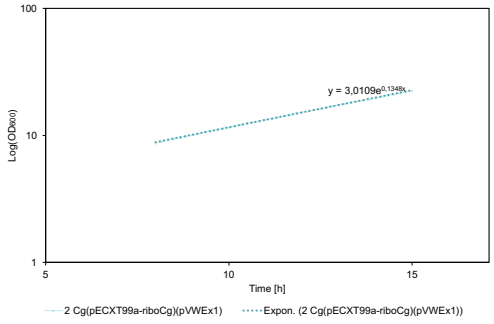

(c) The exponential growth phase of parallel number 2, with its trendline. Equation represented in Table D.34.

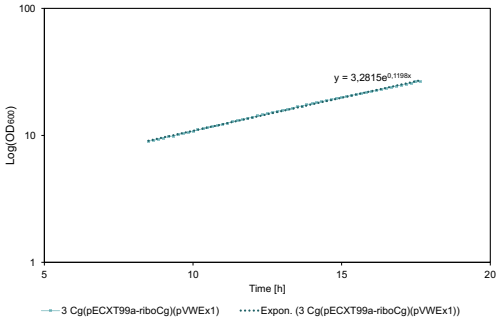

(d) The exponential growth phase of parallel number 3, with its trendline. Equation represented in Table D.34.

Figure D.2: These plots represent the growth curves of three parallels of the strain Cg(pECXT99a-*riboCg*)(pVWEx1-*fbp*) and Cg(pECXT99a-*riboCg*)(pVWEx1), and their corresponding trend lines, in the exponential phase incubated with glucose 1%. The OD_{600} values are plotted against their corresponding time, between the time interval of 0 and 25 hours.

Glucose and fructose as carbon source

With a mixture of glucose 1% and fructose 1% as the carbon source for strains Cg(pECXT99a-*riboCg*)(pVWEx1-*fbp*) and Cg(pECXT99a-*riboCg*)(pVWEx1), the logarithmic OD_{600} with the corresponding trendlines are plotted in Figure D.3, D.4 respectively.

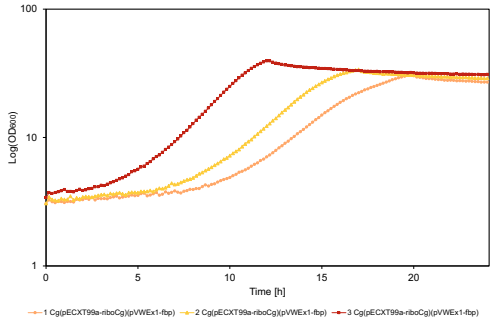

(a) All three parallels with their complete Log(OD_600) values are represented over 25 hours.

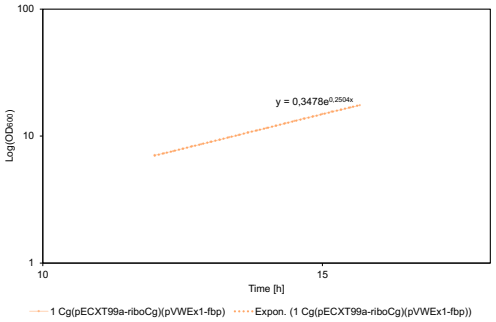

(b) The exponential growth phase of parallel number 1, with its trendline. Equation represented in Table D.34.

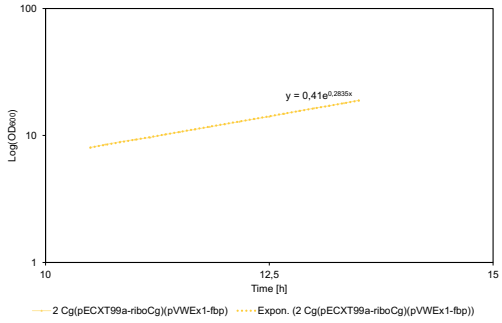

(c) The exponential growth phase of parallel number 2, with its trendline. Equation represented in Table D.34.

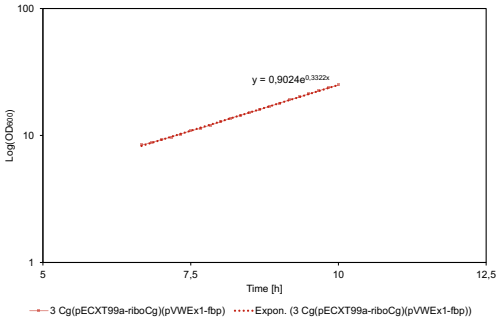

(d) The exponential growth phase of parallel number 3, with its trendline. Equation represented in Table D.34.

Figure D.3: These plots represent the growth curves of three parallels of the strain Cg(pECXT99a-*riboCg*)(pVWEx1-*fbp*) and Cg(pECXT99a-*riboCg*)(pVWEx1), and their corresponding trend lines, in the exponential phase incubated with a mixture of glucose 1% and fructose 1%. The OD_{600} values are plotted against their corresponding time, between the time interval of 0 and 25 hours.

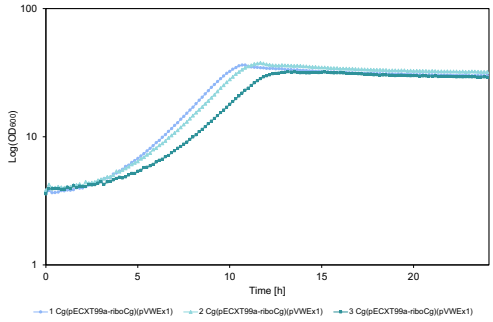

(a) All three parallels with their complete Log(OD_600) values are represented over 25 hours.

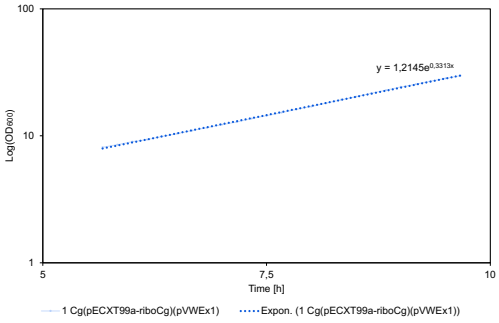

(b) The exponential growth phase of parallel number 1, with its trendline. Equation represented in Table D.34.

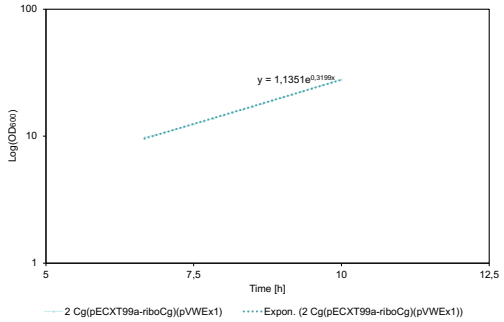

(c) The exponential growth phase of parallel number 2, with its trendline. Equation represented in Table D.34.

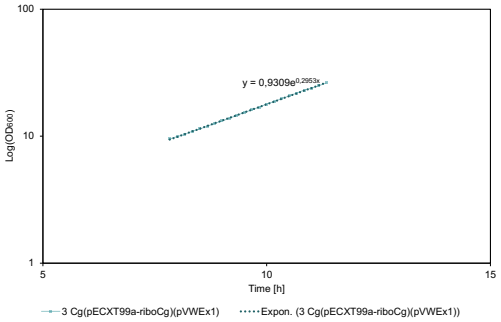

(d) The exponential growth phase of parallel number 3, with its trendline. Equation represented in Table D.34.

Figure D.4: These plots represent the growth curves of three parallels of the strain Cg(pECXT99a-*riboCg*)(pVWEx1-*fbp*) and Cg(pECXT99a-*riboCg*)(pVWEx1), and their corresponding trend lines, in the exponential phase incubated with glucose 1% and fructose 1%. The OD_{600} values are plotted against their corresponding, between the time interval of 0 and 25 hours.

Fructose as carbon source

With fructose 1% as the carbon source for strains Cg(pECXT99a-*riboCg*)(pVWEx1-*fbp*) and Cg(pECXT99a-*riboCg*)(pVWEx1), the logarithmic OD_{600} with the corresponding trendlines are plotted in Figure D.5 and D.6 respectively.

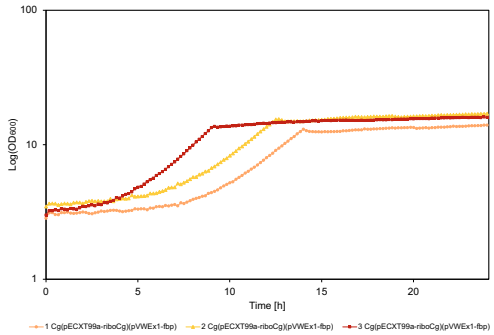

(a) All three parallels with their complete Log(OD_600) values are represented over 25 hours.

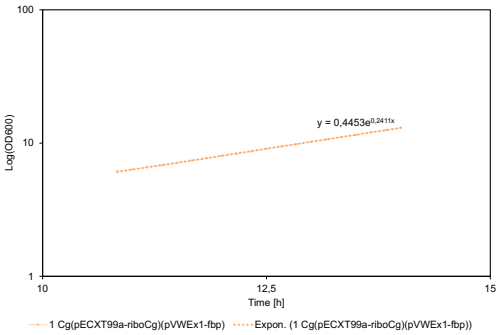

(b) The exponential growth phase of parallel number 1, with its trendline. Equation represented in Table D.34.

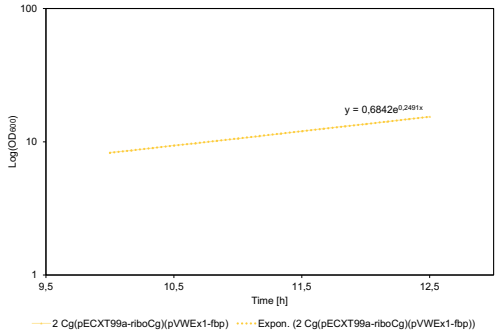

(c) The exponential growth phase of parallel number 2, with its trendline. Equation represented in Table D.34.

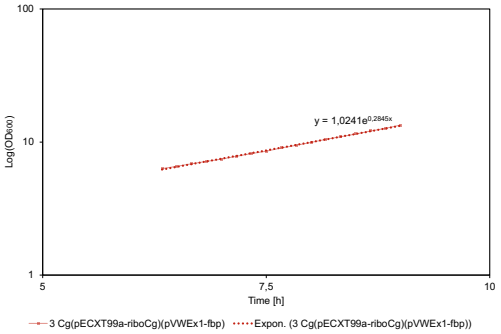

(d) The exponential growth phase of parallel number 3, with its trendline. Equation represented in Table D.34.

Figure D.5: These plots represent the growth curves of three parallels of the strain Cg(pECXT99a-*riboCg*)(pVWEx1-*fbp*) and Cg(pECXT99a-*riboCg*)(pVWEx1), and their corresponding trend lines, in the exponential phase incubated with fructose 1%. The logarithmic OD_{600} values are plotted against their corresponding time, between the time interval of 0 and 25 hours.

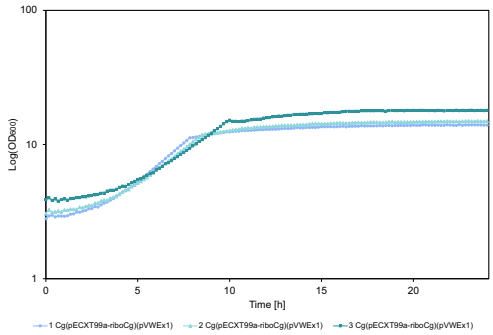

(a) All three parallels with their complete Log($OD_6$00) values are represented over 25 hours.

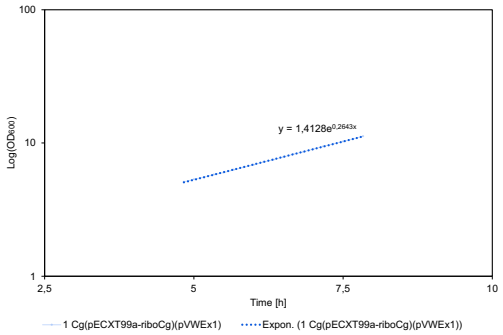

(b) The exponential growth phase of parallel number 1, with its trendline. Equation represented in Table D.34.

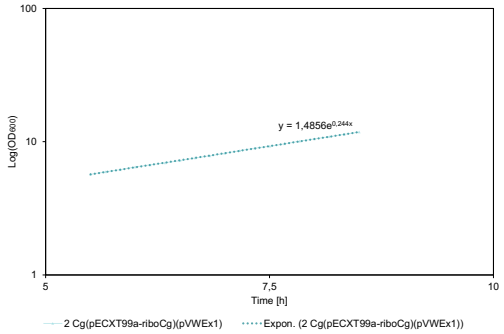

(c) The exponential growth phase of parallel number 2, with its trendline. Equation represented in Table D.34.

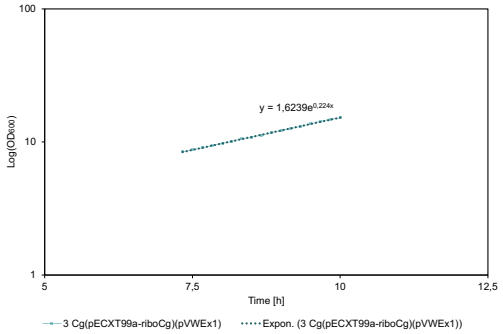

(d) The exponential growth phase of parallel number 3, with its trendline. Equation represented in Table D.34.

Figure D.6: These plots represent the growth curves of three parallels of the strain Cg(pECXT99a-*riboCg*)(pVWEx1-*fbp*) and Cg(pECXT99a-*riboCg*)(pVWEx1), and their corresponding trend lines, in the exponential phase incubated with fructose 1%. The OD_{600} values are plotted against their corresponding time, between the time interval of 0 and 25 hours.

c

D.3.2 Trendlines for the CgΔ*altR*(pECXT99a-*riboCg*) and CgΔ*altR*(pECXT99a) strains

For the three conditions sett for strains CgΔ*altR*(pECXT99a-*riboCg*) and CgΔ*altR*(pECXT99a) , the trend lines are given in Table D.35. The trend lines are found from the plots given in Figure D.7, D.8, D.9, D.10, D.11 and D.12. From the trendlines, the specific growth rate is found. These values are given in Chapter 5.2.1, Table 5.2.

Table D.35: Equations for the trend lines of strain CgΔ*altR*(pECXT99a-*riboCg*) and CgΔ*altR*(pECXT99a) at different carbon source conditions, found from Figures D.7, D.8, D.9, D.10, D.11 and D.12, are represented with their corresponding sample number.

Carbon source	Amount [%]	Sample nr	**CgΔ*altR*(pECXT99a-*riboCg*)**	**CgΔ*altR*(pECXT99a)**
Glucose	1	1	$y = 4.4975\ e^{0.1055x}$	$y = 1.7188\ e^{0.256x}$
	1	2	$y = 3.6977\ e^{0.1177x}$	$y = 1.8019\ e^{0.2431x}$
	1	3	$y = 3.5543\ e^{0.1391x}$	$y = 1.6247\ e^{0.2403x}$
Glucose and Mannitol	1 + 1	1	$y = 0.6197\ e^{0.0702x}$	$y = 0.4916\ e^{0.4058x}$
	1 + 1	2	$y = 1.3431\ e^{0.1493x}$	$y = 0.0619\ e^{0.2909x}$
	1 + 1	3	$y = 1.3163\ e^{0.2095x}$	$y = 0.0363\ e^{0.3686x}$
Mannitol	1	1	$y = 0.8146\ e^{0.1101x}$	$y = 0.7098\ e^{0.3268x}$
	1	2	$y = 0.8344\ e^{0.1453x}$	$y = 0.0736\ e^{0.2998x}$
	1	3	$y = 1.3142\ e^{0.1711x}$	$y = 0.0748\ e^{0.2834x}$

Glucose as carbon source

With glucose 1% as the carbon source for strains CgΔ*altR*(pECXT99a-*riboCg*) and CgΔ*altR*(pECXT99a) , the logarithmic OD_{600} with the corresponding trendlines are plotted in Figure D.7 and D.8 respectively.

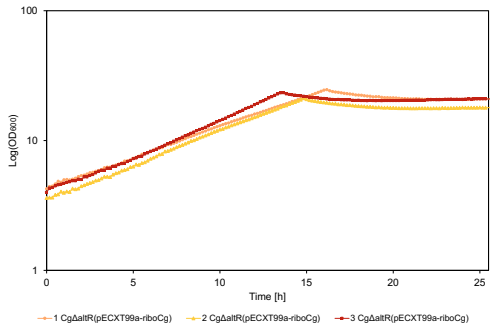

(a) All three parallels with their complete Log(OD_600) values are represented over 25 hours.

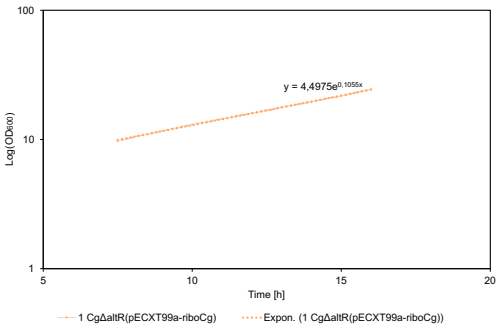

(b) The exponential growth phase of parallel number 1, with its trendline. Equation represented in Table D.35.

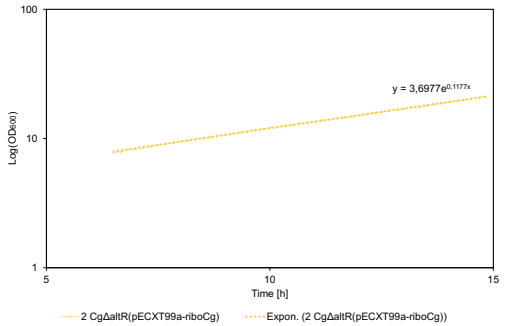

(c) The exponential growth phase of parallel number 2, with its trendline. Equation represented in Table D.35.

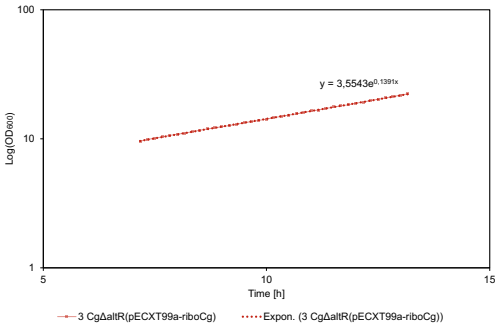

(d) The exponential growth phase of parallel number 3, with its trendline. Equation represented in Table D.35.

Figure D.7: These plots represent the growth curves of three parallels of the strain CgΔ*altR*(pECXT99a-*riboCg*) and their corresponding trend lines, in the exponential phase incubated with a mix of glucose 1%. The OD_{600} values are plotted against their corresponding time, between the time interval of 0 and 25 hours.

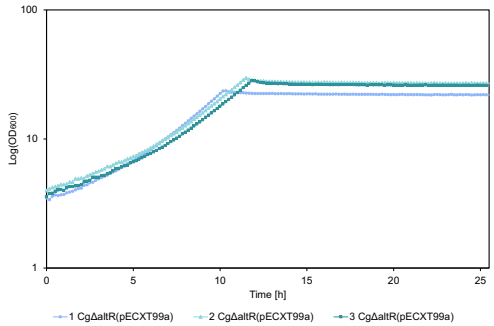

(a) All three parallels with their complete Log(OD_600) values are represented over 25 hours.

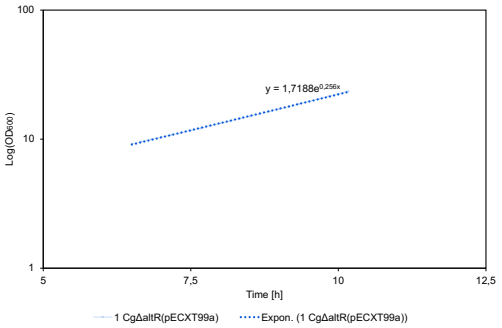

(b) The exponential growth phase of parallel number 1, with its trendline. Equation represented in Table D.35.

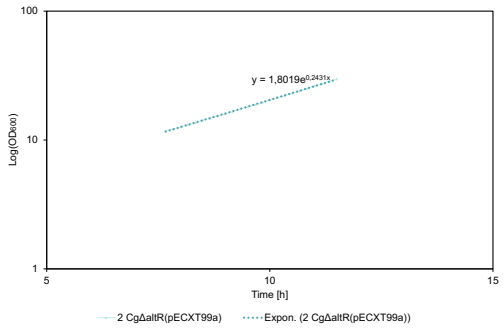

(c) The exponential growth phase of parallel number 2, with its trendline. Equation represented in Table D.35.

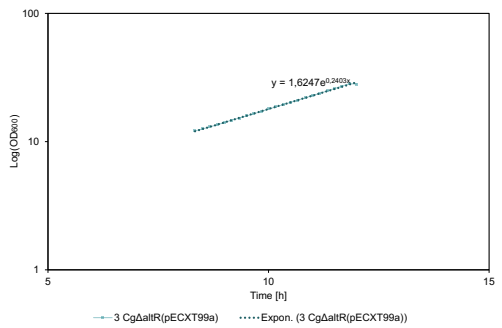

(d) The exponential growth phase of parallel number 3, with its trendline. Equation represented in Table D.35.

Figure D.8: These plots represent the growth curves of three parallels of the strain CgΔ*altR*(pECXT99a) and their corresponding trend lines, in the exponential phase incubated with a mix of glucose 1%. The OD_{600} values are plotted against their corresponding time, between the time interval of 0 and 25 hours.

Glucose and Mannitol as carbon source

With glucose 1% as the carbon source for strains CgΔ*altR*(pECXT99a-*riboCg*) and CgΔ*altR*(pECXT99a) , the logarithmic OD_{600} with the corresponding trendlines are plotted in Figure D.9 and D.10 respectively.

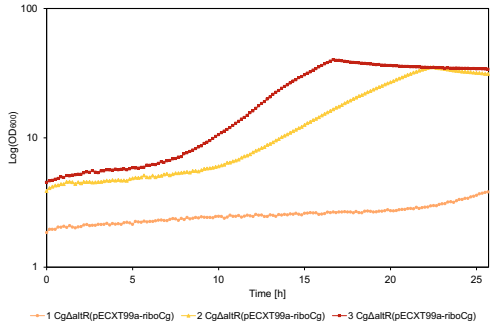

(a) All three parallels with their complete Log($OD_6$00) values are represented over 25 hours.

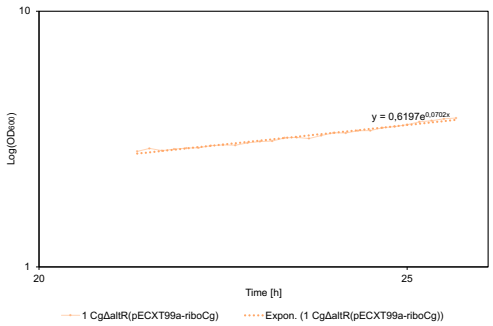

(b) The exponential growth phase of parallel number 1, with its trendline. Equation represented in Table D.35.

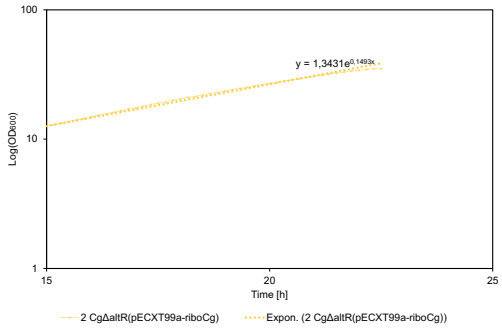

(c) The exponential growth phase of parallel number 2, with its trendline. Equation represented in Table D.35.

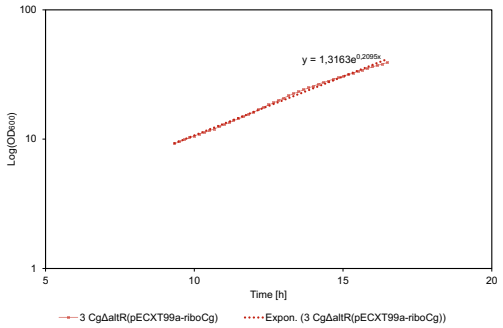

(d) The exponential growth phase of parallel number 3, with its trendline. Equation represented in Table D.35.

Figure D.9: These plots represent the growth curves of three parallels of the strain CgΔ*altR*(pECXT99a-*riboCg*) and their corresponding trend lines in the exponential phase incubated with a mix of glucose 1% and mannitol 1%. The OD_{600} values are plotted against their corresponding time, between the time interval of 0 and 25 hours.

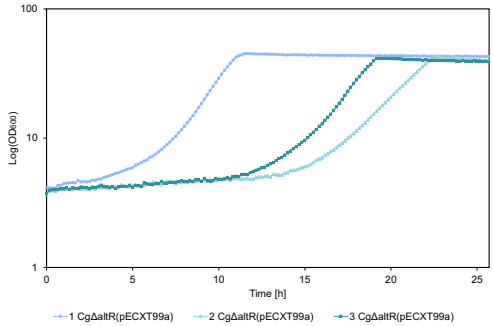

(a) All three parallels with their complete Log($OD_6$00) values are represented over 25 hours.

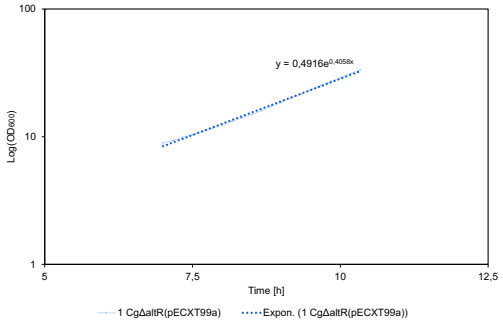

(b) The exponential growth phase of parallel number 1, with its trendline. Equation represented in Table D.35.

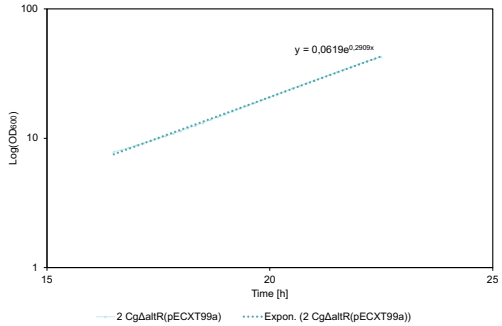

(c) The exponential growth phase of parallel number 2, with its trendline. Equation represented in Table D.35.

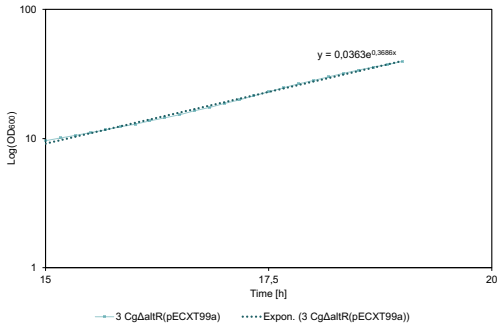

(d) The exponential growth phase of parallel number 3, with its trendline. Equation represented in Table D.35.

Figure D.10: These plots represent the growth curves of three parallels of the strain CgΔ*altR*(pECXT99a) and their corresponding trend lines, in the exponential phase incubated with glucose 1% and mannitol 1%. The OD_{600} values are plotted against their corresponding time, between the time interval of 0 and 25 hours.

Mannitol as carbon source

With glucose 1% as the carbon source for strains CgΔ*altR*(pECXT99a-*riboCg*) and CgΔ*altR*(pECXT99a) , the logarithmic OD_{600} with the corresponding trendlines are plotted in Figure D.11 and D.12 respectively.

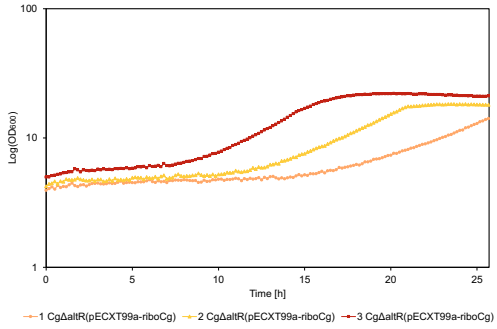

(a) All three parallels with their complete Log(OD_600) values are represented over 25 hours.

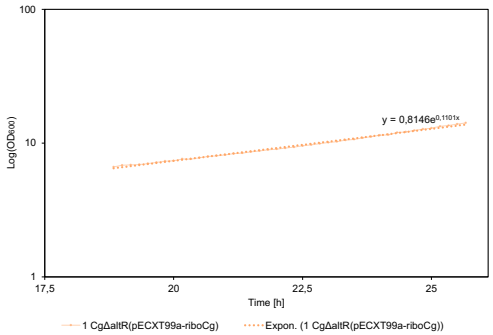

(b) The exponential growth phase of parallel number 1, with its trendline. Equation represented in Table D.35.

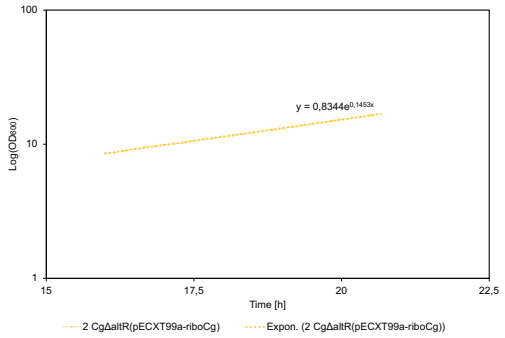

(c) The exponential growth phase of parallel number 2, with its trendline. Equation represented in Table D.35.

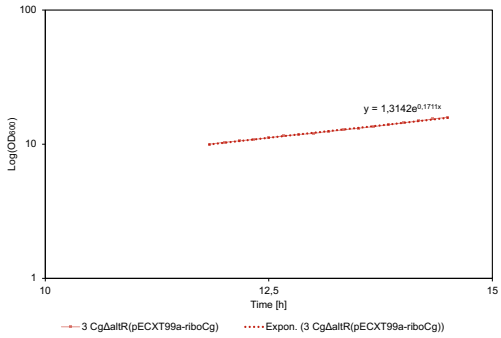

(d) The exponential growth phase of parallel number 3, with its trendline. Equation represented in Table D.35.

Figure D.11: These plots represent the growth curves of three parallels of the strain CgΔ*altR*(pECXT99a-*riboCg*) and their corresponding trend lines, in the exponential phase incubated with mannitol 1%. The OD_{600} values are plotted against their corresponding time, between the time interval of 0 and 25 hours.

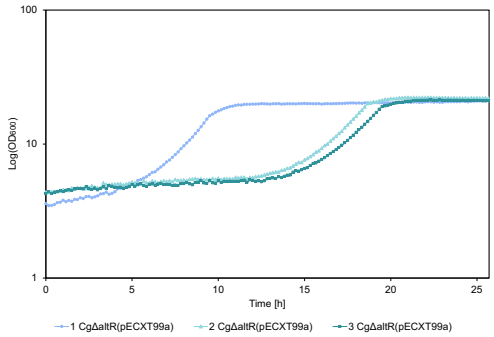

(a) All three parallels with their complete Log(OD_600) values are represented over 25 hours.

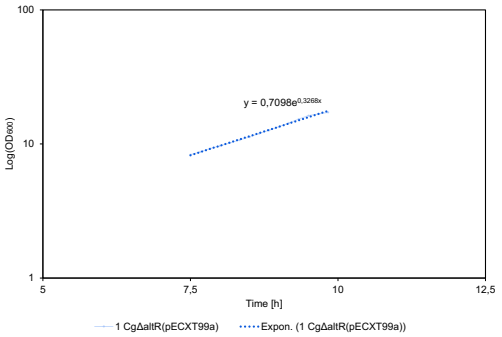

(b) The exponential growth phase of parallel number 1, with its trendline. Equation represented in Table D.35.

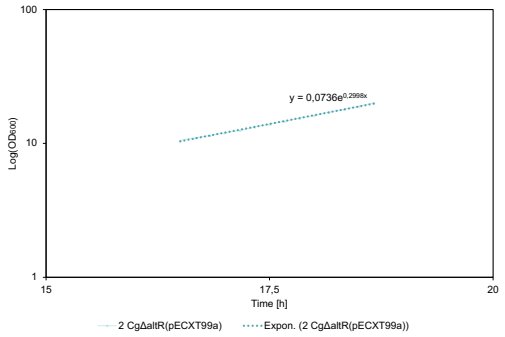

(c) The exponential growth phase of parallel number 2, with its trendline. Equation represented in Table D.35.

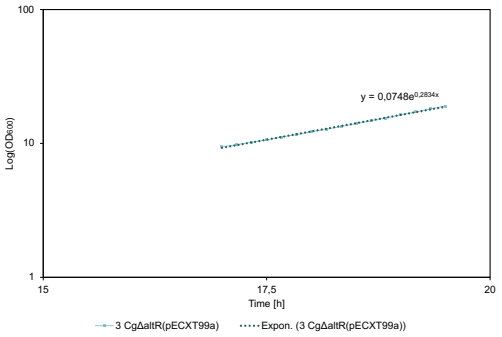

(d) The exponential growth phase of parallel number 3, with its trendline. Equation represented in Table D.35.

Figure D.12: These plots represent the growth curves of three parallels of the strain CgΔ*altR*(pECXT99a) and their corresponding trend lines, in the exponential phase incubated with mannitol 1%. The OD_{600} values are plotted against their corresponding time, between the time interval of 0 and 25 hours.

D.3.3 Trendlines for the Cg(pECXT99a-*riboCg*)(pSH1-*xylAB*) and Cg(pECXT99a-*riboCg*)(pSH1) strains

For the three conditions sett for strains Cg(pECXT99a-*riboCg*)(pSH1-*xylAB*) and Cg(pECXT99a-*riboCg*)(pSH1), the trend lines are given in Table D.36. The trend lines are found from the plots given in Figure D.13, D.14, D.15, D.16, D.17 and D.18. From the trendlines, the specific growth rate is found. These values are given in Chapter 5.2.1, Table 5.3.

Table D.36: Equations for the trend lines of strain Cg(pECXT99a-*riboCg*)(pSH1-*xylAB*) and Cg(pECXT99a-*riboCg*)(pSH1) at different carbon source conditions, found from Figures D.13, D.14, D.15, D.16, D.17 and D.18, are represented with their corresponding sample number.

Carbon source	Amount [%]	Sample nr	**Cg(pECXT99a-*riboCg*)(pSH1-*xylAB*)**	**Cg(pECXT99a-*riboCg*)(pSH1)**
Glucose	1	1	$y = 3.3305\ e^{0.1229x}$	$y = 2.5229\ e^{0.1305x}$
	1	2	$y = 2.9975\ e^{0.1255x}$	$y = 2.8426\ e^{0.1360x}$
	1	3	$y = 3.0375\ e^{0.1257x}$	$y = 2.7959\ e^{0.1272x}$
Glucose and Xylose	1 + 1	1	$y = 1.3637\ e^{0.0896x}$	$y = 3.1546\ e^{0.0104x}$
	1 + 1	2	$y = 1.6188\ e^{0.1261x}$	$y = 2.3456\ e^{0.1214x}$
	1 + 1	3	$y = 1.9929\ e^{0.1321x}$	$y = 1.0955\ e^{0.1131x}$
Xylose	1	1	$y = 1.4139\ e^{0.0085x}$	$y = 0.6251\ e^{0.0043x}$
	1	2	$y = 1.1663\ e^{0.0062x}$	$y = 0.6384\ e^{0.0037x}$
	1	3	$y = 2.7995\ e^{0.0376x}$	$y = 0.5706\ e^{0.0035x}$

Glucose as carbon source

With glucose 1% as the carbon source for strains Cg(pECXT99a-*riboCg*)(pSH1-

xylAB) and Cg(pECXT99a-*riboCg*)(pSH1), the logarithmic OD_{600} with the corresponding trendlines are plotted in Figure D.13 and D.14 respectively.

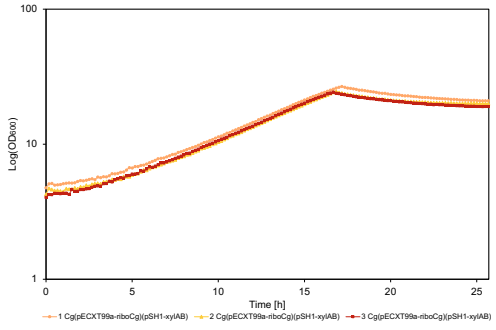

(a) All three parallels with their complete Log($OD_6$00) values are represented over 25 hours.

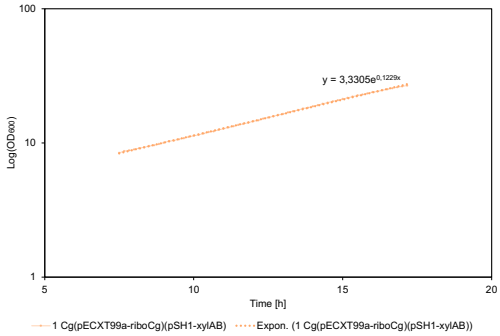

(b) The exponential growth phase of parallel number 1, with its trendline. Equation represented in Table D.36.

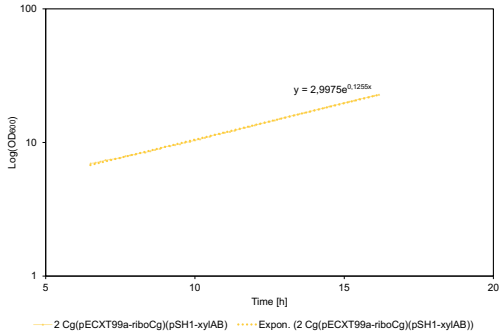

(c) The exponential growth phase of parallel number 2, with its trendline. Equation represented in Table D.36.

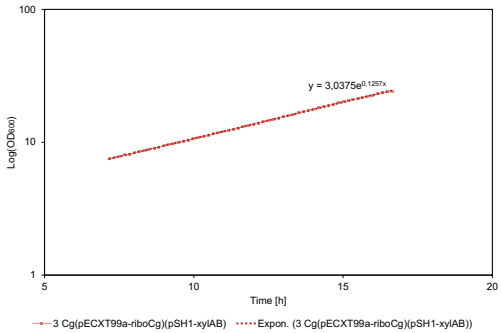

(d) The exponential growth phase of parallel number 3, with its trendline. Equation represented in Table D.36.

Figure D.13: These plots represent the growth curves of three parallels of the strain Cg(pECXT99a-*riboCg*)(pSH1-*xylAB*), and their corresponding trend lines, in the exponential phase incubated with a mixture of glucose 1%. The OD_{600} values are plotted against their corresponding time, between the time interval of 0 and 25 hours.

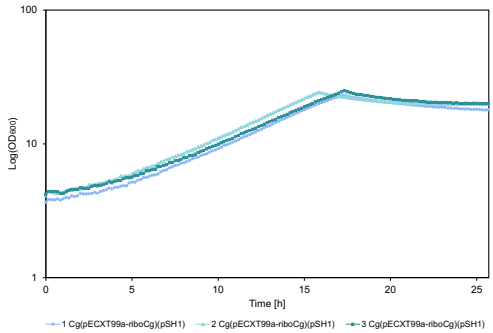

(a) All three parallels with their complete Log(OD_600) values are represented over 25 hours.

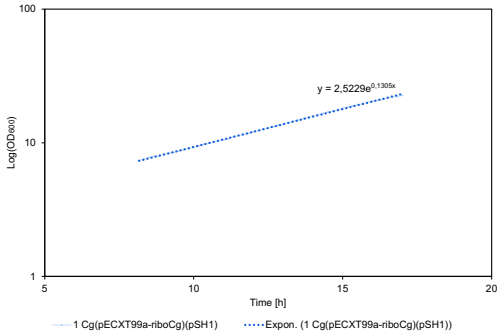

(b) The exponential growth phase of parallel number 1, with its trendline. Equation represented in Table D.36.

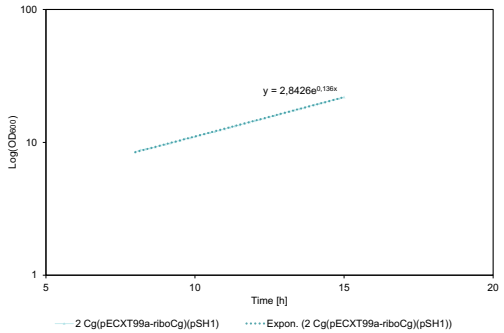

(c) The exponential growth phase of parallel number 2, with its trendline. Equation represented in Table D.36.

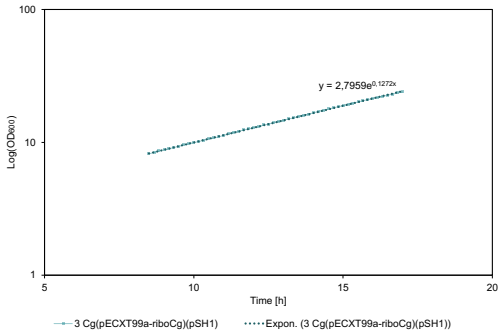

(d) The exponential growth phase of parallel number 3, with its trendline. Equation represented in Table D.36.

Figure D.14: These plots represent the growth curves of three parallels of the strain Cg(pECXT99a-*riboCg*)(pSH1) and their corresponding trend lines, in the exponential phase incubated with a mixture of glucose 1%. The OD_{600} values are plotted against their corresponding time, between the time interval of 0 and 25 hours.

Glucose and Xylose as carbon source

With a mixture of glucose 1% and xylose 1% as the carbon source for strains Cg(pECXT99a-*riboCg*)(pSH1-*xylAB*) and Cg(pECXT99a-*riboCg*)(pSH1), the logarithmic OD_{600} with the corresponding trendlines are plotted in Figure D.15 and D.16 respectively.

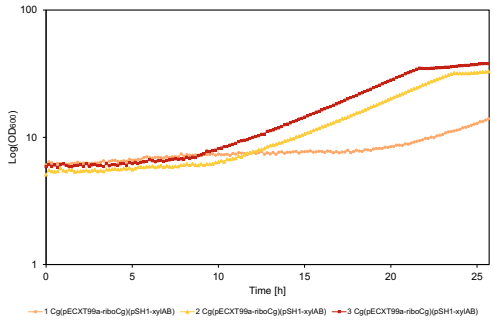

(a) All three parallels with their complete Log(OD_600) values are represented over 25 hours.

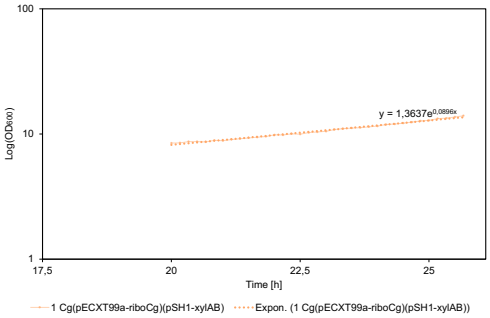

(b) The exponential growth phase of parallel number 1, with its trendline. Equation represented in Table D.36.

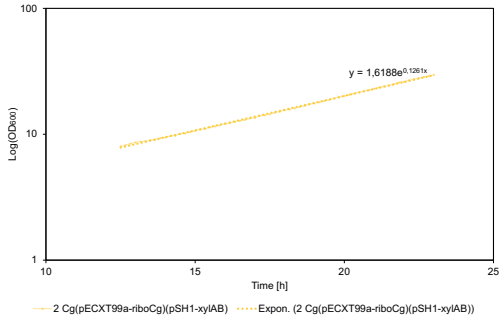

(c) The exponential growth phase of parallel number 2, with its trendline. Equation represented in Table D.36.

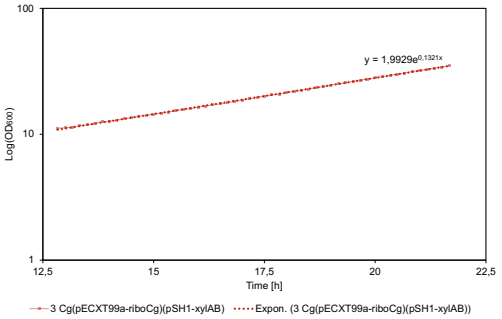

(d) The exponential growth phase of parallel number 3, with its trendline. Equation represented in Table D.36.

Figure D.15: These plots represent the growth curves of three parallels of the strain Cg(pECXT99a-*riboCg*)(pSH1-*xylAB*), and their corresponding trend lines, in the exponential phase incubated with a mixture of glucose 1% and xylose 1%. The OD_{600} values are plotted against their corresponding time, between the time interval of 0 and 25 hours.

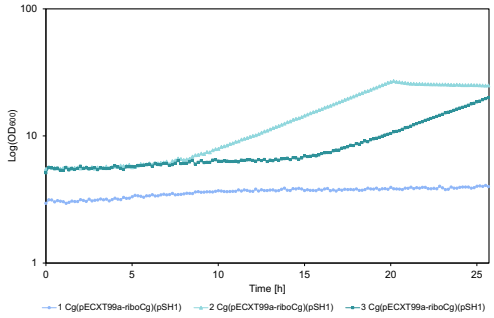

(a) All three parallels with their complete Log(OD_600) values are represented over 25 hours.

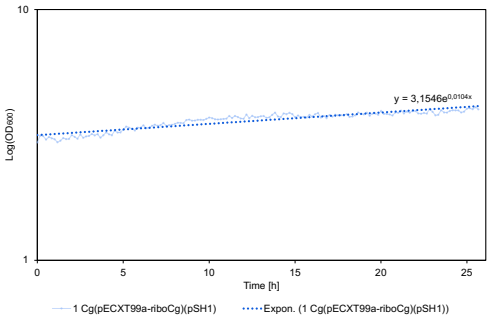

(b) The exponential growth phase of parallel number 1, with its trendline. Equation represented in Table D.36.

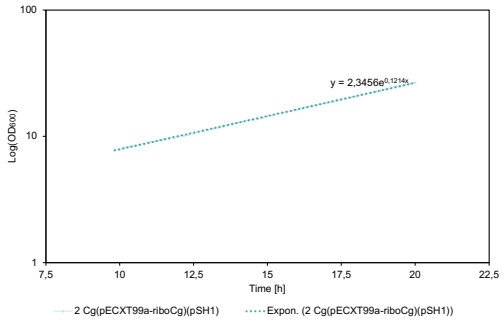

(c) The exponential growth phase of parallel number 2, with its trendline. Equation represented in Table D.36.

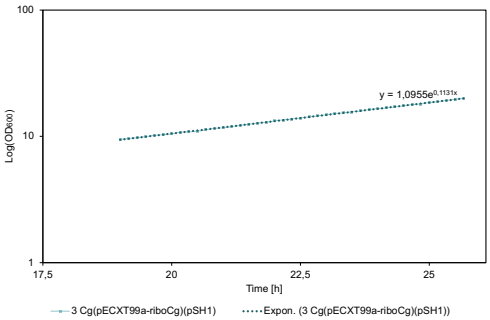

(d) The exponential growth phase of parallel number 3, with its trendline. Equation represented in Table D.36.

Figure D.16: These plots represent the growth curves of three parallels of the strain Cg(pECXT99a-*riboCg*)(pSH1) and their corresponding trend lines, in the exponential phase incubated with a mixture of glucose 1% and xylose 1%. The OD_{600} values are plotted against their corresponding time, between the time interval of 0 and 25 hours.

Xylose as carbon source

With xylose 1% as the carbon source for strains Cg(pECXT99a-*riboCg*)(pSH1-*xylAB*) and Cg(pECXT99a-*riboCg*)(pSH1), the logarithmic OD_{600} with the corresponding trendlines are plotted in Figure D.17 and D.18 respectively.

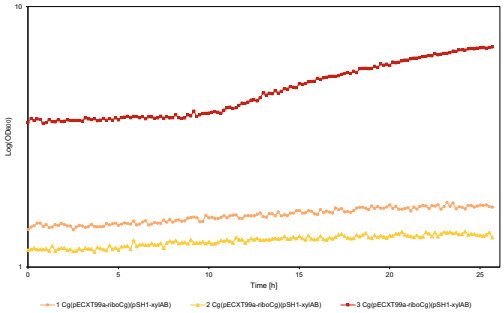

(a) All three parallels with their complete Log(OD_600) values are represented over 25 hours.

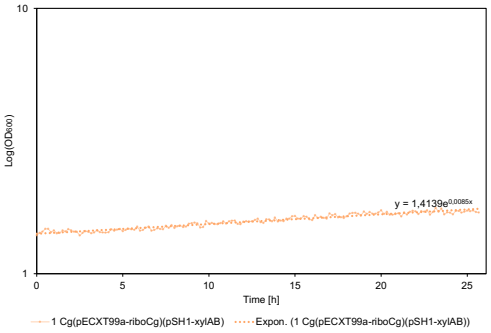

(b) The exponential growth phase of parallel number 1, with its trendline. Equation represented in Table D.36.

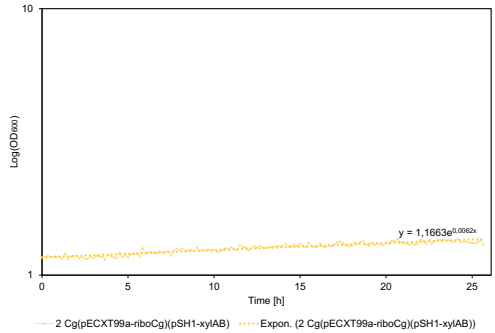

(c) The exponential growth phase of parallel number 2, with its trendline. Equation represented in Table D.36.

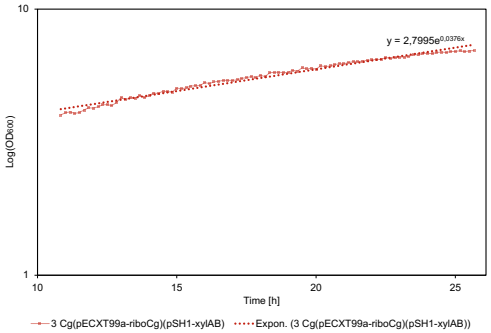

(d) The exponential growth phase of parallel number 3, with its trendline. Equation represented in Table D.36.

Figure D.17: These plots represent the growth curves of three parallels of the strain Cg(pECXT99a-*riboCg*)(pSH1-*xylAB*), and their corresponding trend lines, in the exponential phase incubated with xylose 1%. The OD_{600} values are plotted against their corresponding time, between the time interval of 0 and 25 hours.

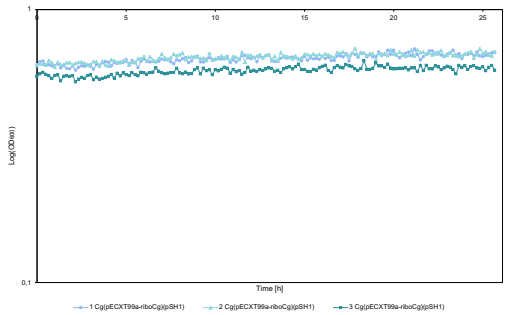

(a) All three parallels with their complete Log($OD_6$00) values are represented over 25 hours.

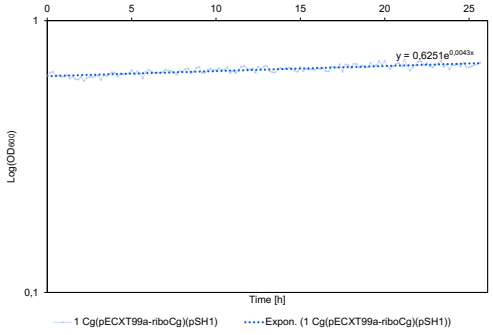

(b) The exponential growth phase of parallel number 1, with its trendline. Equation represented in Table D.36.

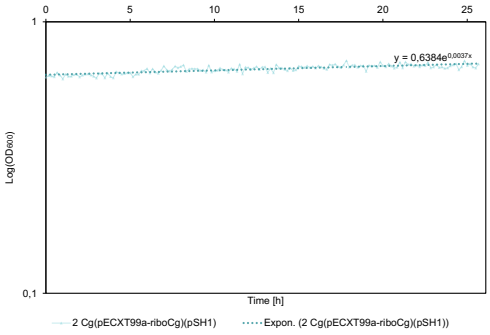

(c) The exponential growth phase of parallel number 2, with its trendline. Equation represented in Table D.36.

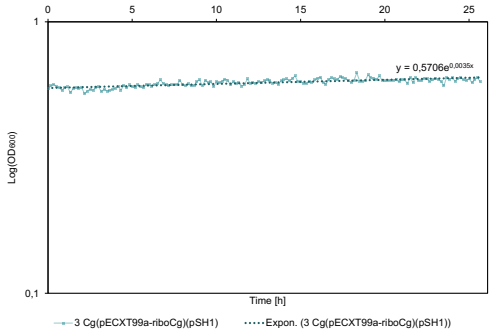

(d) The exponential growth phase of parallel number 3, with its trendline. Equation represented in Table D.36.

Figure D.18: These plots represent the growth curves of three parallels of the strain Cg(pECXT99a-*riboCg*)(pSH1) and their corresponding trend lines, in the exponential phase incubated with xylose 1%. The OD_{600} values are plotted against their corresponding time, between the time interval of 0 and 25 hours.

D.4 Biomass and biomass yield calculations

The biomass and biomass yield for the strains final values were calculated, utilising Equation D.6 and D.7. The final sample was chosen because all samples were in a stationary phase at this point.

$$\text{Biomass}_i = \text{Correlation factor} \cdot \text{OD}_{600(i)} \tag{D.6}$$

The correlation factor utilised in this thesis was set to 0.343, based on personal conclusions with Dr. Pérez García. The $OD_{600(i)}$ values here refer to the final average OD_{600} value for each strain in different conditions.

$$\text{Biomass yield}_\text{i} = \frac{\text{Biomass}_\text{i}}{C_{\text{Carbon source}}} \tag{D.7}$$

$C_{\text{Carbon source}}$, refers to the concentration of carbon source used, which varies for experiments performed on the different strains. It was either set to 10 g/L or 20 g/L, dependent on the presence of a sole carbon source or multiple.

The average and standard deviation values of the biomass and biomass yield were calculated, and are given in Table 5.1, 5.2 and 5.3for the different strains.

E HPLC

In the following chapter the calculations done from the HPLC values found for fermentations done by biolector and bioreactor will be represented. Their was an HPLC performed to analyse the amount of product present in different samples, but for the fermentation performed in a bioreactor the samples were also analysed for xylose.

E.1 HPLC standards

Four standards with known riboflavin and xylose concentrations were examined to analyse the riboflavin titer and xylose titer from the HPLC samples respectively. The concentration, retention time, area and height of the standards are given in Table E.37 and E.38. The retention time for riboflavin is given at around 4.2 minutes, and the retention time for xylose is given at 10.4 minutes.

Table E.37: Standard samples of riboflavin with their know concentrations, and their correlating retention time, area and height values from the HPLC analysis.

Standard concentration [g/L]	Retention time	Area	Height
0.005	4,149	43154025	4611142
0.0025	4,18	22137833	2326810
0.00125	4,215	11191040	1183194
0.000625	4,226	5450460	574133

Table E.38: Standard samples of xylose with their know concentrations, and their correlating retention time, area and height values from the HPLC analysis.

Standard concentration [g/L]	Retention time	Area	Height
10	10.384	21927.1	450.2
1	10.367	2086.0	87.1
0.1	10.405	203.2	13.0

The heights given for the two different compounds were then plotted against the known concentrations, giving the plots shown in Figure E.19 and E.20. From this, the slope of the curves were found to be 919 908 215.65 and 42.61 respectively. These values were utilised in the calculations of riboflavin and xylose titer of the HPLC samples.

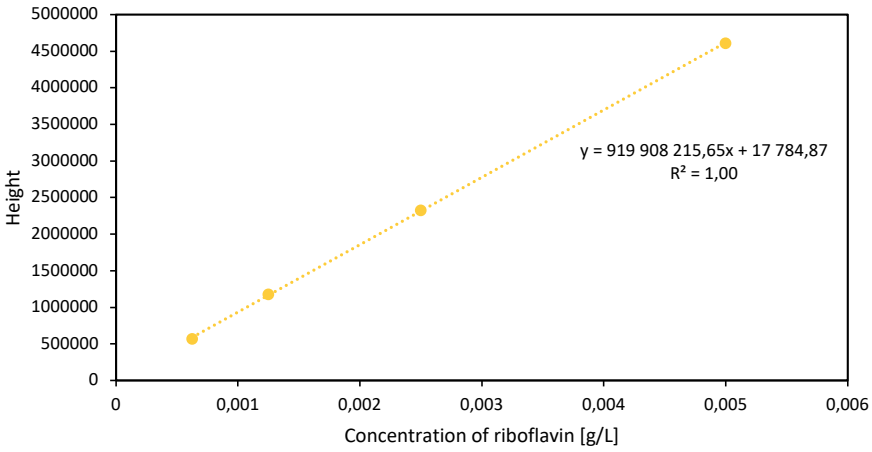

Figure E.19: Height values of the riboflavin standards given from the HPLC analysis with their corresponding concentrations. The trend line for the samples is given by the dotted line and equals the equation y = 919 908 215.65x + 17 784.87

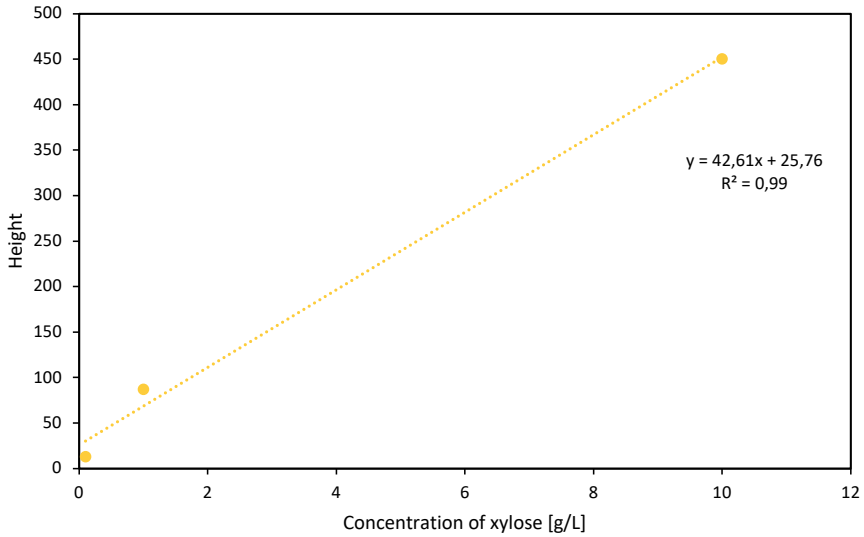

Figure E.20: Height values of the xylose standards given from the HPLC analysis with their corresponding concentrations. The trend line for the samples is given by the dotted line and equals the equation y = 42.61x + 25.76

E.2 HPLC calculations

The height and retention time for riboflavin and xylose were found through HPLC analysis. These values are given in Table 5.4 and 5.7 for riboflavin from the biolector and bioreactor fermentation samples, and in Table 5.8 for xylose from the bioreactor fermentation samples. From the height values, the compound titers could be calculated with Equation E.1. Here H_{ji} represents the height for the compound j in sample i. S_j represents the standard slope for compound j, given from the plots represented in Appendix E.1. D_i is the dilution factor for sample i.

$$C_i = \frac{H_{\mathrm{ji}}}{S_{\mathrm{j}}} \cdot D_{\mathrm{i}} \tag{E.1}$$

The yield (Y_i) and volumetric productivity(VP_i) of the product for the samples were then analysed by utilising Equation E.2 and E.3. $\mathrm{C}_{\mathrm{Carbon\ source}}$ is the carbon source concentration for the different conditions, while t is the hour the final sample for the experiment was taken.

$$Y_{\mathrm{i}} = \frac{C_{\mathrm{i}}}{C_{\mathrm{Carbon\ source}}} \tag{E.2}$$

$$VP_{\mathrm{i}} = \frac{C_{\mathrm{i}}}{t} \tag{E.3}$$

E.2.1 Biolector

From the biolector fermentation, one sample of each strain in each condition was analysed for riboflavin. The height values(H_{i}) were utilised to calculate the correlation coefficients (R_{i}) from the estimated riboflavin output values from the biolector(Y_{i}), by using Equation E.4, they are further represented in Table E.39.

$$R_{\mathrm{i}} = \frac{H_{\mathrm{i}}}{Y_{\mathrm{i}}} \tag{E.4}$$

Table E.39: For the different combinations of strains, one sample for each condition is represented with their height value, output value from the biolector, and the correlation coefficient between them at the final point of the experiments. G, F, M and X stands for glucose, fructose, mannitol and xylose.

Strain	Sample nr.	Carbon source	Height	Value from biolector	Correlation coefficient
Cg(pECXT99a-*riboCg*)(pVWEx1-*fbp*)	2	G	30240709	1.53	19765169.28
Cg(pECXT99a-*riboCg*)(pVWEx1-*fbp*)	1	G + F	20648237	1.79	11535327.93
Cg(pECXT99a-*riboCg*)(pVWEx1-*fbp*)	3	F	13806302	1.46	9456371.233
CgΔ*altR*(pECXT99a-*riboCg*)	3	G	30072488	1.6	18795305
CgΔ*altR*(pECXT99a-*riboCg*)	2	G + M	42372466	1.76	24075264.77
CgΔ*altR*(pECXT99a-*riboCg*)	3	M	17264714	1.61	10723424.84
Cg(pECXT99a-*riboCg*)(pSH1-*xylAB*)	3	G	33978187	1.55	21921410.97
Cg(pECXT99a-*riboCg*)(pSH1-*xylAB*)	1	G + X	11216126	1.69	6636760.947
Cg(pECXT99a-*riboCg*)(pSH1-*xylAB*)	3	X	11566446	1.42	8145384.507

The height of every sample was then calculated through Equation E.5 with the correlation factors for each strain in different conditions.

$$H_{\mathrm{i}} = \frac{R_{\mathrm{i}}}{Y_{\mathrm{i}}} \tag{E.5}$$

The height values were further used to calculate the average titer, yield and volumetric productivity at 25 hours, with their correlating standard deviation values. The final values are given in Table 5.5, alongside the carbon source concentrations.

E.2.2 Bioreactor

From the bioreactor, each sample was analysed for both riboflavin and xylose. The retention time and height values are respectively represented in Table 5.7 and 5.8.

F Bioreactor

This Chapter includes the values taken from the fermentation in the bioreactor, including further calculations done with these values. The volume of the reactor from 0 to 48.5 hours was at 0.5 L, increasing to 0.6 L when adding the feeding solvent of 5% xylose at this point. This change in volume has been taken into account for the different calculations.

F.1 OD_{600} values

In Table F.40 the initial OD_{600} values are represented. The values found have then been corrected with the dilution factor that has been caused by the feed solution of 5 % xylose started at 48.5 hours. The volume was increased from 0.5 litres to 0.6 litres, resulting in an increasing percentage of 20. The initial values taken after 48.5 hours have therefore been multiplied by 20 %, correcting the dilution factor, and are represented in Table F.40.

Table F.40: The initial OD_{600} values taken from the strain Cg(pECXT99a - *riboCg*)(pSH1-xylAB), inoculated with 1 % xylose, are represented in this table. Furthermore the corrected OD_{600} values have been calculated from the change in volume during the feed phase of the fermentation, and are also represented here with the samples correlated volume.

Sample hour [h]	0	2	4	6	12	13	18	20	22	24	26	28	44	46.5	48.5	51	53	55	57	68	70	72
Solution volume [L]	0.5	0.5	0.5	0.5	0.5	0.5	0.5	0.5	0.5	0.5	0.5	0.5	0.5	0.5	0.5	0.6	0.6	0.6	0.6	0.6	0.6	0.6
Initial sampled OD_{600}	0.12	0.12	0.14	0.17	0.4	0.56	0.9	1.2	1.6	1.8	2.2	2.6	5	7	6	6	6	6	6	7	6	6
Corrected OD_{600}	0.12	0.12	0.14	0.17	0.4	0.56	0.9	1.2	1.6	1.8	2.2	2.6	5	7	6	7.2	7.2	7.2	7.2	8.4	7.2	9.6

F.2 Calculations

This subchapter will include the calculations performed from the corrected OD_{600} values, represented in the Table F.40, and the HPLC values found from the fermentation samples. The calculations for the fermentation have been divided into two segments. The first segment is the batch fermentation from 0 to 48.5 hours, and the second is the fermentation with the feeding from 48.5 to 72 hours.

F.2.1 Calculations of the growth rates

From the corrected OD_{600} values, the growth rates for the exponential phase of the two phases were found by utilising Equation D.5. The logarithmic values of the OD_{600} values were plotted against the sample times, giving Figure F.21a and F.21b.

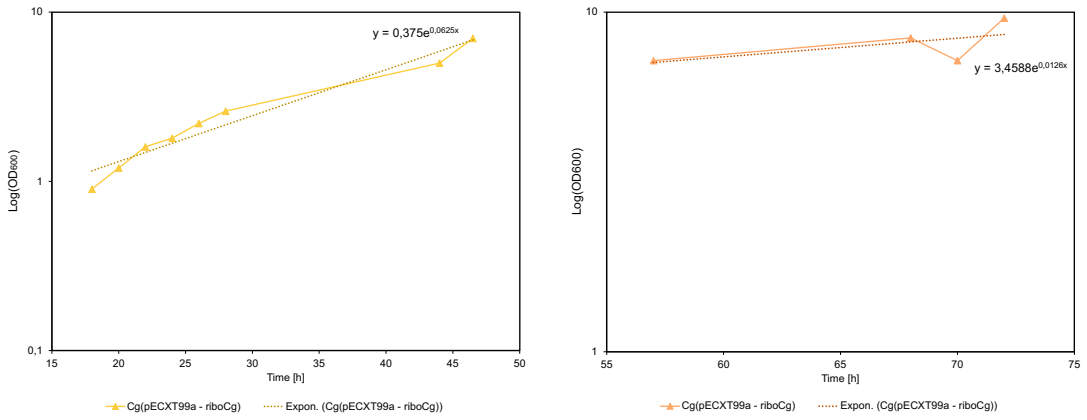

(a) **(b)**

Figure F.21: Growth rates for the to segments for the fermentation of the third parallel for Cg(pECXT99a-*riboCg*)(pSH1-*xylAB*).

The trendlines for the two phases of fermentation are respectively y = $0.375e^{0.0625}$ and y = $3.4588e^{0.0126}$, resulting in the growth rates 0.06 and 0.01.

F.2.2 Titer calculations

From the fermentation, each sample was analysed for both riboflavin and xylose. The retention time and height values are respectively represented in Table 5.7 and 5.8. The titer values of the two compounds were calculated from the HPLC height values and the slope from the standard curve, given in Appendix E.1. This was done by utilising Equation E.1. The calculated initial titer values alongside the correlating sample times are represented in Table F.41. The titer values for the samples taken during the fermentation with feeding were corrected for the dilution factor of 20 %, resulting in the titer values represented in Table 5.7 and 5.8.

Table F.41: This Table shows the initial calculated riboflavin and xylose titers over time, with the correlating solution volume of the reactor at the sampling point. These values are then corrected for the feed dilution factor, and the final titer results are represented in Table 5.7 and 5.8, respectively.

Sample hour [h]	0	2	4	6	12	13	18	20	22	24	26	28	44	46.5	48.5	51	53	55	57	68	70	72
Solution volume [L]	0.5	0.5	0.5	0.5	0.5	0.5	0.5	0.5	0.5	0.5	0.5	0.5	0.5	0.5	0.5	0.6	0.6	0.6	0.6	0.6	0.6	0.6
Riboflvin initial titer [mg/L]	0.05	0.08	0.31	1.11	10.68	12.89	29.61	51.96	49.91	55.09	86.38	97.40	280.83	252.83	364.75	302.95	296.34	272.20	359.13	707.60	676.10	558.74
Xylose initial titer [g/L]	11.41	11.12	11.01	10.54	9.15	8.61	8.12	8.21	8.10	7.60	7.39	9.13	6.52	6.08	5.77	10.44	11.48	11.43	12.95	10.47	7.91	6.71

F.2.3 Carbon source consumption calculations

From the xylose titer calculations, the consumed titer(U_i) of the carbon source could be calculated at the different sample times i. This was done by utilising Equation F.1 for the final point of the batch fermentation at 48.5 hours and the final point of the complete fermentation at 72 hours.

$$U_i = U_j - C_i \tag{F.1}$$

C_i represents the titer of xylose, given in Table 5.8, for the consumption point i being analysed. The final titer concentrations for the two segments are 5.36 mg/L and 13.10 mg/L. U_j is the carbon source consumption at the starting point of the segment being analysed. This value is 0 g/L for the batch phase, but for the feeding phases, it would be the carbon consumption value of the final point of the batch fermentation, 5.63 g/L. The total carbon source consumption is the sum of the two phasess consumption values. The calculated values are represented in Table F.42.

Table F.42: In this Table the carbon source consumption amount of xylose is represented for the two phasess of the fed-bath fermentation, the batch phases from 0 - 48.5 hours and the feed phases from 48.5 - 72 hours, as well as the total consumption through the complete fermentation.

Sample hour [h]	Carbon source consumption [g/L]
0 - 48.5	5.63
48.5 - 72	7.46
0 - 72	13.20

F.2.4 Biomass and biomass yield

Equation D.6 and D.7 were utilised to calculate the biomass and biomass yield values for the two phases. Results are represented in Table 5.9. For the calculation of the biomass yield, the consumption values in Table F.42 were defined as the carbon source titer values used for the correlating points, using the total consumption value for the final fermentation point.

F.2.5 Product yield and volumetric productivity

The riboflavin product yield and volumetric productivity were calculated with Equation E.2 and E.3. The carbon source concentration values utilised were for the final point of the two fermentation phases, at the time 48.5 and the total consumption value at 72 hours, respectively, represented in Table F.42. The final results are described in Table 5.10 with their correlating titer and time.

Thea Isabel Bakken

Potential of using alternative carbon sources for the production of riboflavin with engineered *C. glutamicum*

NTNU
Norwegian University of
Science and Technology